ERROR ANALYSIS OF ANGLE AND RANGE ESTIMATION IN A RANGE LIMITED ANTENNA SYSTEM USING MUSIC AND MODIFIED ROOT PISARENKO ALGORITHMS

Zarak A. Khan

Thesis submitted to the Faculty of the Virginia Polytechnic Institute and State University in partial fulfillment of the requirement for the degree of

Master of Science
in
Electrical Engineering

Dr. Amir I. Zaghloul, Chair
Dr. William A. Davis
Dr. Jeffrey H. Reed

December 2003

Key words: Direction-finding algorithms, MUSIC, Modified Root Pisarenko, Range Limited Antenna

ERROR ANALYSIS OF ANGLE AND RANGE ESTIMATION IN A RANGE LIMITED ANTENNA SYSTEM USING MUSIC AND MODIFIED ROOT PISARENKO ALGORITHMS

Zarak A. Khan

ABSTRACT

The Range Limited Antenna (RLA) has the ability to track and pin-point RF devices operating within a certain accepted range. Using two antenna arrays, each made up of several elements, direction-finding algorithms such as MUSIC and Modified Root Pisarenko (MRP) are used to estimate the angles of arrival of incoming signals. Using the estimated angles of arrival, a range estimation algorithm is used to estimate the distance of the emitter from the antenna array.

The aim of this thesis is to check the sensitivity of the range estimation and to form a statistical analysis for such conditions. Conditions of error are introduced into the system and several extensive Monte Carlo simulations are run for both MUSIC and MRP. Upon simulating physical errors in the antenna set-up, it is realized that the range estimation algorithm is sensitive to the slightest of phase shift differences, cable loss differences, mixer mismatches, and antenna mismatches.

Dedication

This effort is dedicated to my parents.

ACKNOWLEDGEMENTS

Before anyone else, I would want to thank God for having given me the strength to reach this wonderful moment of my life. All praises and thanks are to Him.

I would like to thank my advisor, Dr. Amir Zaghloul, whose wonderful guidance made this experience a most enjoyable one. I thank him for advising me during my research, counseling me during my studies, and providing a supportive environment for me to carry out my M.S. research. Also, I would want to thank my committee members, Dr. Davis and Dr. Reed for their very wonderful co-operation and support.

I would like to thank Dr. Ivica Kopriva of the George Washington University, who has been a great help during the course of my research. He has been a wonderful mentor and tutor. Also, I thank Dr. Wasyl Wasylkiwskyj, also of GWU, for his valuable advice and suggestions.

I cannot find the words to express my feelings of gratitude towards my father, Tahir A. Khan, and my mother, Nilofer Tahir Khan. I thank them for their encouragement throughout the course of my life. Without their support, I would never be able to achieve my goals. Furthermore, I would want to thank my sisters, Kashmala and Sherbano for their love and patience towards me.

At this point, I thank my uncle, Dr. Waqar Mohmand and my aunt, Sarah Iman for their wonderful support and encouragement during my stay in Alexandria, VA. I am proud to have them as close members of my family.

In the end, I would say that during the course of our lives we encounter many people who help us, guide us, share their valuable time with us and provide support in whatever way possible. I thank them all.

Table of Contents

List of Figures

List of Tables

Chapter 1
Introduction

The work presented in this thesis is based on an effort to analyze, design, build and test a Range Limited Antenna (RLA) that has the ability to track and pin-point RF devices operating within a certain accepted range.

The Range Limited Antenna (RLA) would be able to receive signals from sources inside a certain range and reject all signals from emitters outside this range. The antenna that has been designed consists of two ten-element patch arrays. The four center elements in each array are excited while the other six elements are terminated in 50 ohm impedances. The patch antennas are connected via SMA cables to phase shifters, mixers, and power dividers. Upon receiving incident signals, the array response is input to a direction-finding algorithm. The algorithm then produces estimated angles of arrival that are then used to estimate the range of the emitter.

1.1 Motivation

The range estimation algorithm uses the estimated angles of arrival at the two antenna arrays to produce a range estimate of the emitter from the center of the array. The dependence of the estimated range on the angles of arrival can be seen in the derivation given in the Appendix A. Although these angles can be accurate in theoretical conditions, there was a need to see its practical performance in conditions of random errors as the algorithm is sensitive to the slightest of changes in estimated angles. Extensive simulations were needed to check these trends. The work presented in this thesis covers these simulations and presents them as tolerance levels to the reader. Factors such as transmission line lengths, phase shifters, frequency mixers, cable gains, etc. were taken into account.

1.2 Contribution

The work covered in this thesis is representative of the required analysis for the RLA to check its sensitivity to different practical environments. Extensive Monte Carlo simulations were run for different conditions of error. The statistical data produced has been recorded for future reference. Most importantly, these results have been summarized into reference tables that define tolerance levels for the system. This gives the advantage of knowing bounds of random error within which useful results can be produced.

1.3 Overview of Thesis

Following this introduction, Chapter 2 describes the physical structure used for the RLA. It also presents some pictorial representations so that the reader finds it easier to visualize the equipment designed and used. Although the antenna elements chosen for the RLA design and implementation were patch elements, the error analysis in this thesis is independent of the element type and in cases where element patterns are required, dipole elements are assumed. Chapter 3 covers the array response and the theoretical concepts explaining the direction-finding algorithms used for the project. MUSIC and Modified Root Pisarenko (MRP) algorithms were chosen. Chapter 4 presents the results of various and extensive MATLAB simulations using the Monte Carlo techniques for MUSIC. These results show the errors that are introduced into the system when different conditions of inconsistencies are taken into consideration. Chapter 5 presents the results of various and extensive MATLAB simulations using the Monte Carlo techniques for Modified Root Pisarenko. This chapter also covers the effect of using an extended array where passive elements are added to the antenna array to equalize the effects of mutual couplings. The results show that the process is very effective. Chapter 6 gives a summary of the work done and some recommendations for future work.

Chapter 2
Range Limited Antenna

This chapter gives the background necessary to understand the antenna configuration and simulations used in the Range Limited Antennas (RLA) project. It describes the patch antenna used, its advantages and disadvantages, the properties of substrates, and characteristics of co-axial feeds. A few drawings illustrate the construction of the antenna. Also, a block diagram of the RLA system is given for a clearer understanding of the signal path.

2.1 The patch antenna

A microstrip antenna or patch antenna has a conducting patch at the top which is usually a copper or gold foil. This is followed by a dielectric that has the patch and feed photo-etched to it. Following the substrate is the metallic bottom ground plane that is aluminum or copper. RLA used a square patch with given dimensions. It is important to note that the simulations discussed in Chapter 4 and Chapter 5 used dipole antennas. The following picture shows the patch antenna used for the project.

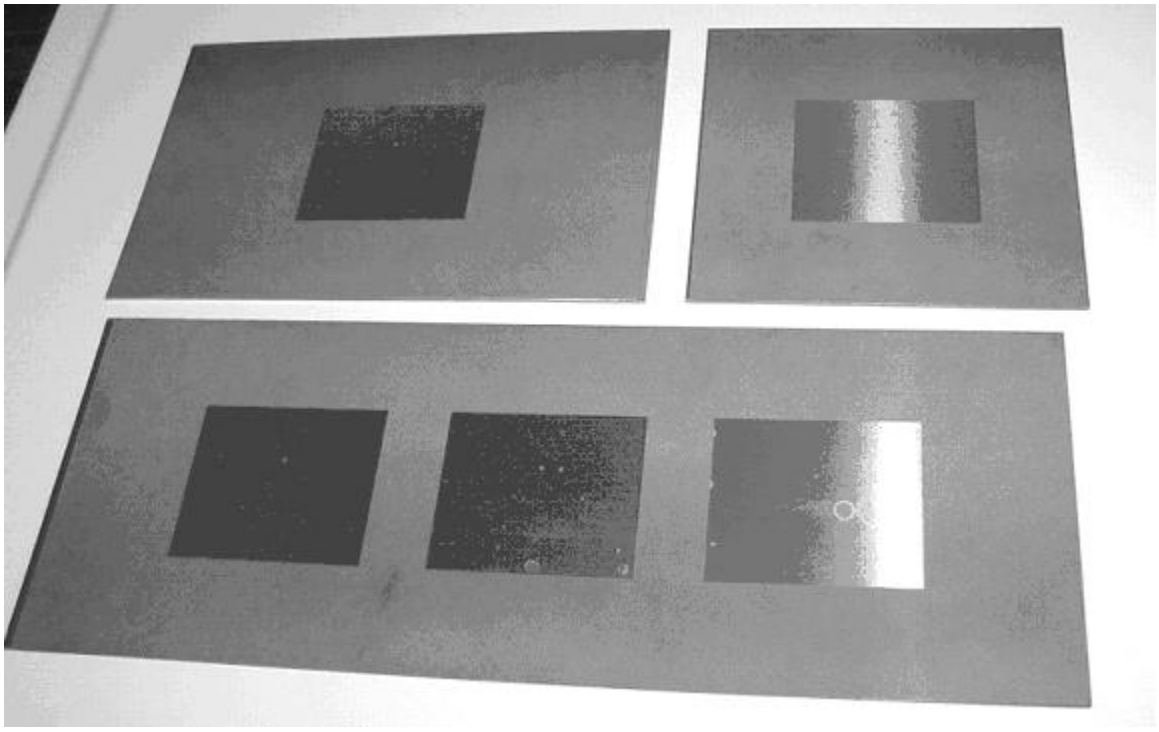

Figure 2.1: Antenna patches with substrate used in RLA

2.2 Advantages and disadvantages of a patch antenna

The following are some of the various advantages and disadvantages of a microstrip antenna [Garg1]:

Advantages:

- Low volume
- Linear and circular polarizations with regular-simple feeds possible
- Feed lines can be made with the antenna
- Low cost to fabricate
- Light weight

Disadvantages:

- Narrow bandwidths for thin substrates
- High levels of cross-polarization and mutual coupling at high frequencies

- Large losses in array feed lines
- Radiation into half-space
- High dielectric constant substrates may give poor efficiency and narrow bandwidth
- Radiation from feed lines

2.3 Properties of substrates

Any antenna design has the substrate [Garg2] as an important determining factor as it provides both electrical and mechanical properties by using the dielectric material. Some properties of substrates are given below:

- Dielectric constant
- Variation of losses with frequency, temperature
- Cost
- Strain relief
- Thickness uniformity
- Permittivity
- Tensile strength
- Dimensional stability

It is important to note that the type of substrate used depends on the particular application. Dielectric constants for microstrip antenna substrates vary between $2.2 \le e_r \le 16$. Applications that require high efficiency, large bandwidth, and loosely bound fields use thick substrates with low dielectric constants [Bahl1]. However, these have the limitation of increased antenna size. In comparison, thin substrates contribute to a reduced factor of element size, radiation and coupling in the antenna along with greater losses giving lower efficiency and smaller bandwidths [Bahl1]. It is also important to note that by increasing the height of the substrate, surface waves are introduced which has an affect on antenna patterns and polarizations [Bahl1].

2.4 Co-axial Antenna Feeds

The type of feed given to the antenna depends on the application. Furthermore, amongst the many available techniques, complexity is an important factor that decides this factor. Transmission line feeds, co-axial feeds, aperture coupled feeds, buried feeds, slot feeds, and proximity coupled feeds are the most commonly used [Ban1]. The feed-type used for the RLA is the co-axial feed that is perpendicular to the patch and ground plane. This feed has two cylinders of which the inner conductor is connected to the patch after passing through the dielectric and ground plane whereas the outer conductor is connected to the ground plane. This gives the feed and patch a shield from each other. Also, the position of the feed along the patch varies the input impedance. The figure below shows this configuration [Ban1]:

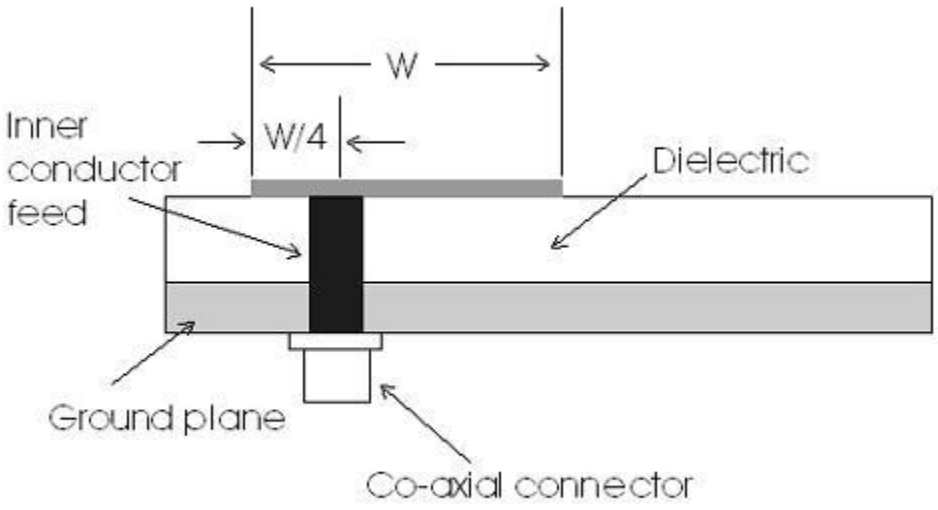

Figure 2.2: Side view of the co-axial feed

2.5 Pictorial representation of RLA

This section gives some pictorial representations used for the design of the Range Limited Antenna. Figure 2.3 shows the flexibility of the antenna with reference to the

angle of elevation. This comes with the use of a ball and socket support that allows the antenna axis to be moved in the vertical plane. The internal details of the figure for each block supporting an aluminum plate show the phase shifters, mixers, cables, etc used. Figure 2.4 gives the final shape of the RLA. The two antenna arrays used are shown as rectangular planes on the top of the aluminum plate. The tripod mounts are adjustable in vertical height.

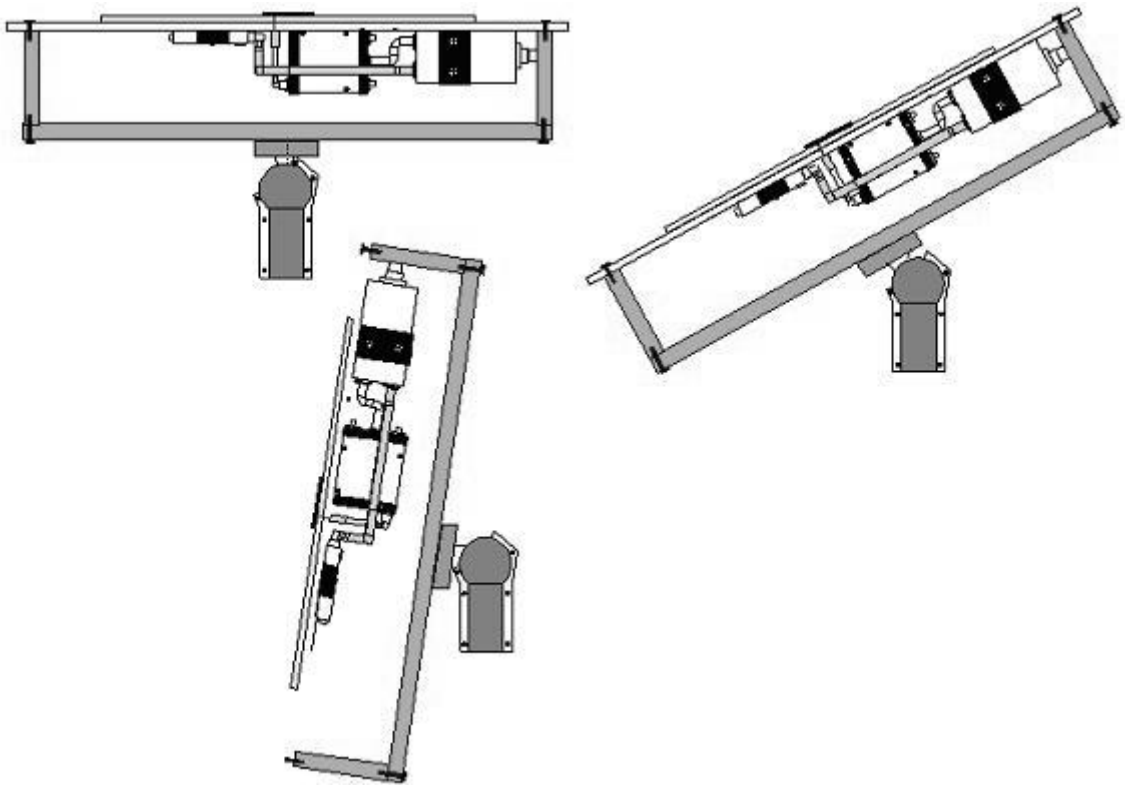

Figure 2.3: Side view of the antenna set-up

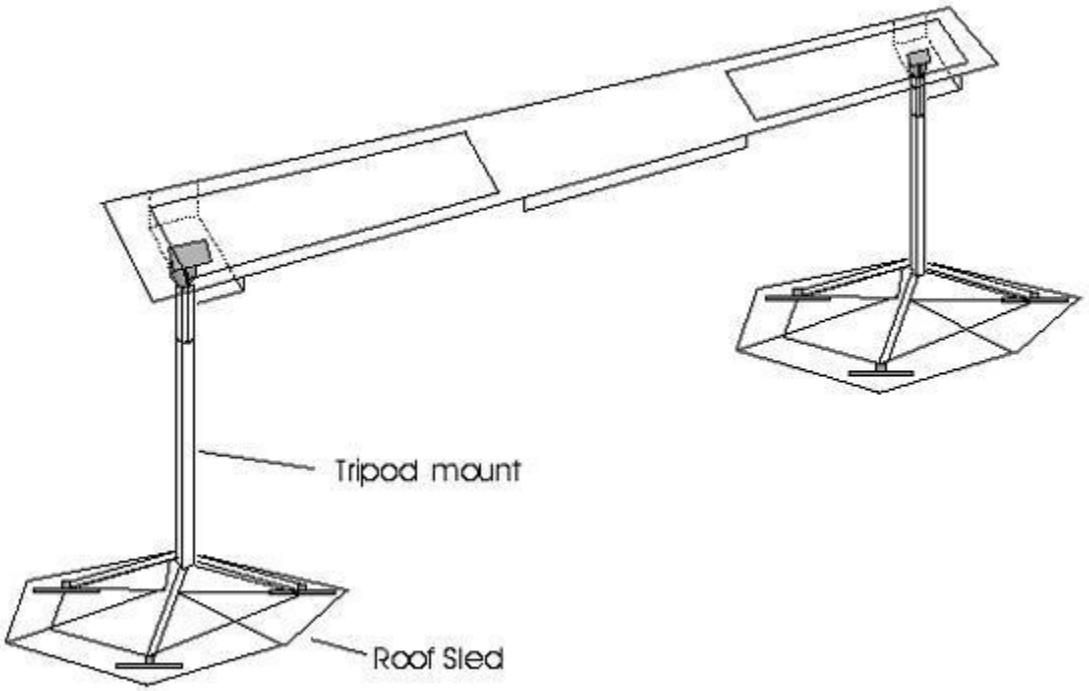

Figure 2.4: Range Limited Antenna

2.6 Block Diagram representation of RLA

Antenna elements are connected to frequency mixers via coaxial cables. These cables form an input to the mixer at radio frequency in the range of 1.8-2.1 GHz. The second input to the mixer comes from the local oscillator. The local oscillator's output is used with the incoming signal to produce sum or difference tones. Phase shifters are inserted in the LO signal path to equalize the signal phase for all antenna elements when the signal is incident in the broadside direction. Figure 2.5 represents the system concept.

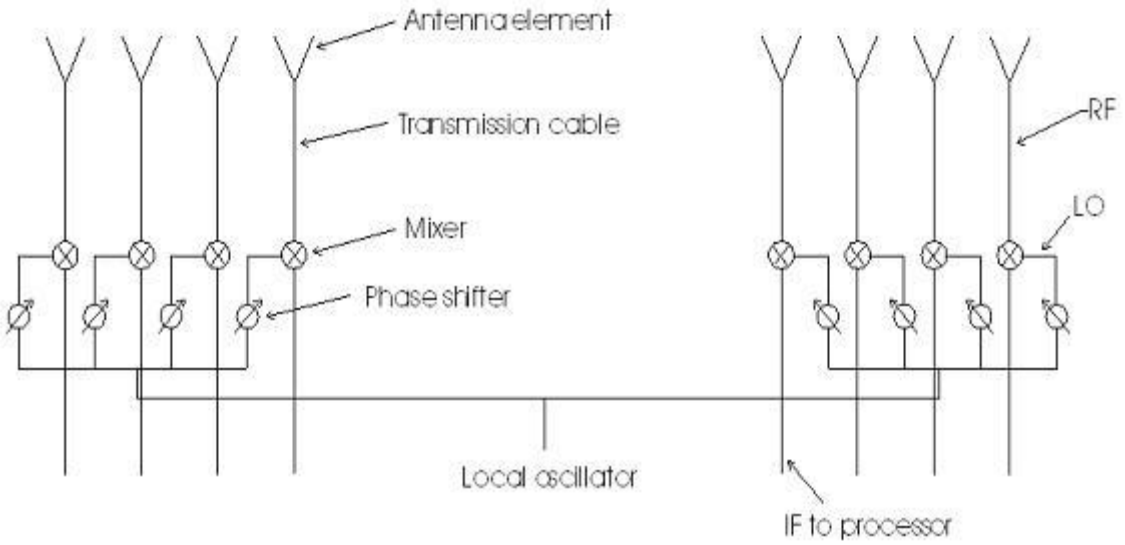

Figure 2.5: Block diagram of array components

Chapter 3

Direction-finding Algorithms

This chapter gives a theoretical background of the antenna array response and the direction-finding algorithms. MUSIC, Blind MUSIC, Root MUSIC, Modified Pisarenko, Modified Root Pisarenko, and Prony's method are the common direction-finding algorithms used. Amongst these algorithms, Prony is the only algorithm that can work in multipath where the incoming signals are correlated [Kop1]. For the Range Limited Antenna (RLA) project, MUSIC and Modified Root Pisarenko were used. MUSIC is able to work under coupled and decoupled conditions. However, it does require that the array be calibrated with respect to the steering vector. On the other hand, Modified Root Pisarenko requires equalized radiation patterns so that it can get a uniform steering vector [Kop2]. The equalization was done using a model for an infinite array. These concepts will be explained later on in this chapter.

It is important to note that for small errors in the system, the direction-finding algorithms are greatly affected. Furthermore, as the errors are increased the performance degrades till a threshold where the direction of arrival of the incoming signal is not resolved [Frid1].

3.1 The Array Model

The antenna array response can be described by the following equation [Kop5]:

$$z(t) = As(t) + n(t) \tag{3.1}$$

The individual vectors given in Equation 3.1 are given below where:

z (t) = $[\, z_1(t)\ z_2(t)\ z_3(t)\ \ldots\ldots z_N(t)\,]^T$ represents the output of the I-Q channels.

A = $[\, a(\theta_1,\varphi_1)\ a(\theta_2,\varphi_2)\ a(\theta_3,\varphi_3)\ \ldots\ldots a(\theta_L,\varphi_L)\,]$ represents the steering matrix.

s(t) = $[\, s_1(t)\ s_2(t)\ s_3(t)\ \ldots\ldots s_L(t)\,]^T$ represents the narrowband source signal.

n(t) = $[\, v_1(t)\ v_2(t)\ v_3(t)\ \ldots v_N(t)\,]^T$ represents the additive Gaussian noise.

The variable *L* denotes the number of emitted signals and *N* gives the number of antenna array elements. Each element of A is an N-element column vector that gives the steering vector corresponding to the Direction-of-Arrival of the j-th signal. The vector s(t) is an LxT vector with T as the sample size. Multiplying s(t) and A gives an NxT vector.

For the RLA simulations, N was taken to be 4 for each of the two arrays. In simulations using MRP, N was changed to 10 with 4 active and 6 passive elements. Considering an array's m-th element and its center element, the difference in phase between a signal's components arriving at the two is given by the following [Lib1]:

$$\Delta\psi = \beta\Delta d_m = \beta\left(x_m \cos\phi \sin\theta + y_m \sin\phi \sin\theta\right) \tag{3.2}$$

where $\beta = \dfrac{2\pi}{\lambda}$ is the free space wave number, and λ is the wavelength.

The spacing between the antenna array elements can be assumed to be 0.5λ. The array is referred to as a linear, equally-spaced array. Figure 3.1 shows the array used with an emitter at a certain distance. The plane wave incident on the array has the direction of arrival as (ϕ,θ) relative to the horizontal axis of the antenna array. $\dfrac{D}{2}$ is the distance of the center of the 4-element array to the origin. θ is the elevation angle measured from the zenith. ϕ is the azimuth angle. R is the distance of the source or emitter from the origin.

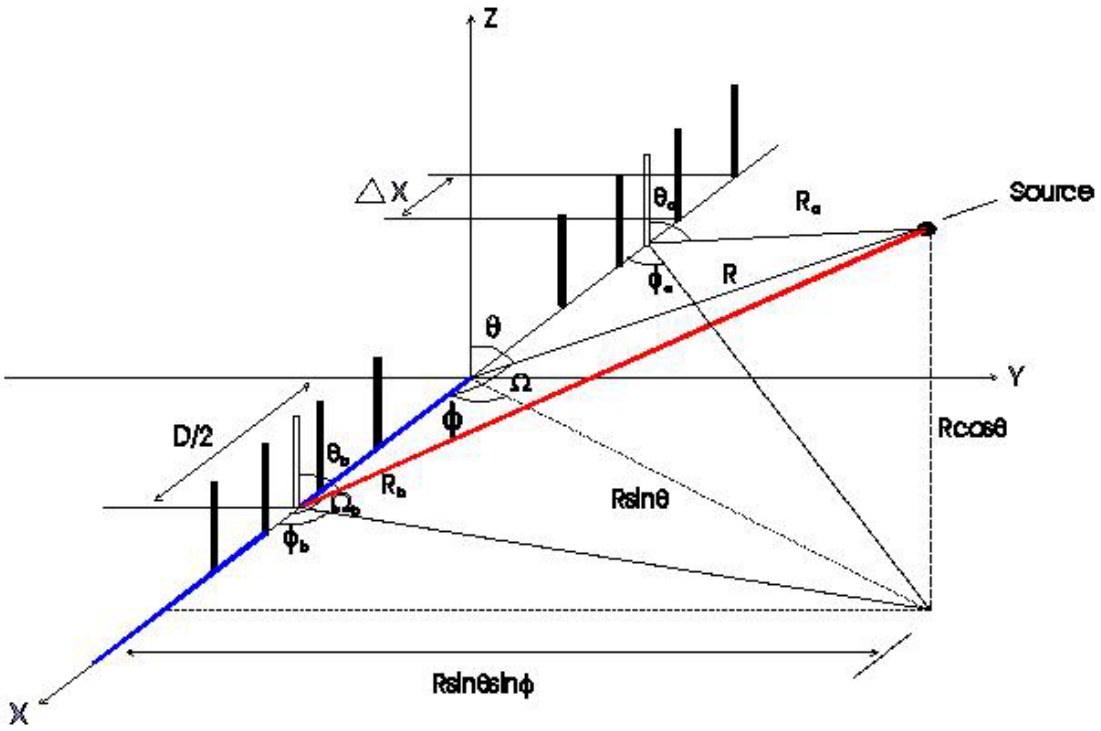

Figure 3.1: Angles of arrival for emitter at distance R from origin

Since the elements are spaced equally apart, the element location on the x-axis is given by [Lib1]:

$$x_m = m\Delta x \tag{3.3}$$

where m is the element number with 1 being the inner most element from the origin. Δx is the distance between two consecutive antenna elements of the same array. It is important to note in Figure 3.1, that the origin is between the two four element arrays.

The signal at the m-th element is [Lib1]:

$$s_m(t) = Gs(t)e^{-i\beta m\Delta d} \tag{3.4}$$

$$s_m(t) = Gs(t)e^{-i\beta m\Delta x\cos\phi\sin\theta} \tag{3.5}$$

with G representing the directional gain of the emitters. The array response is calculated with a summation of individual responses of the weighted antenna elements. This is as shown below [Lib1]:

$$z(t) = \sum_{m=0}^{M-1} w_m u_m(t) = Gs(t) \sum_{m=0}^{M-1} w_m e^{-i\beta m \Delta x \cos\phi \sin\theta} \tag{3.6}$$

From Equation 3.1 it can be seen that the steering matrix has the element patterns as a part of it. The steering vector that describes the phase of the signal at each antenna element relative to the center element phase is made up of the following elements [Kop5]:

$$a_n(\theta_j, \phi_j) = \hat{f}_n(\theta_j, \phi_j)c \tag{3.7}$$

where $c = ink_0 d \sin(\theta_j)\cos(\varphi_j)$ with θ as the elevation angle and φ as the azimuth angle. The subscript 'j' refers to the j-th emitter. 'n' refers to the element number. d gives the inter-element spacing in terms of λ, the wavelength. The element pattern for the dipole antenna element array is given as below [Kop5]:

$$\hat{f}_n(\theta_j, \phi_j) = -i\sqrt{\frac{3}{8\pi}} \sin\theta_j 2 \sum_{m=1}^{N} Y_{nm} e^g \tag{3.8}$$

where $g = i(m-n)k_0 d \sin(\theta_j)\cos(\varphi_j)$. At this point, it is worth mentioning that the ratio of the received signal available at the array output, z(t) or the array response with the signal Gs(t) measured at the reference element as a function of θ and φ is called the array factor. In other words, each antenna element can be taken to have its field, which when multiplied with the array factor gives the total E-field of the antenna array. Using pattern multiplication for arrays, the overall array factor is calculated. As shown by the equations above, this factor is taken to be a function of the number of elements on the

array, their geometrical arrangement, the excitation amplitude and phases of the elements, the relative patterns of the elements, and the inter-element spacing [Ban2].

From Equation 3.8, Y_{nm} represents the elements of the admittance matrix that is given by [Kop5]:

$$Y = \left(I + Z\right)^{-1} \tag{3.9}$$

For a single element antenna, the impedance is only dependent on its current distribution. However, in the presence of other elements, current distribution and radiated fields vary along with the impedance of the antenna. Therefore, the input impedance of an antenna depends on the self impedance and mutual impedance. In this case, self impedance is the impedance of the element without the presence of other elements. Mutual impedance, on the other hand, is the impedance between the driver element and other elements [Ban3]. The normalized mutual impedance matrix with Z_{nm} set to $1\,\Omega$ for the dipole antenna element array is given by the following [Kop5]:

$$Z_{nm} = 1 \text{ for n=m} \tag{3.10-a}$$

$$Z_{nm} = \left(\frac{3}{2}\right)\left\{i\left(\left|n-m\right|k_0 d\right)^{-1} + \left(\left|n-m\right|k_0 d\right)^{-2} - i\left(\left|n-m\right|k_0 d\right)^{-3}\right\} e^{\left(-ik_0 d\left|n-m\right|\right)} \text{ for n} \neq \text{m} \tag{3.10-b}$$

3.2 MUSIC Algorithm

The Multiple Signal Classification (MUSIC) [Sch1] algorithm is the most popular amongst its class of signal classification algorithms. It can estimate several parameters for a given source with extremely high resolution. It can be used to estimate the direction of arrival for emitters, the signal strengths, the cross-correlations, the noise power, the polarizations, etc [Lib2]. However, this comes at a cost of needing an array response to be calibrated and stored accurately. Furthermore, it requires a priori knowledge of the

spatial statistics of background noise and interferences [Swi1]. Another drawback of the algorithm is that the time consumed for the running of the algorithm is very high. This highlights its need for extensive hardware in practical set-ups for runs that would not allow calculation times greater than a few milliseconds. MUSIC also requires the incoming signals to be uncorrelated. This highlights the problem of the algorithm not functioning in conditions of multipath.

The array response and noise covariance are difficult parameters to estimate correctly in practice due to changes in certain surrounding conditions. Weather, environment, antenna location and temperature can bring a change in the response of the array [Swi1]. Also gain and phase errors can affect the overall response. Another error can be accounted for by taking into account the physical antenna element set-ups and the distances between them. For calibrated arrays of identically spaced and oriented elements, the array response resolution meets the condition for MUSIC to perform well. However, practically the array elements will not be equally spaced or oriented. Even the slightest change can bring a change in the response degrading the overall performance [Swi1].

To account for noise in the surrounding environment is a difficult process to satisfy. Furthermore, channel crosstalk, reverberation and several other sources can add to the changing environment for noise [Swi1]. These then add up to the received signal affecting the performance of the algorithm. The signal subspace methods that are applied assume that the power of each channel is equal and that the noise fields are independent with reference to channels. Assuming L emitters producing signals, with an N element array, we have N signals received that are combinations of the emitted signals. This is given by [Lib3]:

$$z = As + n \tag{3.11}$$

The MUSIC algorithm exploits the eigenstructure of the input covariance matrix by estimating the sample co-variance of the complex baseband outputs. It works on the covariance matrix that is given below [Lib3]:

$$R_{zz} = E[zz^H] = AE[ss^H]A^H + E[nn^H] \tag{3.12}$$

$$E[nn^H] = \sigma_n^2 I \tag{3.13}$$

$$E[ss^H] = R_{ss} \tag{3.14}$$

R_{ss} represents the covariance of the sources and σ_n^2 is the noise variance. Furthermore, R_{ss} is an LxL matrix. It is important to note that Equation 3.13 represents an assumption of uncorrelated noise between the antenna elements. There may be signal phase cancellations from particular directions, but that does not make the cross correlation zero. Furthermore, the correlation of noise should account for bandwidth and the elements being very close to each other in relation to the bandwidth. Therefore, this could be a highlighted problem with the way the algorithm has been used for this specific case. Using eigenvalue decomposition, the noise and signal subspace decompose giving the following [Kop5]:

$$R_{zz} = E\Lambda E^H = E_s \Lambda_s E_s^H + E_n \Lambda_n E_n^H \tag{3.15}$$

Λ represents the NxN diagonal matrix with eigenvalues. The two signal subspaces shown in the equation above are orthogonal to each other. The former represents the signal subspace and the latter represents the noise subspace. Their being orthogonal gives us an important relationship because the steering vectors containing the Directions-of-Arrival in the signal subspace [Lib2]. A search through the array vectors gives the arrival angles of the incoming signal as the projections of the signals onto the noise subspace gives us zero. From Equation 3.15, it can be seen that R_{zz} has eigenvalues $\lambda_1, ..., \lambda_N$. Taking the number of linearly statistically independent signals to be equal to *L*, the rank of R_{zz} will be *L* if $N \geq L$ [Was2]. Also, for implementation of the algorithm, *L* is estimated using a technique discussed later on. As the steering vectors are independent, the rank of *A* is *L* as well. Taking this into account, $AR_{ss}A^H$ is an NxN matrix with rank equal to *L*.

Accordingly, *N-L* of the eigenvalues of $AR_{ss}A^H$ are equal to zero for the null-space [Was2]. The *N-L* eigenvectors e_j required to construct the noise subspace are given below [Was3]:

$$A^H e_j = 0 \text{ for } j=L+1, L+2,...,N \tag{3.16}$$

$$E_n = [e_{L+1} \; e_{L+2} \ldots\ldots \; e_N] \tag{3.17}$$

The matrix shown above is an *Nx(N-L)* matrix as each vector has *N* rows. As the signal subspace steering vectors are orthogonal to the noise subspace eigenvectors, for angles corresponding to the Direction of Arrival (DOA) of the incoming signals, we have:

$$a^H(\Omega)E_n E_n^H a(\Omega) = 0 \tag{3.18}$$

$$P_{Music}(\Omega) = \frac{1}{a^H(\Omega)E_n E_n^H a(\Omega)} \tag{3.19}$$

Ideally, Equation 3.18 would give a 0 in the direction of the angle of arrival of the signal due to the signal sub-space being orthogonal to the defined noise sub-space. However, in practical scenarios, Equation 3.18 does not give an exact zero as the vectors cannot be completely orthogonal. Taking the reciprocal as shown in Equation 3.19, peaks are related to the DOA, Ω where $\cos\Omega_j = \cos\phi_j \sin\theta_j$.

The *L* factor can be estimated using a number of methods of which the most prominent are Akaike's Information Criterion, the Minimum Description Length Criterion, and the Singular Value Decomposition Method [Camp1]. For simulations, the latter has been used by taking into account the first *L* singular values that lie above a certain threshold called the noise floor. This is shown below where ε is the threshold value [Kop5]:

$$\hat{L} = \arg_L \min\left\{ \frac{\sum_{i=1}^{L} \sigma_i^2}{\sum_{i=1}^{N} \sigma_i^2} > \varepsilon \right\} \tag{3.20}$$

3.3 Angle of Arrival Estimation using MUSIC

The major disadvantage of this algorithm is the time it takes to find the direction of incoming signals. This is because it searches through the angle domain with a run of the algorithm for each point. Furthermore, the performance of MUSIC depends on the accuracy of the measured radiation patterns. In theory, the radiation patterns can be calculated at any required resolution to be used in the denominator of Equation 3.19. However, in practical scenarios measurements of these patterns is only possible to a certain level. Also, there is always an uncertainty in the measurements of the magnitude and phase of the element patterns. For these simulations, only the theoretical case has been considered.

Figures 3.2-3.4 show the accuracy of the MUSIC spectrum for simple cases of an emitter being located at a distance of 1000m with parameters given in Table 3.1. It should be noted that although the gain for dipole elements is approximately 2dB, taking 0dB gives us a change in reference only. This is due to the variation in results not dependent on different gains considered.

N = 4	**d =** $\lambda / 2$
Directional gain of the emitter, G = 1	**Local oscillator freq.,** $f_0 = 1.875 \times 10^9$ **Hz**
Bit duration, $T_b = 1 \times 10^{-4}$ **s**	**Number of pulses,** N_p **= 1000**
Modulation type = QPSK	**Antenna type = Half-wave dipole antenna**
$\theta = 90^0$	**Power of emitter, P = 0.1W**
Sampling frequency, $f_s = 2 \times 10^5$ **Hz**	**Noise factor, NF = 10.0 dB**
SNR = 40 dB	$\phi = 120^0$

Table 3.1: Parameters for simulations using MUSIC

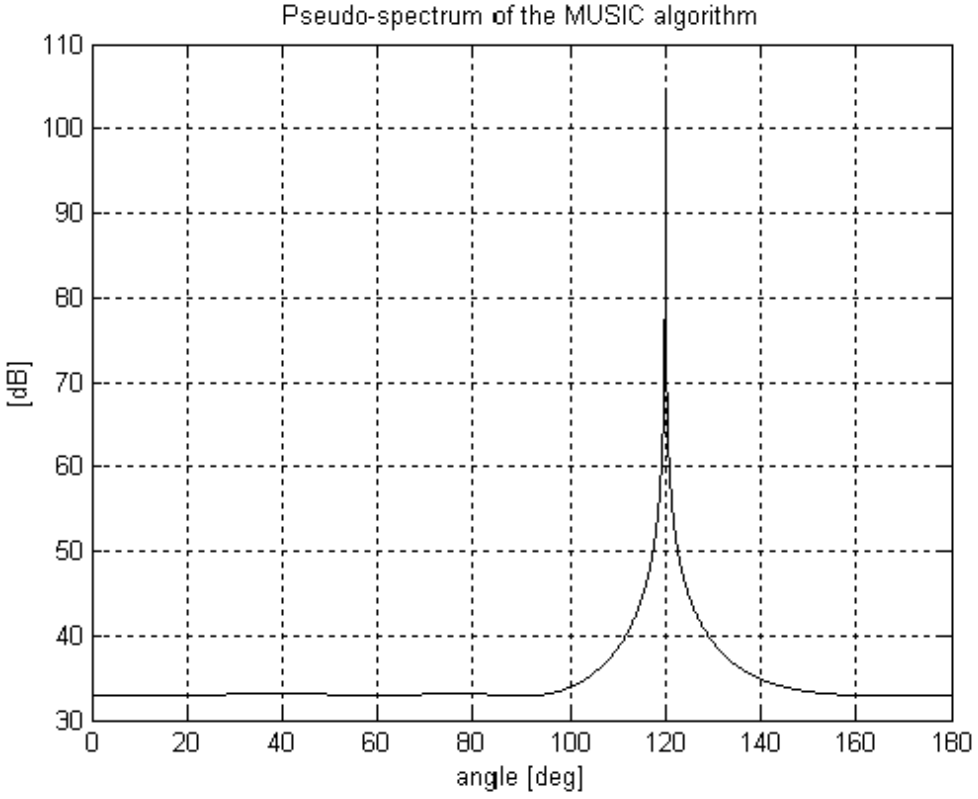

Figure 3.2: Angular position estimation using MUSIC with 0.01^0 search resolution

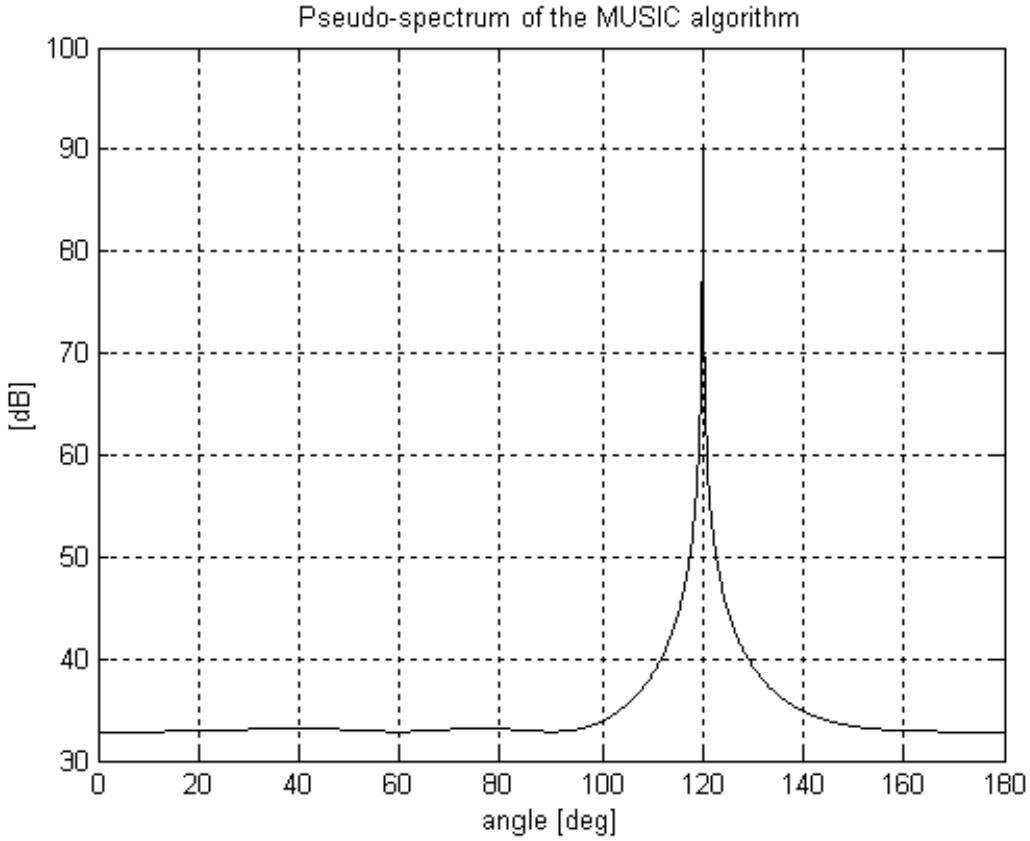

Figure 3.3: Angular position estimation using MUSIC with 0.1^0 search resolution

Almost similar spectrums are obtained for both arrays. The angle to array A is $\phi_a = 119.97^0$. From Figure 3.3, the estimated angle for array A using MUSIC is 120^0. On the other hand, the angle to array B is $\phi_b = 120.02^0$ and the estimated angle for array B using MUSIC is 120^0. It should be noted that due to the resolution, the estimated angles are the same.

For 2 emitters $\phi_1 = 120^0$ and $\phi_2 = 150^0$. The SNR used for this case is 53 dB. Also, the search resolution used is 0.01^0. This is shown in Figure 3.4.

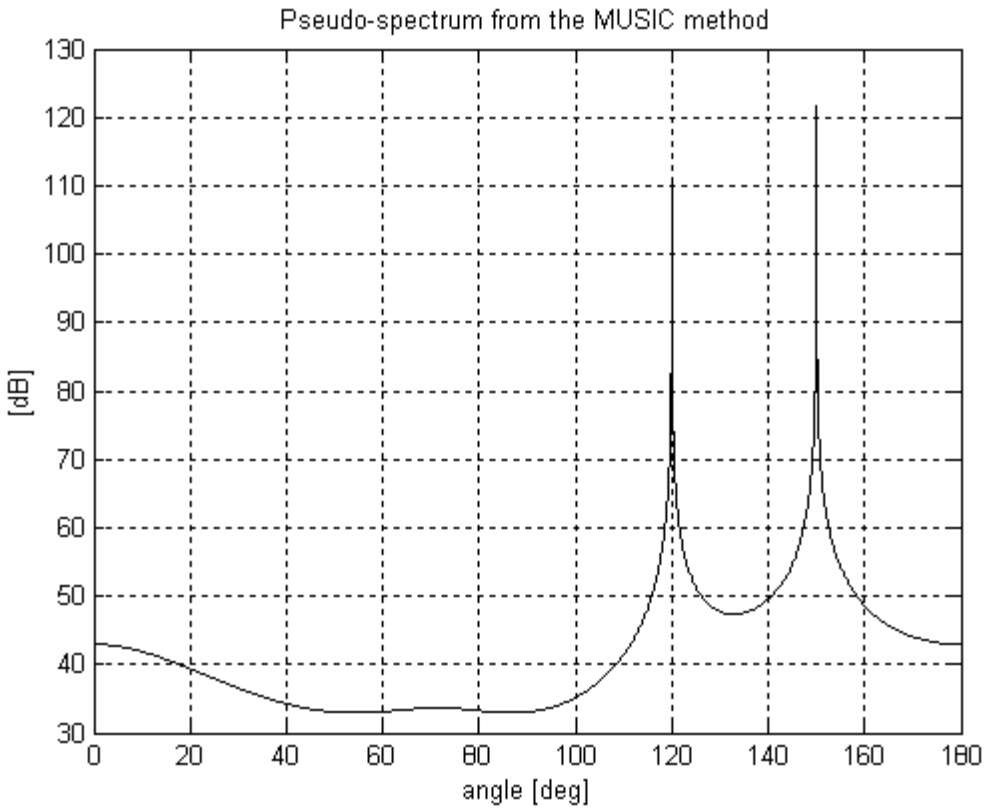

Figure 3.4: Angular position estimation for 2 emitters using MUSIC with 0.01^0 search resolution

Array-A calculates the positions of the two emitters as:

$\phi_{1a} = 119.9752^0$; $\phi_{2a} = 149.9821^0$

Array-B calculates the positions of the two emitters as:

$\phi_{1b} = 120.0248^0$; $\phi_{2b} = 150.0179^0$

MUSIC's implementation on Array-A estimates the following angles:

$\phi_{1a(MUSIC)} = 119.9800^0$; $\phi_{2a(MUSIC)} = 149.9800^0$

MUSIC's implementation on Array-B estimates the following angles:

$\phi_{1b(MUSIC)} = 120.0200^0$; $\phi_{2b(MUSIC)} = 150.0200^0$

The higher SNR value used for the 2 emitter case makes the performance comparable to the single emitter case.

The angles calculated above are for the theoretical case with no errors due to the physical set-up. Later on, it shall be shown that even the slightest introduction of errors into the system brings drastic changes to the angles estimated.

3.4 Mutual Coupling and Decoupling

Before going into the explanation of the Modified Root Pisarenko (MRP) algorithm, it is important to explain what coupling and decoupling in an antenna array means. Also, this section will explain the steps taken to counteract this effect in order to get equalized radiation patterns. This, as mentioned before, is useful for the performance of the MRP algorithm.

3.4.1 Mutual Coupling

Mutual coupling occurs due to the influence of antenna elements over each other due to the interaction of energy between them. The element radiation patterns, relative separation, and orientation of the elements are some of the factors that influence the degree of coupling involved in an antenna array [Ban3]. To make this clear, the example of a plane wave incident on an array is taken. Taking the case of element 1, the plane wave induces a current in it. However, some of the energy of the wave is reflected back into space so that it is incident on the other elements. Therefore, the resultant energy incident on the other element is a vector sum of the incident wave's energy and the parasitic energy present due to coupling. Also, the terminating impedances of the antenna elements affect mutual coupling as it influences the re-radiated energy [Ban3]. Thus, to reduce the effects of coupling, terminating impedances can be optimized. Furthermore, the mutual coupling model used does not tackle the varying currents in the antenna elements. Adding extra passive elements in the form of an extended array reduces this variation giving better results.

3.4.2 Decoupling

Equation 3.10 gives the theoretical mutual impedance matrix. However, in practical scenarios this has to be based on measurements of the scattering matrix *S* of the antenna array and on the downconverter reflection matrix. The scattering matrix is used as shown below [Kop5]:

$$Z = R_g (I + S)(I - S)^{-1} \tag{3.21}$$

where R_g is the internal impedance of the voltage generator and I denotes the identity matrix. Using this, the decoupling matrix *P* that has to be applied to the baseband array response signal is [Kop5]:

$$P = \left(Z + R_g I\right)\left(Z_{Diagonol} + R_g I\right)^{-1} \tag{3.22}$$

where Z is the impedance matrix, $Z_{Diagonol}$ represents the self-impedances, R_g is the internal impedance of the voltage generator and I denotes the identity matrix. Equation 3.22 assumes equal length for all antenna elements. As shown earlier, the steering vector for a linear array is given as [Kop4]:

$$a(\theta,\phi) = -\frac{i}{\sqrt{\zeta_0}}[\hat{f_1}(\theta,\phi)\ \hat{f_2}(\theta,\phi)e^{ik_0 d\xi}\ \hat{f_3}(\theta,\phi)e^{ik_0 2d\xi} \ldots \hat{f_N}(\theta,\phi)e^{ik_0(N-1)d\xi}]^T \tag{3.23}$$

where $\xi_j = \sin(\theta_j)\cos(\varphi_j)$, ζ_0 is the characteristic impedance of free space with a value of $377\,\Omega$, and $\hat{f_N}(\theta,\phi)$ is the radiation pattern of the N-th element with terminated circuit conditions. It should be noted that these patterns are not isotropic as there is coupling in the array [Kop3]. By applying the decoupling transformation, as given by as Equation 3.22 to the baseband signal, a uniformly weighted steering vector is formed as given below [Kop4]:

$$a(\theta,\phi) = -\frac{i}{\sqrt{\zeta_0}} \hat{f}^0(\theta,\phi)[1 \;\; e^{ik_0 d\xi} \;\; e^{ik_0 2d\xi} \;\; e^{ik_0 3d\xi} \;\ldots\ldots\; e^{ik_0 (N-1)d\xi}]^T \qquad (3.24)$$

where $\hat{f}^0(\theta,\phi)$ is a factor that gives the isolated radiation pattern of the antenna elements with open circuit conditions [Kop3]. Mathematically, $\hat{f}_n(\theta,\phi)$ can be written as the following [Kop4]:

$$\hat{f}_n(\theta,\phi) = \sum_{m=1}^{N} e^{-ik_0 d(n-1)\xi} (Z_{mn} + Z_{gm}) R_{gm}^{-1/2} Y_{mn} R_{gn}^{1/2} e^{-ik_0 d(m-1)\xi} \hat{f}^0(\theta,\phi) \qquad (3.25)$$

In the above equation, we have the Q_{nm} factor which is equal to $(Z_{mn} + Z_{gm}) R_{gm}^{-1/2} Y_{mn} R_{gn}^{1/2}$. This factor is present due to the mutual coupling in the array and has the following:

Z_{mn} = array impedance matrix

Z_{gm} = internal impedance of m-th antenna element

R_{gm} = Re (internal impedance of m-th element)

R_{gn} = Re (internal impedance of n-th element)

The baseband response of the n-th antenna element is given as [Kop4]:

$$z_n(t) = -\frac{i\lambda}{\sqrt{\zeta_0}} \sum_{l=1}^{L} \hat{f}_n(\theta_l,\phi_l) e^{i(n-1)k_0 d\xi_l} s_l(t) + v_n(t) \qquad (3.26)$$

Substituting Equation 3.25 into Equation 3.26, we have [Kop4]:

$$z_n(t) = -\frac{i\lambda}{\sqrt{\zeta_0}} \sum_{l=1}^{L} \sum_{m=1}^{N} e^{-ik_0 d(n-1)\xi} Q_{nm} e^{-ik_0 d(m-1)\xi} \hat{f}^0(\theta_l,\phi_l) e^{ik_0 d(n-1)\xi} s_l(t) + v_n(t) \qquad (3.27)$$

Exponential cancellation gives [Kop4]:

$$z_n(t) = -\frac{i\lambda}{\sqrt{\zeta_0}} \sum_{l=1}^{L} \sum_{m=1}^{N} Q_{nm} e^{ik_0 d(m-1)\xi} \hat{f}^0(\theta_l, \phi_l) s_l(t) + v_n(t) \tag{3.28}$$

Applying the decoupling transform P_{nm} on the baseband response in Equation 3.28, we have cancellation of P_{nm} and Q_{nm} [Kop4]:

$$z_n(t) = -\frac{i\lambda}{\sqrt{\zeta_0}} \sum_{l=1}^{L} e^{ik_0 d(m-1)\xi} \hat{f}^0(\theta_l, \phi_l) s_l(t) + \sum_{n=1}^{N} P_{jn} v_n(t) \tag{3.29}$$

As seen from above, decoupling has been obtained as the patterns are now represented by a factor of the isolated antenna element pattern. Modified Root Pisarenko requires equalized radiation patterns for good performance. As mutual coupling has an effect on the patterns, decoupling allows for it to be used for the practical scenario.

3.5 Equalization of Element Radiation Patterns

For this project, equalized radiation patterns were required as MRP was being used to pin-point emitters in the environment. For infinite arrays, the element patterns are equal [Kop2]. To simulate a similar case for practical purposes, a ten element array was used for each of the two arrays. This is shown in the figure below:

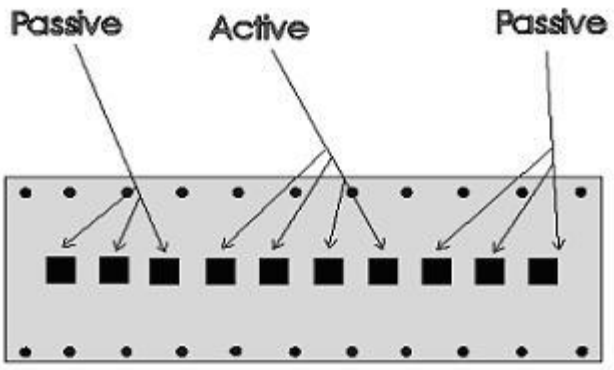

Figure 3.5: Passive elements introduced in array to equalize element patterns

The extra passive elements that are terminated in 50-ohm impedances have the effect of equalizing the radiation patterns for the center active elements. As mentioned earlier, to optimize further equalization of the patterns could have been achieved by optimizing the terminating impedances of the ten elements. However, this was not done for the project [Kop2]. In the analysis, presented in this thesis, dipole elements are assumed.

3.6 Modified Root Pisarenko Algorithm

The second algorithm used for this study is the Modified Root Pisarenko (MRP) algorithm. MRP was developed so that the computational complexity of Modified Pisarenko could be avoided. This is done by using the classical array factor where the mutual coupling effects are cancelled so that the steering vector is uniformly weighted [Was2]. This vector is given as [Was3]:

$$a(\Omega) = \{ e^{ik\Psi} \quad e^{i(k+1)\Psi} \quad e^{i(k+2)\Psi} \ldots\ldots\ldots e^{iN\Psi} \} \tag{3.30}$$

$$= e^{ik\Psi} \{1 \quad e^{i\Psi} \quad e^{i2\Psi} \ldots\ldots\ldots e^{iL\Psi} \} \tag{3.31}$$

where $\Psi = k_0 D\xi$ and $\xi_j = \sin\theta_j \cos\phi_j$. The spectrum for Modified Pisarenko is given by [Was3]:

$$S_{MP}(\Omega) = \frac{1}{\sum_{k=1}^{N-L} a_k^H(\Omega) h_k h_k^H a_k(\Omega)} \tag{3.32}$$

Using the steering vector derived in Equation 3.30 together with the denominator of Equation 3.32, the spectrum of the MRP method is [Kop5]:

$$\Lambda(\Omega) = \sum_{n=1}^{L+1} \sum_{m=1}^{L+1} e^{i(m-n)} H_{nm} \tag{3.33}$$

with H forming an $(L+1)$x$(L+1)$ matrix. This Hermitian matrix is given by [Kop5]:

$$H = \sum_{k=1}^{L+1} h_k h_k^H \tag{3.34}$$

In the equation above, h_k is an $L+1$ vector that is derived using the rank properties of a matrix formed from the sample covariance matrix and the null subspace. Substituting $z = e^{i\Omega}$ into Equation 3.34, we have [Kop5]:

$$\Lambda = z^{-L} P_{2L}(z) \tag{3.35}$$

where $P_{2L}(z)$ is a polynomial that can be referred to from [Kop5]:

$$P_{2N-2}(z) = \sum_{j=1-N}^{N-1} \alpha_j z^{j+N-1} \tag{3.36}$$

Using $2L = 2N - 2$, we have [Kop5]:

$$P_{2L}(z) = \sum_{j=-L}^{L} \beta_j z^{j+L} \tag{3.37}$$

Therefore, for the case of a single emitter, we will have two roots. Furthermore, these roots are computed to give the Direction-of-Arrival angles [Kop5]:

$$\Omega_j = \frac{1}{k_0 d} angle(z_j) \text{ for } j = 1,2,.....,L \tag{3.38}$$

3.7 Angle of Arrival Estimation using Modified Root Pisarenko

The method of equalization using an infinite array model for radiation patterns has not been used for these simulations. Figures 3.6-3.8 show the accuracy of the Modified Root Pisarenko (MRP) spectrum for simple cases of an emitter being located at a distance of 1000m with specifications given in Table 3.2. It should be noted that although the gain for dipole elements is approximately 2dB, taking 0dB gives us a change in reference only. This is due to the variation in results not dependent on different gains considered.

N = 4	**d** $= \lambda / 2$
Directional gain of the emitter, G = 1	**Local oscillator freq.,** $f_0 = 1.875 \times 10^9$ **Hz**
Bit duration, $T_b = 1 \times 10^{-4}$ **s**	**Number of pulses,** N_p **= 1000**
Modulation type = QPSK	**Antenna type = Half-wave dipole antenna**
$\theta = 90^0$ **Sampling frequency,** $f_s = 2 \times 10^5$ **Hz**	**Power of emitter, P = 0.1W** **Noise factor, NF = 10.0 dB**
SNR = 40 dB	$\phi = 120^0$

Table 3.2: Parameters for simulations using MRP

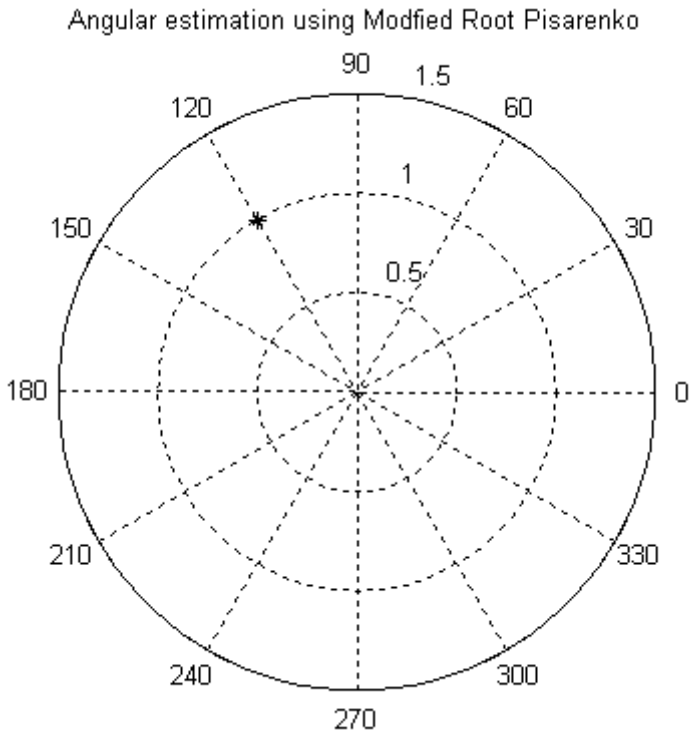

Figure 3.6: Angular position estimation using MRP without coupling

From Figure 3.6 we have:

Array-A calculates the position of the emitter as:

$\phi_{1a} = 119.9752^0$

Array-B calculates the position of the emitter as:

$\phi_{1b} = 120.0248^0$

MRP's implementation on Array-A estimates the following angle:

$\phi_{1a(MRP)} = 119.9746^0$

MRP's implementation on Array-B estimates the following angle:

$\phi_{1b(MRP)} = 120.0256^0$

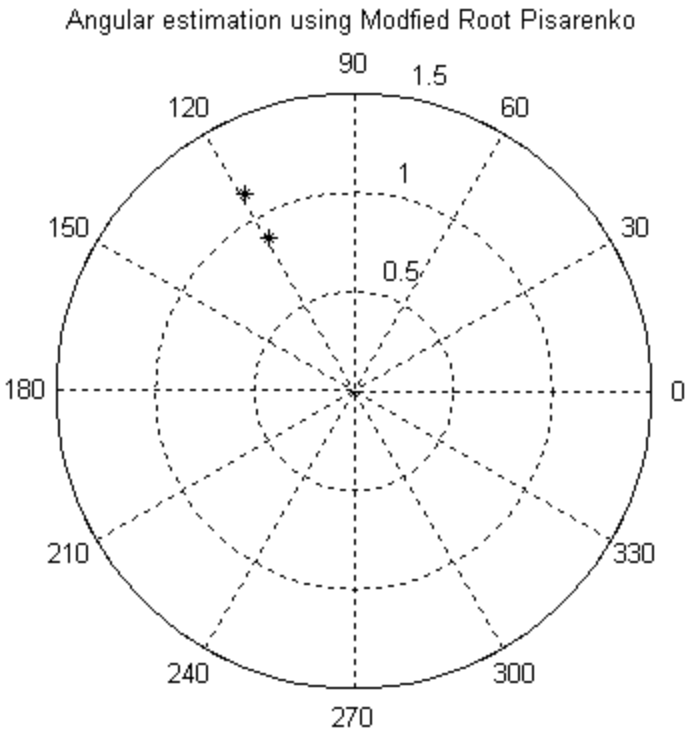

Figure 3.7: Angular position estimation using MRP with coupling

From Figure 3.7 we have:

Array-A calculates the position of the emitter as:

$\phi_{1a} = 119.9752^0$

Array-B calculates the position of the emitter as:

$\phi_{1b} = 120.0248^0$

MRP's implementation on Array-A estimates the following angle:

$\phi_{1a(MRP)} = 119.1215^0$

MRP's implementation on Array-B estimates the following angle:

$\phi_{1b(MRP)} = 119.1649^0$

In comparison to the case without any coupling, this has greater error. This is because the algorithm assumes the array is decoupled, as explained earlier.

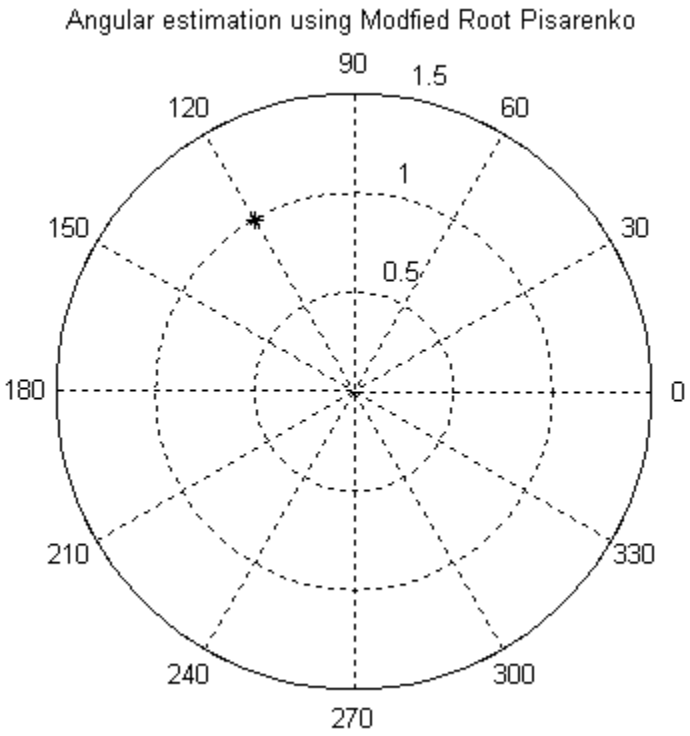

Figure 3.8: Angular position estimation using MRP with coupling and decoupling

From Figure 3.8 we have:

Array-A calculates the position of the emitter as:

$\phi_{1a} = 119.9752^0$

Array-B calculates the position of the emitter as:

$\phi_{1b} = 120.0248^0$

MRP's implementation on Array-A estimates the following angle:

$\phi_{1a(MRP)} = 119.9770^0$

MRP's implementation on Array-B estimates the following angle:

$\phi_{1b(MRP)} = 120.0246^0$

3.8 Range Estimation

The algorithm used for range estimation is based on the angles of the signals at the two arrays. Also, the angles are estimated using the Modified Root Pisarenko algorithm. Equation 3.39 relates the estimated range to the different estimated angles of arrival by the two arrays [Was4]:

$$R = D * \sqrt{\frac{1}{4} + \frac{\sin\theta_a \sin\theta_b \cos(\theta_a - \theta_b)}{\sin^2(\theta_b - \theta_a)}} \tag{3.39}$$

The derivation of Equation 3.39 is given in Appendix A. The parameters θ_a and θ_b are the estimated angles of arrival of the received signals with respect to antenna array A and B with distance D between their mid-points. R is the distance of the source from the center of the array. An important point to take note of is that with increasing distance from the antenna array, the dependence of the algorithm accuracy increases on the slightest of phase errors. This can be proven mathematically or statistically by varying the numerator.

For the 4-element array with d $= \frac{\lambda}{2}$, $\theta = 90^0$, and $\phi = 120^0$ a number of simulations were run using both MUSIC and MRP. A summary of the results from MUSIC are given below to show the effect of increasing emitter distance on the range estimation.

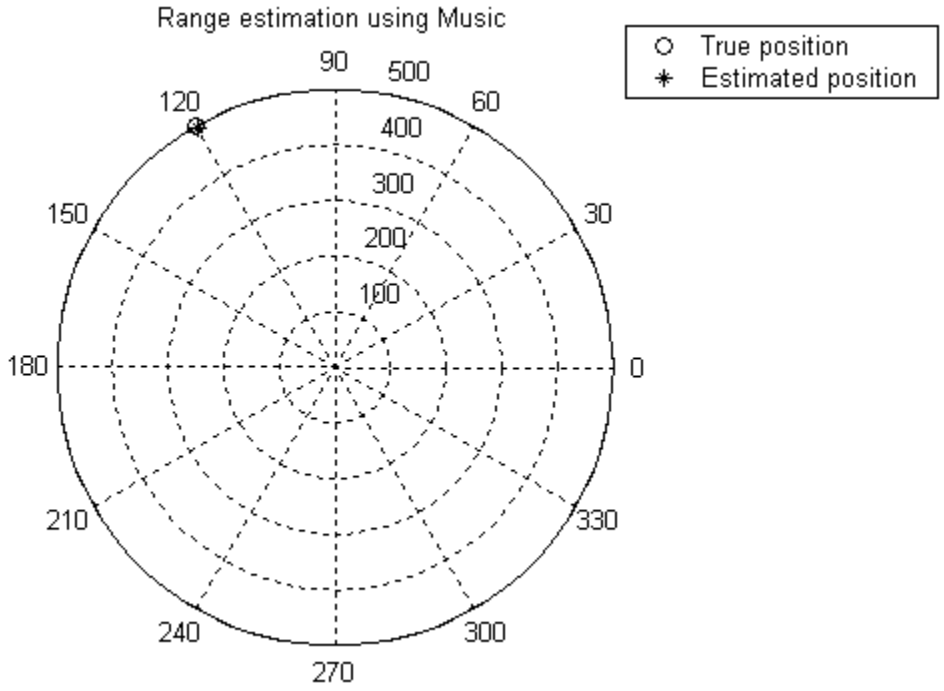

Figure 3.9: Range estimation using MUSIC for r = 500m

For the case shown in Figure 3.9, the estimated range is 496.1959m. Relative error is the fraction of the difference between estimated and real range with respect to the real range. This is -0.0076. At this point, it is important to mention that the relative error cannot be less than -1. $\phi_a = 119.9504^0$ and $\phi_b = 120.0500^0$ give the estimated angles for the two arrays.

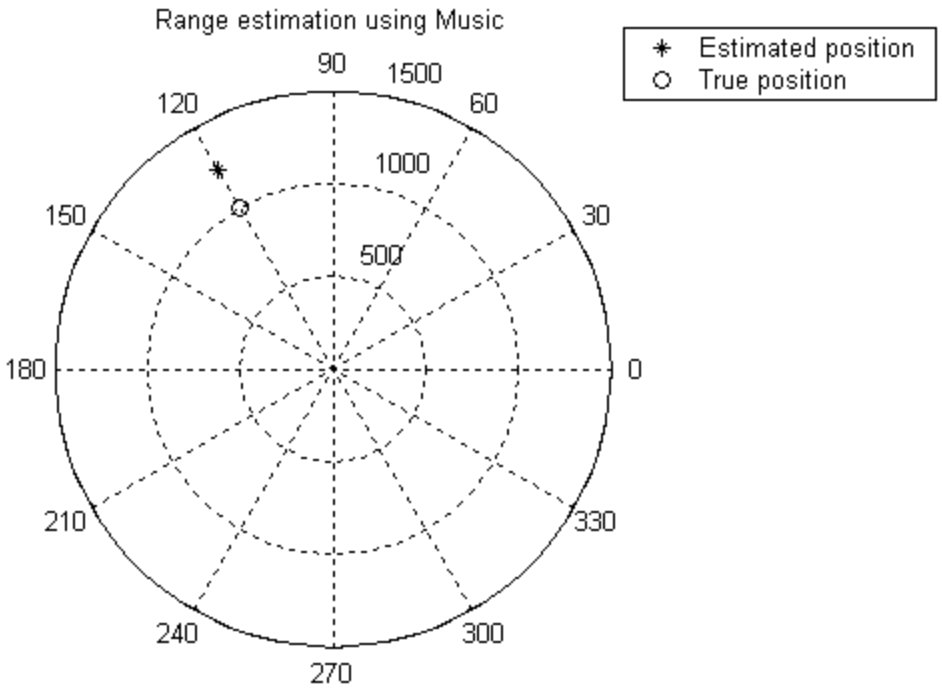

Figure 3.10: Range estimation using MUSIC for r = 1000m

In Figure 3.10, the range estimated is 1240.5 m. This gives us a relative error of 0.2405.

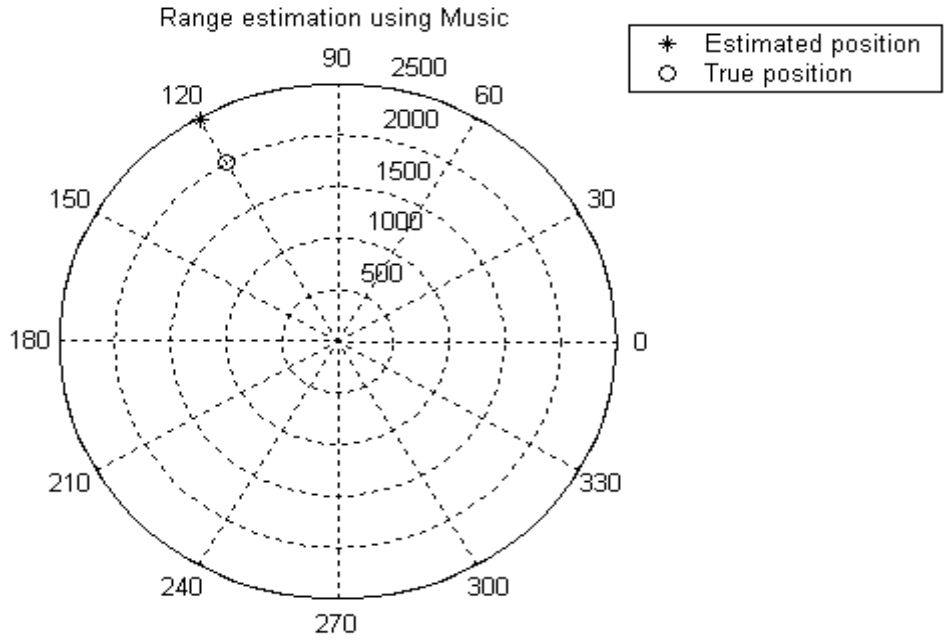

Figure 3.11: Range estimation using MUSIC for r = 2000m

In Figure 3.11, the estimated range is 2481m. Therefore, the relative error is 0.2405. ϕ_a = 119.9900^0 and ϕ_b = 120.0100^0 are the estimated angles for the two arrays.

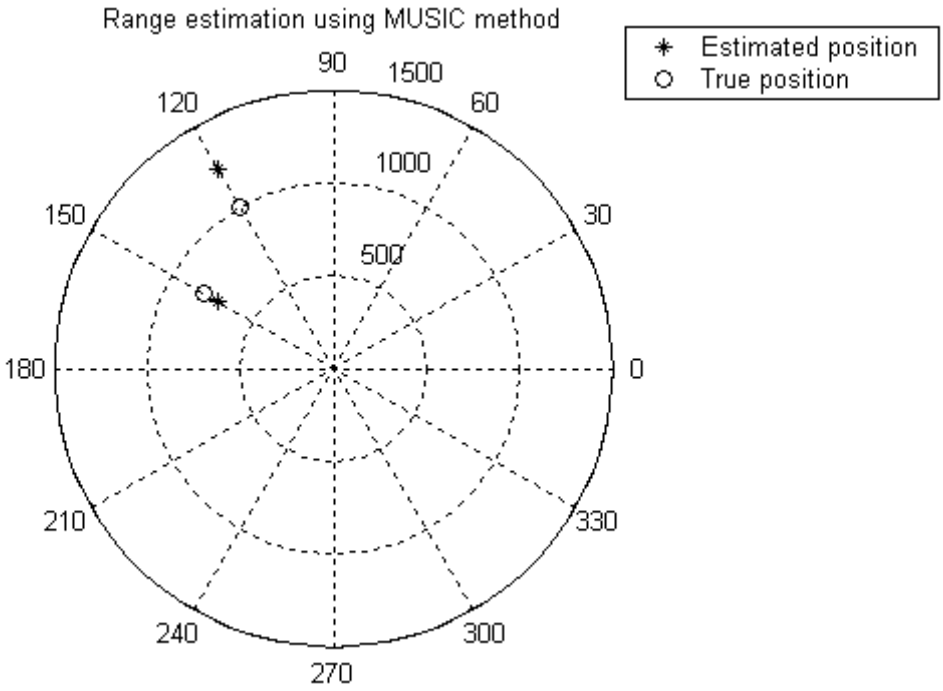

Figure 3.12: Range estimation using MUSIC for r_1 = 1000m and r_2 =800m

In Figure 3.12, the estimated ranges are $r_{1(MUSIC)}$ = 1240.5m and $r_{2(MUSIC)}$ = 716.2m. Therefore, the relative errors are 0.2405 and -0.2838, respectively. It should be seen that the farther the emitter is moved from the array, the greater the effect of even the slightest error in estimated angle. This can only be then improved by increasing the resolution. However, for large ranges this does not remain practical. The following plots show the error in estimated range using MRP.

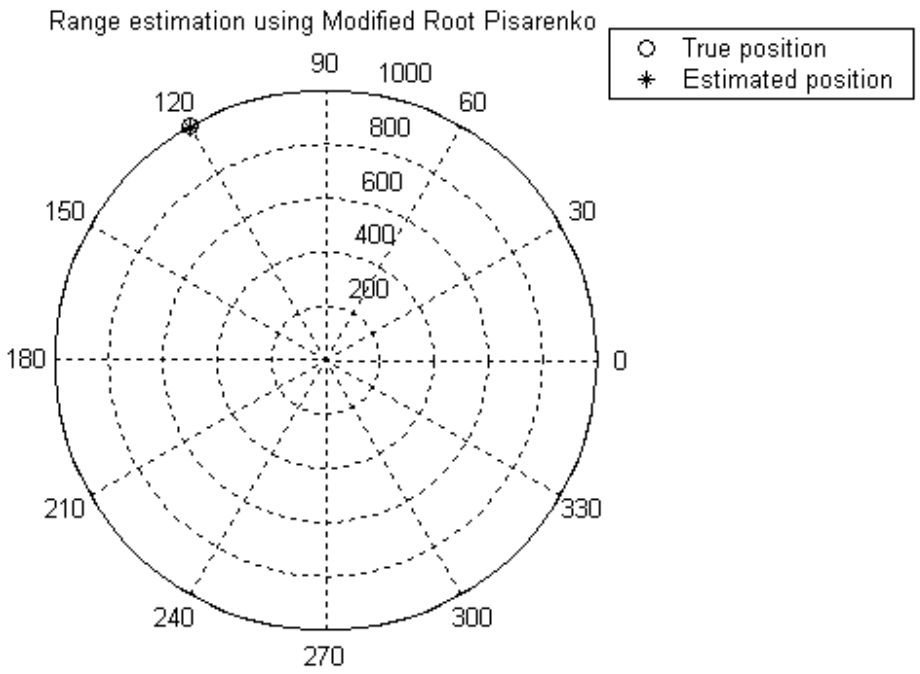

Figure 3.13: Range estimation using MRP for r = 1000m without coupling

In Figure 3.13, the estimated range is 993.6481m. Therefore, the relative error is -0.0064. $\phi_a = 119.9755^0$ and $\phi_b = 120.0255^0$ are the estimated angles for the two arrays.

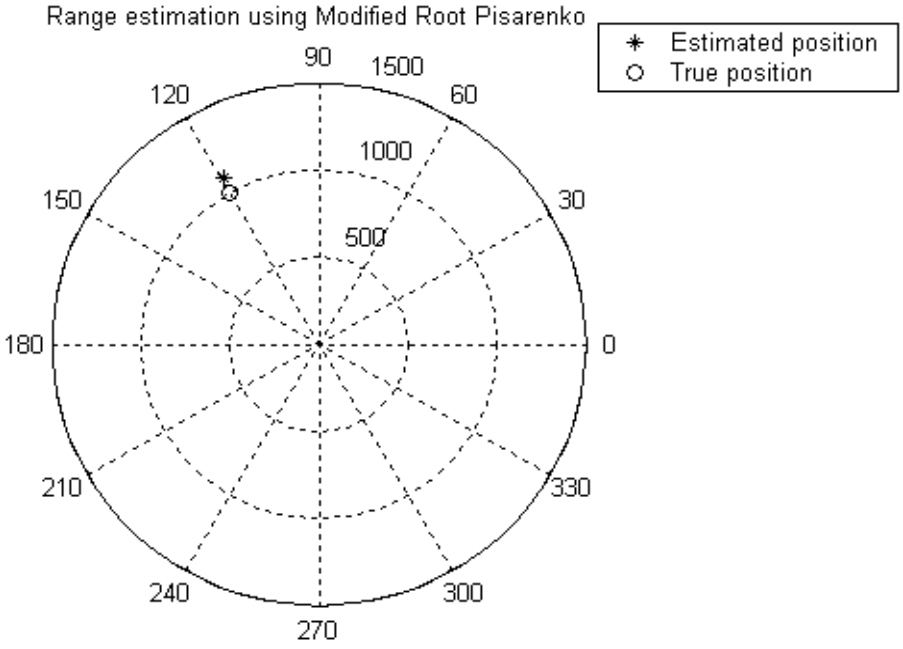

Figure 3.14: Range estimation using MRP for r = 1000m with coupling

In Figure 3.14, the estimated range is 1098.8m. Therefore, the relative error is 0.0988. $\phi_a = 119.1206^0$ and $\phi_b = 119.1662^0$ are the estimated angles for the two arrays.

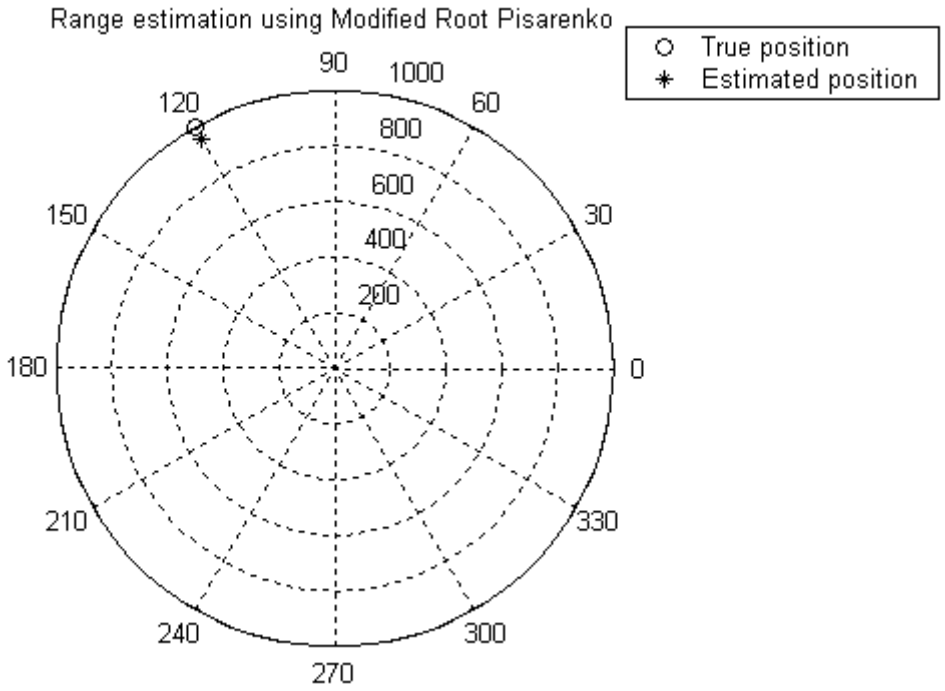

Figure 3.15: Range estimation using MRP for r = 1000m with coupling and decoupling

In Figure 3.15, the estimated range is 950.3650m. Therefore, the relative error is -0.0496. $\phi_a = 119.9743^0$ and $\phi_b = 120.0265^0$ are the estimated angles for the two arrays. This shows that the performance of MRP is much better with the decoupled array, as expected.

Chapter 4
Error Analysis Using MUSIC

This chapter covers results for the error analysis using MUSIC as the Direction-finding Algorithm. The first section gives a block diagram of the signal path. This is used to explain the sequence of errors introduced. Following the block diagram, the section describes errors such as transmission line length differences, phase shifter changes, amplitude changes to the signal, and mismatches used to check the sensitivity of the range estimation algorithm. The second section gives plots representing Monte Carlo simulations run for relative errors in estimated ranges and angles of arrival. Also, the effect of antenna elements on the range estimation is checked by increasing and decreasing the elements to 8 and 2, respectively. The third section gives tolerance tables for the analysis involving MUSIC. The results given in this section can be used as a bound for certain conditions in which the antenna is to be used.

4.1 Description of Error Analysis

Without any random errors introduced, results for a specified emitter range and angle of arrival using MUSIC are the same. On the other hand, even small random errors highlight the dependence of the range algorithm on the accuracy of the estimated angles of arrival for the two arrays. The range estimation algorithm is given by Equation 3.40.

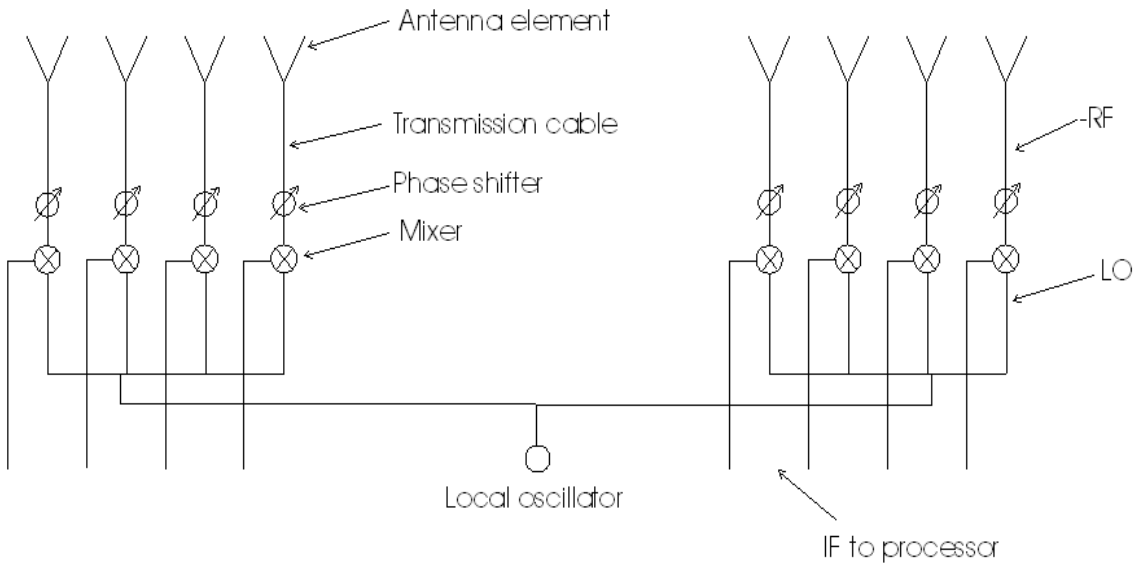

Figure 4.1: Block diagram of array components

Antenna elements are connected to phase shifters via transmission cables. These cables form an input to the mixer at radio frequency in the range of 1.9-2 GHz. The second input to the mixer comes from the local oscillator. The local oscillator's output is used with the incoming signal to produce sum or difference tones. For the purpose of the error analysis, phase shifters are inserted in the path of the RF signal to equalize the signal phase for all antenna elements when the signal is incident in the broadside direction.

The following sub-sections explain errors introduced into the system code.

4.1.1 Transmission line change

The errors in transmission line lengths take the different cables into consideration. Figure 4.1 shows the block diagram of the array components as used in the error analysis.

These cable connections are given in order below:

1) Antenna elements to phase shifter

2) Phase shifter to mixer
3) LO to two-way divider
4) Four-way power divider to mixer

Although each of the 8 cables leading from the array elements is supposed to be of the same length, differences arise due to the cutting of cables, screwing of cables to components, etc. Even the slightest differences in cable lengths can bring phase differences between the eight signals which then affect the over-all performance. The error analysis is based on 3 ranges within which the cable length may vary:

1) $\pm 1mm$
2) $\pm 2mm$
3) $\pm 3mm$

Each error generated is introduced in terms of a random phase shift given by:

$$\Delta\phi = \frac{2\pi}{\lambda}\Delta L \tag{4.1}$$

ΔL refers to the difference in transmission line lengths which implies a change in the array response with the introduction of a phase shift. It can be seen from Equation 4.1 that the introduced error is related to the wavelength of the incoming signal wave. Therefore, for higher frequencies, the random phase shifts increase.

Table 4.1 is a list of simulation cases that were run for changes in transmission line length changes for different ranges (r), azimuth angles (ϕ), elevation angles (θ), and cable length differences (ΔL).

r (m)	Azimuth (ϕ)	Elevation (θ)	ΔL
15	120	90	$\pm 1mm$
15	120	90	$\pm 2mm$
15	120	90	$\pm 3mm$
20	120	90	$\pm 1mm$
20	120	90	$\pm 2mm$
20	120	90	$\pm 3mm$
35	120	90	$\pm 1mm$
35	120	90	$\pm 2mm$
35	120	90	$\pm 3mm$
50	120	90	$\pm 1mm$
50	120	90	$\pm 2mm$
50	120	90	$\pm 3mm$

Table 4.1: Error analysis data points for ΔL

4.1.2 Phase shifter error

Phase shifters are used to tune in the received frequencies from the different antenna elements to one frequency. Taking practical limitations into account, errors are introduced within a certain tolerance as the phase shifter settings are dependent upon physical tuning using a knob.

The error introduced in the analysis has 3 random ranges within which it may vary:

1) $\pm 0.5^{\circ}$

2) $\pm 1^{\circ}$

3) $\pm 3^{\circ}$

The phase error in the signal ($\Delta\phi$) due to the phase shifter error is simply:

$$\Delta\phi = \Delta P \tag{4.2}$$

where ΔP is the phase shifter error. This phase error is related to the equivalent transmission line length change by the power of the exponential as shown:

$$\Delta L = \frac{\lambda}{2\pi}\Delta P \tag{4.3}$$

It is important to note that at $f_0 = 1.875\times10^9\,Hz$ and $c = 3\times10^8\,m/s$. This gives $\lambda = \frac{c}{f_0} = \frac{3\times10^8}{1.875\times10^9} = 0.16m$. Furthermore, $\frac{2\pi}{\lambda} = 39.27$ so that $\Delta L = \frac{\Delta P}{39.27}$. Using this relationship it is shown that:

1) $\Delta P \Rightarrow \pm3^\circ$ corresponds to $\Delta L \Rightarrow \pm0.0013m$
2) $\Delta P \Rightarrow \pm1^\circ$ corresponds to $\Delta L \Rightarrow \pm4.4563\times10^{-4}\,m$
3) $\Delta P \Rightarrow \pm0.5^\circ$ corresponds to $\Delta L \Rightarrow \pm2.2282\times10^{-4}\,m$

The phase changes vary between the given ranges. Also, they are randomly distributed into each array element. Therefore, the phase shifter errors correspond to a magnified version of the transmission line length errors. Furthermore, the introduced error is related to the wavelength of the incoming signal wave. Therefore, for higher frequencies, the random phase shifts increase. The following simulations were run for changes in phase shifter errors:

r (m)	Azimuth (ϕ)	Elevation (θ)	ΔP
15	120	90	$\pm 0.5^0$
15	120	90	$\pm 1^0$
15	120	90	$\pm 3^0$
20	120	90	$\pm 0.5^0$
20	120	90	$\pm 1^0$
20	120	90	$\pm 3^0$

35	120	90	$\pm 0.5^0$
35	120	90	$\pm 1^0$
35	120	90	$\pm 3^0$
50	120	90	$\pm 0.5^0$
50	120	90	$\pm 1^0$
50	120	90	$\pm 3^0$

Table 4.2: Error analysis data points for ΔP

4.1.3 Antenna Mismatch

In a mismatched antenna system, the available power is determined by the degree of mismatch between the antenna elements and the transmission lines. This mismatch is a function of the impedance of the lines and the antenna input impedance and is given below:

$$\frac{P_{reflected}}{P_{incident}} = |\Gamma|^2 = \left|\frac{VSWR-1}{VSWR+1}\right|^2 \tag{4.4}$$

where

Γ = the voltage reflection co-efficient at the antenna input terminals

VSWR = voltage standing wave ratio at the antenna input terminals

The reflection coefficient Γ (S_{11} in the *S*-parameters) can be taken to lie randomly within the following ranges:

1) $\Gamma = 0 \Leftrightarrow 0.05$
2) $\Gamma = 0 \Leftrightarrow 0.1$
3) $\Gamma = 0 \Leftrightarrow 0.2$

Mathematically, this is given by:

$$\Delta Error = \sqrt{1 - |\Gamma|^2} \tag{4.5}$$

The square root indicates analysis on voltage parameters. The following simulations were run to analyze the effect on the overall performance due to antenna mismatch:

r (m)	Azimuth (ϕ)	Elevation (θ)	Γ
15	120	90	$0 \Leftrightarrow 0.05$
15	120	90	$0 \Leftrightarrow 0.1$
15	120	90	$0 \Leftrightarrow 0.2$
20	120	90	$0 \Leftrightarrow 0.05$
20	120	90	$0 \Leftrightarrow 0.1$
20	120	90	$0 \Leftrightarrow 0.2$
35	120	90	$0 \Leftrightarrow 0.05$
35	120	90	$0 \Leftrightarrow 0.1$
35	120	90	$0 \Leftrightarrow 0.2$
50	120	90	$0 \Leftrightarrow 0.05$
50	120	90	$0 \Leftrightarrow 0.1$
50	120	90	$0 \Leftrightarrow 0.2$

Table 4.3: Error analysis data points for the antenna mismatch factor

4.1.4 IF Mismatch

This section describes the errors due to the mixer mismatch at the IF port. The VSWR values at the IF port depend on the power level introduced into the LO port. Using a 10.3 dBm power input on the LO port, the VSWR is less than 1.17 according to typical mixer specifications. Values of the VSWR are related to the reflection coefficient via the following formula:

$$VSWR = \frac{1+|\Gamma|}{1-|\Gamma|} \tag{4.6}$$

where Γ is the reflection coefficient. The S-parameters are taken from this coefficient assuming an absolute value for the coefficient. Using a range of $1 \Leftrightarrow 1.33$ for the VSWR values, we have:

$$1 = \frac{1+|\Gamma|}{1-|\Gamma|} \tag{4.7}$$

$$1-|\Gamma| = 1+|\Gamma| \tag{4.8}$$

The above equations give $\Gamma = 0$ as the lower limit

$$1.33 = \frac{1+|\Gamma|}{1-|\Gamma|} \tag{4.9}$$

$$1.33 - 1.33|\Gamma| = 1+|\Gamma| \tag{4.10}$$

$$0.33 = 2.33|\Gamma| \tag{4.11}$$

The above equations give $\Gamma = \frac{0.33}{2.33} = 0.1416$ as the upper limit. Therefore, Γ lies in the range $0 \Leftrightarrow 0.1416$. The following simulations were run for the IF port mixer mismatch with given values of Γ:

r (m)	Azimuth (ϕ)	Elevation (θ)	Γ
15	120	90	$0 \Leftrightarrow 0.05$
15	120	90	$0 \Leftrightarrow 0.1$
15	120	90	$0 \Leftrightarrow 0.1416$
20	120	90	$0 \Leftrightarrow 0.05$
20	120	90	$0 \Leftrightarrow 0.1$
20	120	90	$0 \Leftrightarrow 0.1416$
35	120	90	$0 \Leftrightarrow 0.05$
35	120	90	$0 \Leftrightarrow 0.1$
35	120	90	$0 \Leftrightarrow 0.1416$
50	120	90	$0 \Leftrightarrow 0.05$
50	120	90	$0 \Leftrightarrow 0.1$
50	120	90	$0 \Leftrightarrow 0.1416$

Table 4.4: Error analysis data points for the IF mismatch factor

4.1.5 Gain factor

Along the transmission lines, mixers and other components, the signal undergoes certain amplitude changes due to the gain effect. These random changes can be taken into consideration using the following mathematical analysis:

$$\Delta A = xdB \tag{4.12}$$

The ΔA term refers to the difference in amplitude that has been brought about due to the gain effect. This term then brings in a change into the array response as a multiple, as shown below:

$$\Delta A = 20\log a \tag{4.13}$$

$$a = 10^{\frac{x}{20}} \tag{4.14}$$

r (m)	Azimuth (ϕ)	Elevation (θ)	ΔA
15	120	90	$\pm 0.1dB$
15	120	90	$\pm 0.5dB$
15	120	90	$\pm 1dB$
20	120	90	$\pm 0.1dB$
20	120	90	$\pm 0.5dB$
20	120	90	$\pm 1dB$
35	120	90	$\pm 0.1dB$
35	120	90	$\pm 0.5dB$
35	120	90	$\pm 1dB$
50	120	90	$\pm 0.1dB$
50	120	90	$\pm 0.5dB$
50	120	90	$\pm 1dB$

Table 4.5: Error analysis data points for the effect of amplitude

4.2 Simulations for the Error Analysis Using MUSIC

The simulations shown in this section have been derived using Monte Carlo simulations. For each simulation, 500 runs were performed where the number was dependent on the time consumed. Furthermore, each simulation generated three different histograms that are described as follows:

Histogram A shows the relative error in phase for array A. This is described as follows:

$$\Omega_{Arel} = \frac{\Omega_{Aest} - \Omega_a}{\Omega_a} \tag{4.15}$$

Histogram B shows the relative error in phase for array B. This is described as follows:

$$\Omega_{Brel} = \frac{\Omega_{Best} - \Omega_b}{\Omega_b} \tag{4.16}$$

Histogram C shows the relative error in estimated range for the whole antenna array set-up. This is described as follows:

$$r_{rel} = \frac{R - r}{r} \tag{4.17}$$

The parameters Ω_{Aest} and Ω_{Best} are the estimated angles of arrival of the received signals with respect to antenna arrays A and B. R and r are the estimated distance and the original range of the emitter from the mid-point of the antenna array. As an example, Figures 4.4 and 4.5 show the histograms representing a specific case for the effect of transmission line length changes:

r (m)	Azimuth (ϕ)	Elevation (θ)	ΔL
15	120	90	$\pm 1mm$

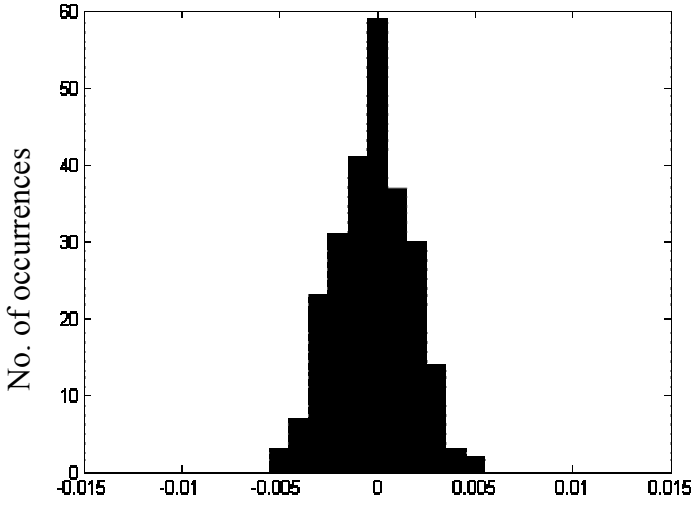

Figure 4.2: Histogram representing Ω_{Arel}

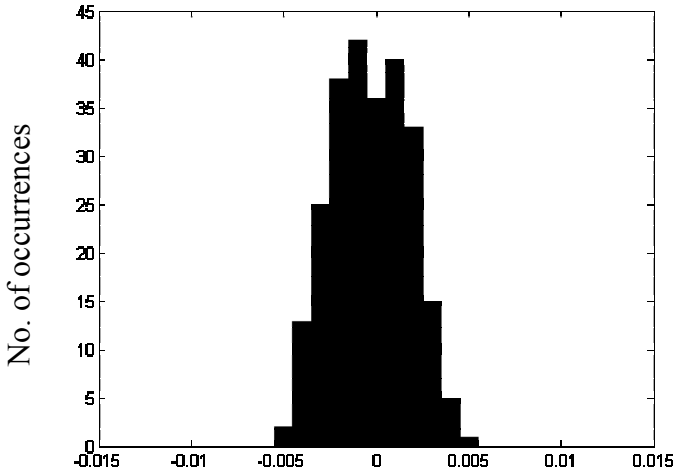

Figure 4.3: Histogram representing Ω_{Brel}

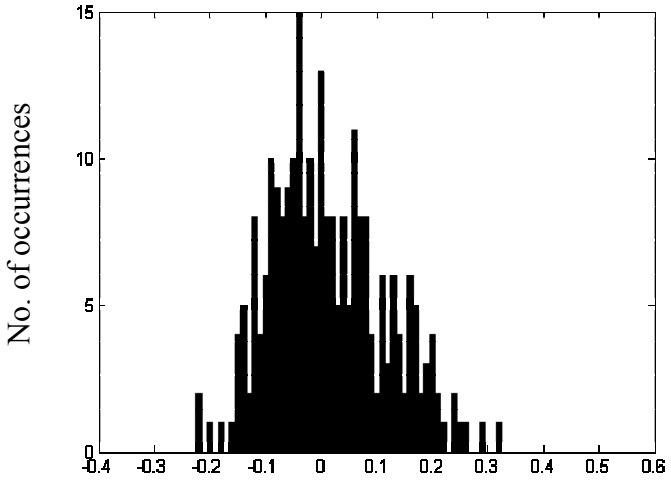

Figure 4.4: Histogram representing r_{rel}

The following table shows the means and standard deviations for the figures above.

	Ω_{Arel}	Ω_{Brel}	r_{rel}
Mean	-2.3051×10^{-4}	2.9145×10^{-4}	0.0119
Standard deviation	0.0019	0.0020	0.1027

Table 4.6: Means and standard deviations for histograms representing $\Delta L = \pm 1mm$

4.2.1 Errors due to transmission line change

It can be seen from the figures above that all three represent approximate Gaussian distributions. For the case representing errors in estimated angles, the means are almost 0. At this point, it is important to point out that the number of simulations run was limited due to the time and resources available. Therefore, increasing the number would have further shifted the means close to 0. These histograms have been collected as a statistical analysis for each introduced error. The following figures show the trends that Ω_{Arel}, Ω_{Brel}, and r_{rel} reflect for the cases listed in Table 4.1.

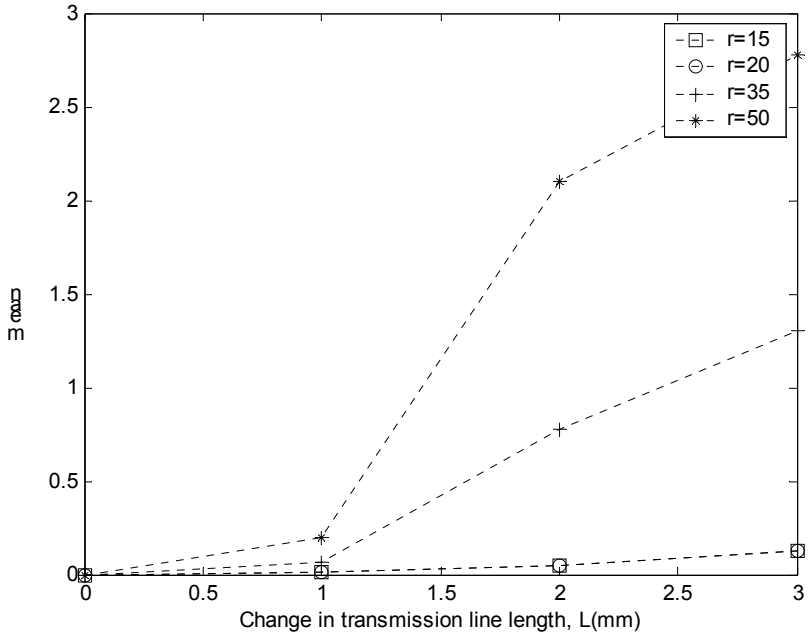

Figure 4.5: Effect of ΔL on means for r_{rel}, N=4

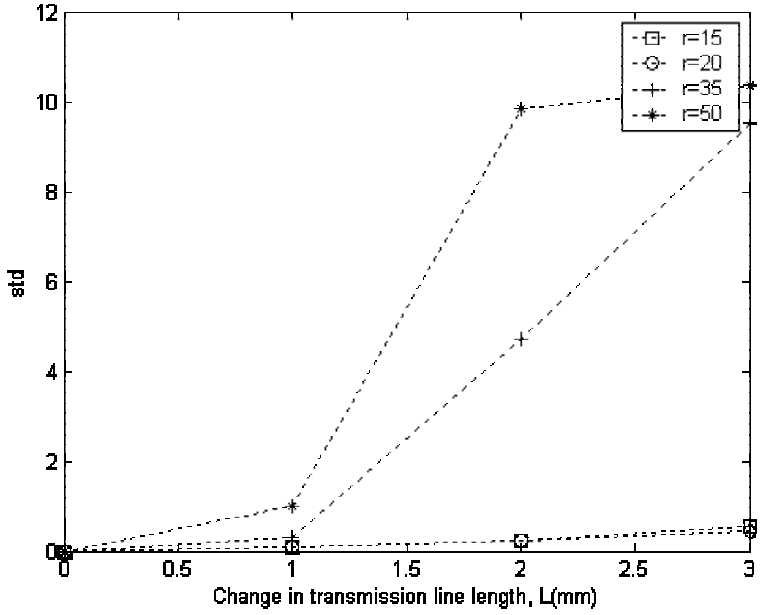

Figure 4.6: Effect of ΔL on standard deviations for r_{rel}, N=4

Figures 4.5 and 4.6 show the increasing mean and standard deviation for range errors in the specified range of increasing transmission line length errors.

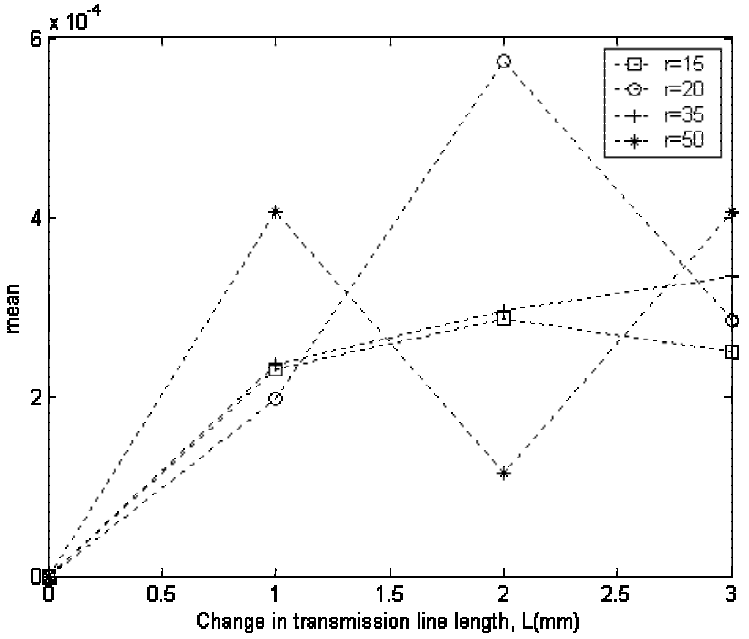

Figure 4.7: Effect of ΔL on means for Ω_{Arel}, N=4

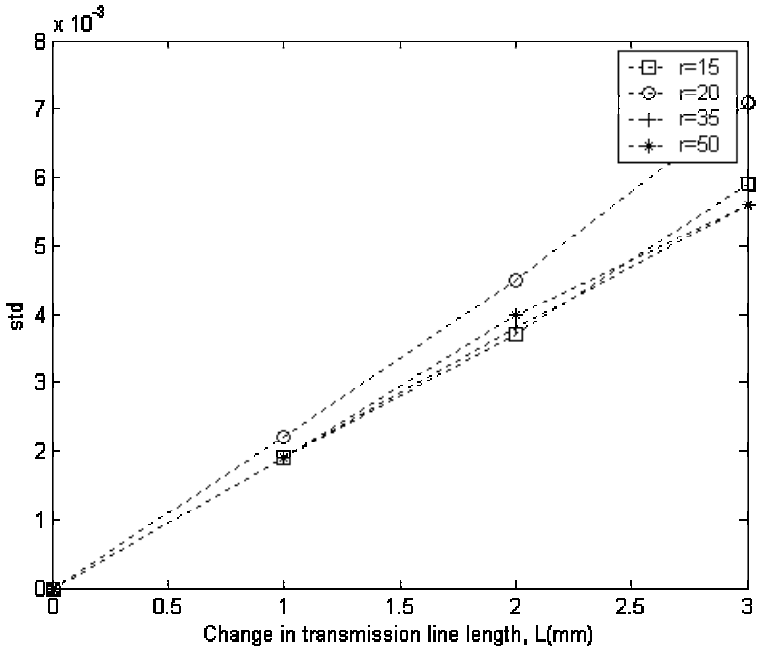

Figure 4.8: Effect of ΔL on standard deviations for Ω_{Arel}, N=4

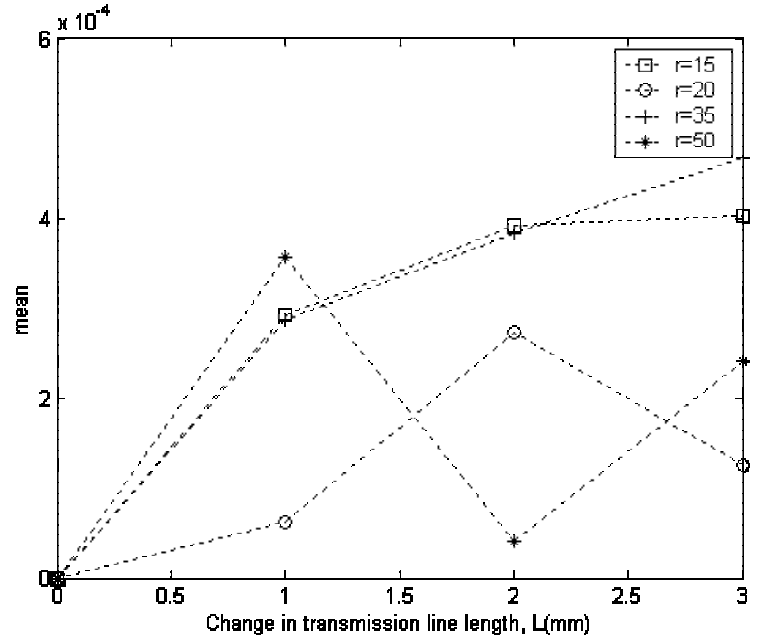

Figure 4.9: Effect of ΔL on means for Ω_{Brel}, N=4

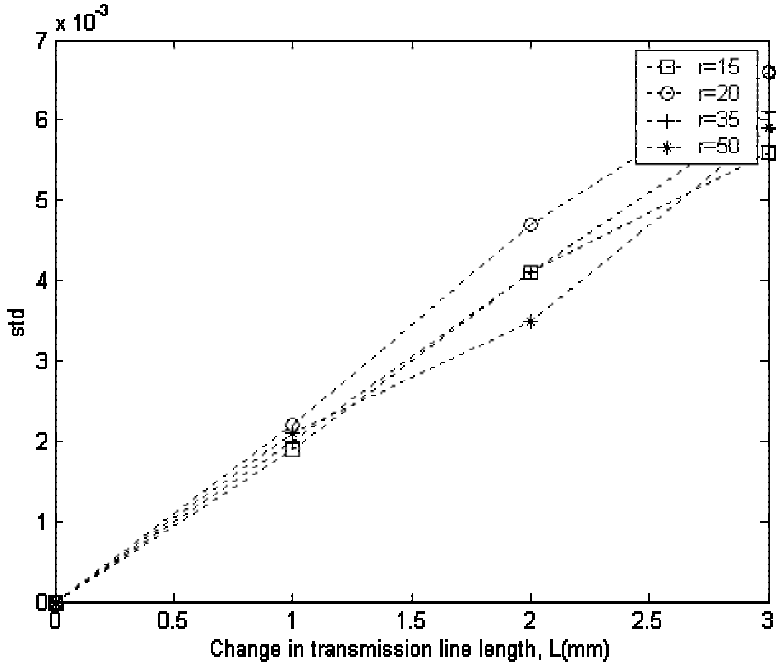

Figure 4.10: Effect of ΔL on means for Ω_{Brel}, N=4

Figures 4.7 and 4.9 do not show any clear trends with increasing transmission line lengths. However, Figures 4.8 and 4.10 show very clearly that the standard deviations increase.

4.2.2 Errors due to phase shifter changes

The following figures show the trends that Ω_{Arel}, Ω_{Brel}, and r_{rel} reflect when data for Table 4.2 is brought together.

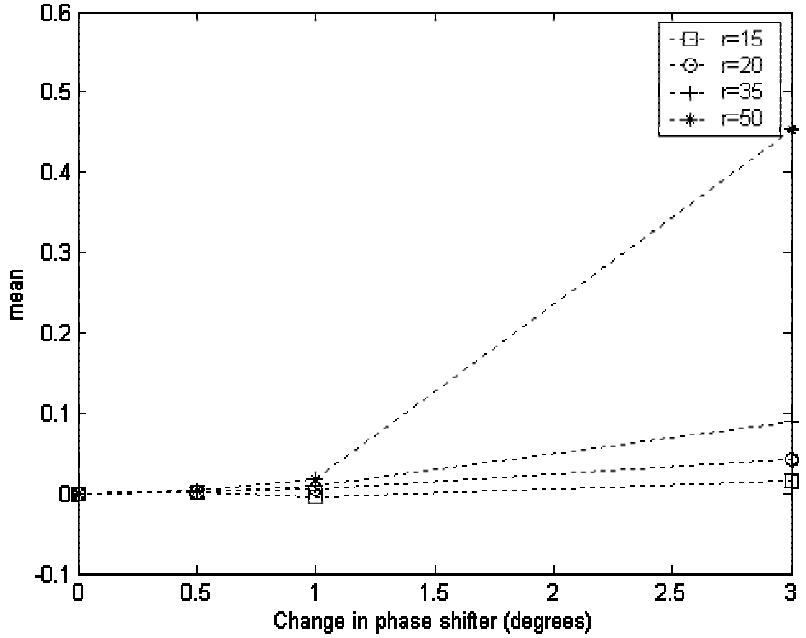

Figure 4.11: Effect of ΔP on means for r_{rel}, N=4

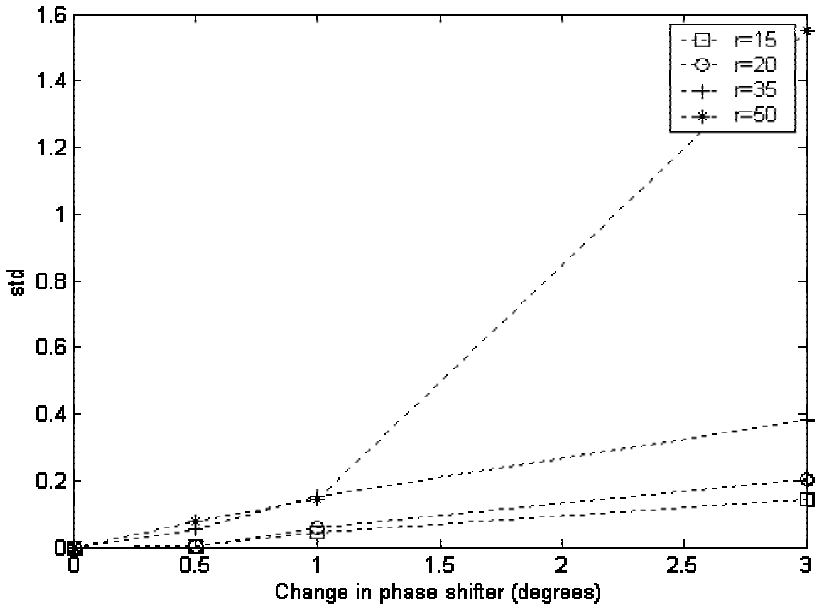

Figure 4.12: Effect of ΔP on standard deviations for r_{rel}, N=4

It can be seen that Figures 4.11 and 4.12 are magnified versions of Figures 4.5 and 4.6. Mathematical explanations for this have been given earlier.

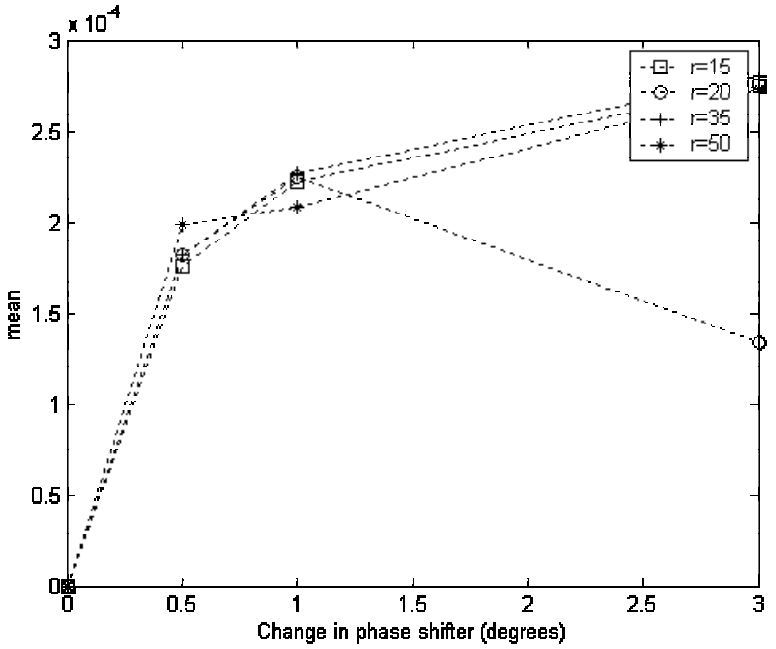

Figure 4.13: Effect of ΔP on means for Ω_{Arel}, N=4

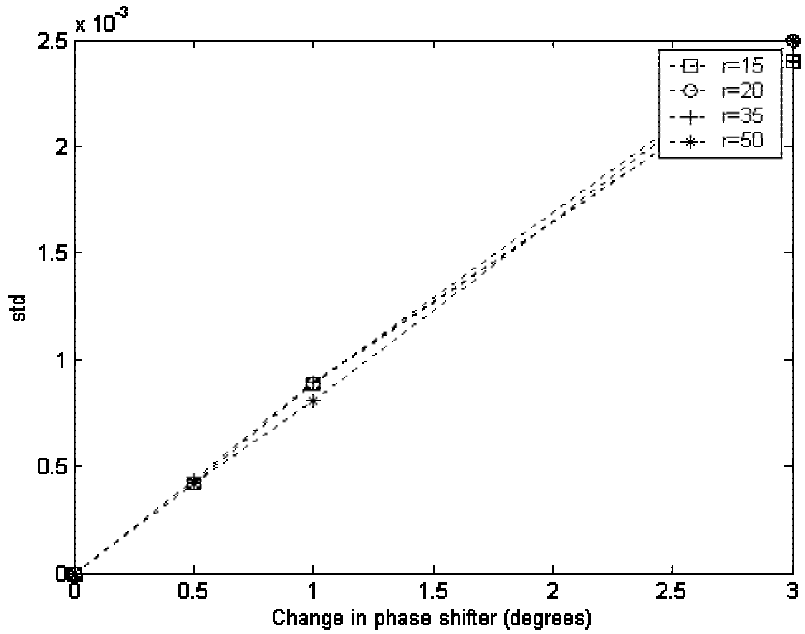

Figure 4.14: Effect of ΔP on standard deviations for Ω_{Arel}, N=4

Figure 4.13 shows the small change in means for the relative error with increasing phase shifter error. Its maximum graphical value is held at $3x10^{-4}$. On the other hand, Figure 4.7 holds a maximum at $6x10^{-4}$. A similar trend can be seen for Figures 4.14 and 4.8.

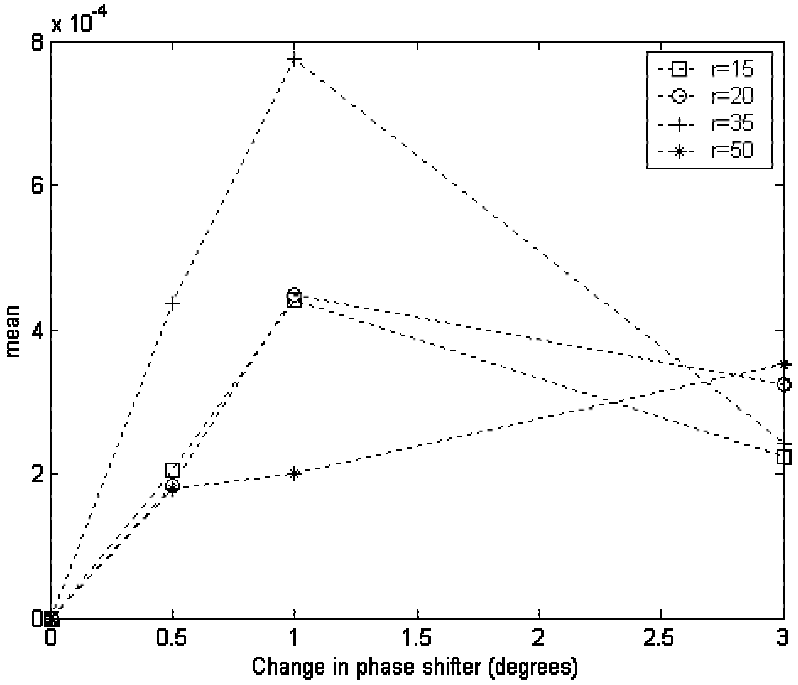

Figure 4.15: Effect of ΔP on means for Ω_{Brel}, N=4

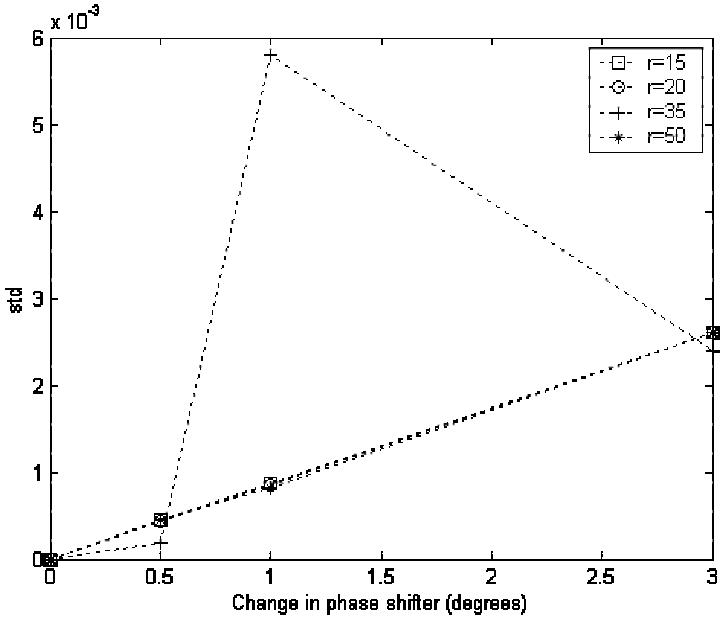

Figure 4.16: Effect of ΔP on standard deviations for Ω_{Brel}, N=4

Apart from one data point, Figure 4.15 shows the general trend to be close to $4x10^{-4}$. The standard deviations show trends of increase towards the maximum value of $2.5x10^{-3}$. In comparison, Figure 4.10 shows a maximum value of $6x10^{-3}$.

4.2.3 Errors due to antenna mismatch

The following figures show the trends that Ω_{Arel}, Ω_{Brel}, and r_{rel} reflect when data for Table 4.3 is brought together.

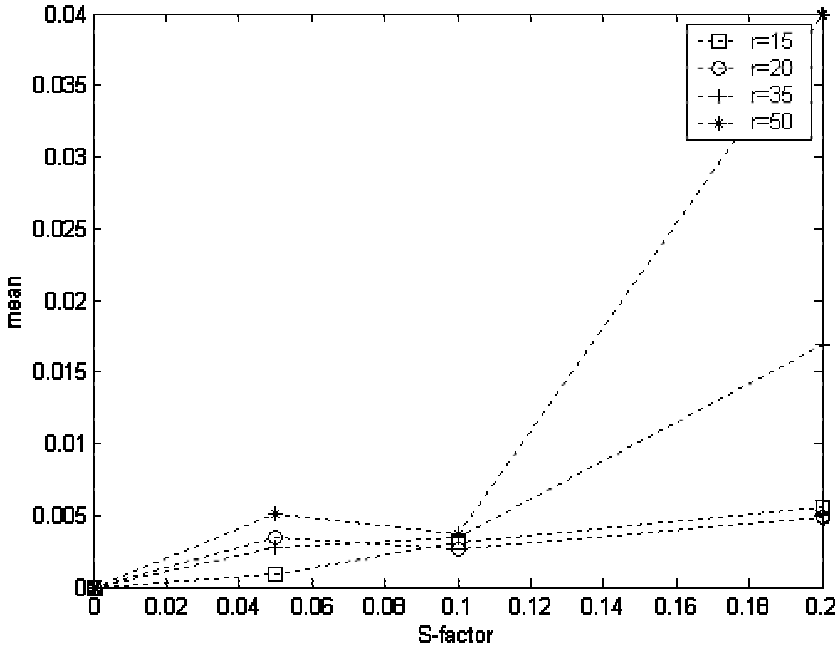

Figure 4.17: Effect of antenna mismatch on means for r_{rel}, N=4

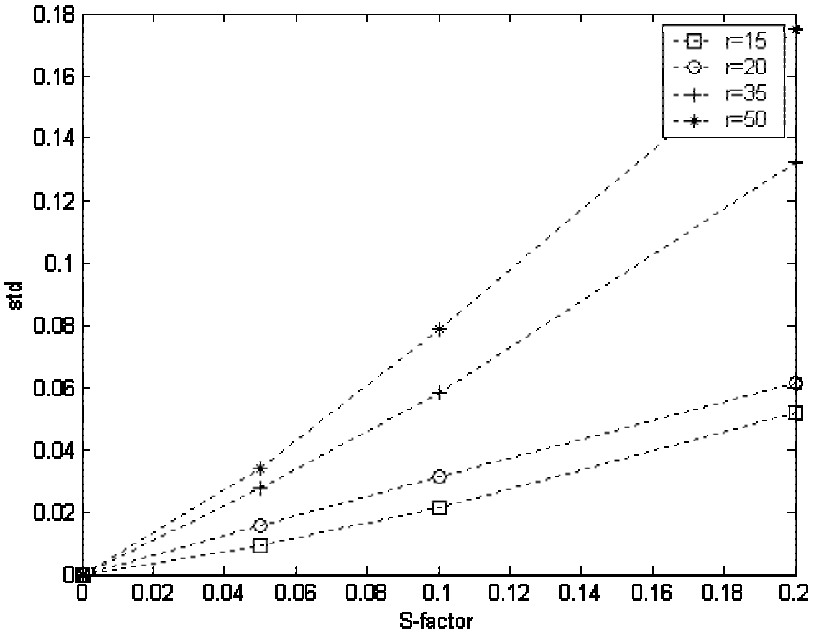

Figure 4.18: Effect of antenna mismatch on standard deviations for r_{rel}, N=4

The increasing standard deviations in Figure 4.18 show that increasing the S-factor brings a greater standard deviation for error in the estimated range. The dip in Figure 4.17 at S = 0.1 can be attributed to the low number of simulations used for these results. Furthermore, the standard deviation of the relative range error stays within a maximum of 0.18.

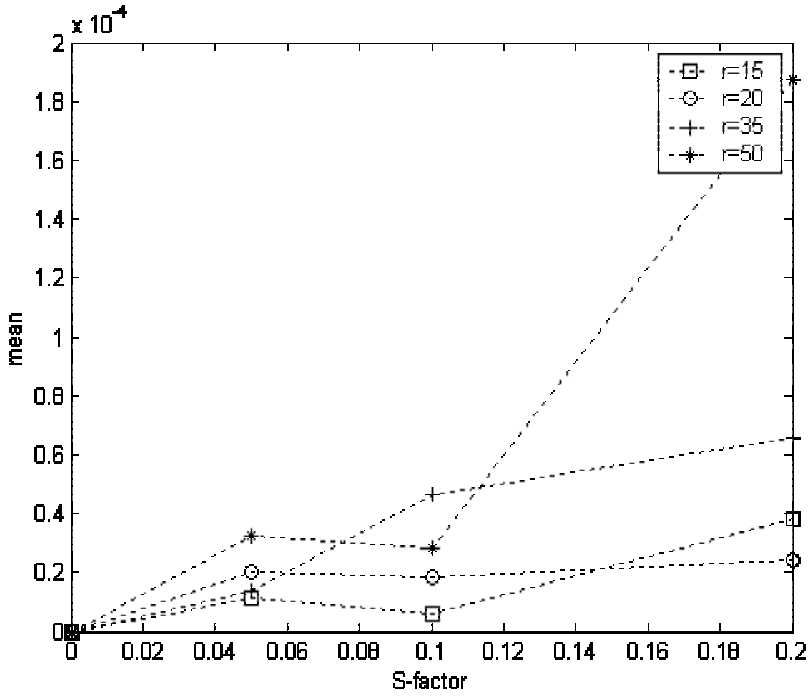

Figure 4.19: Effect of antenna mismatch on means for Ω_{Arel}, N=4

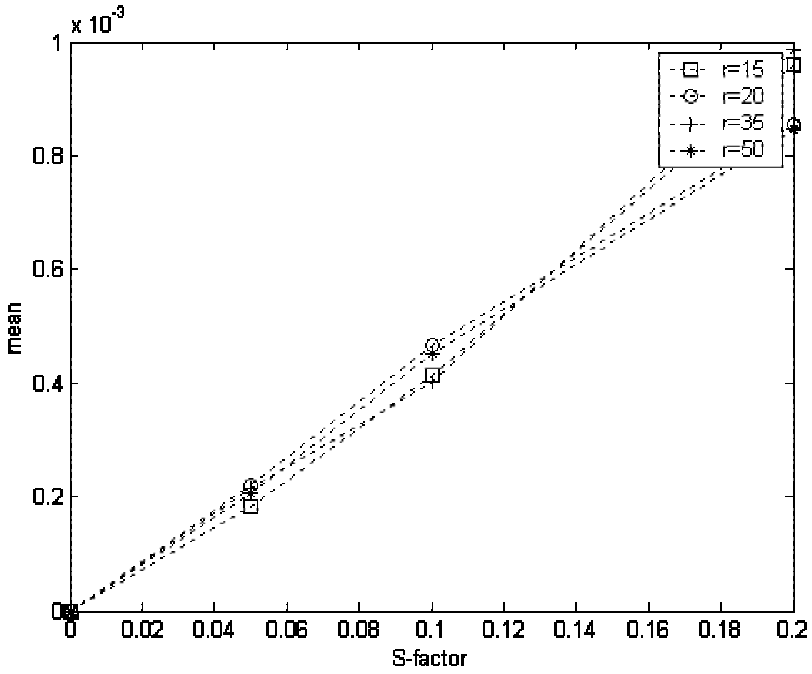

Figure 4.20: Effect of antenna mismatch on standard deviations for Ω_{Arel}, N=4

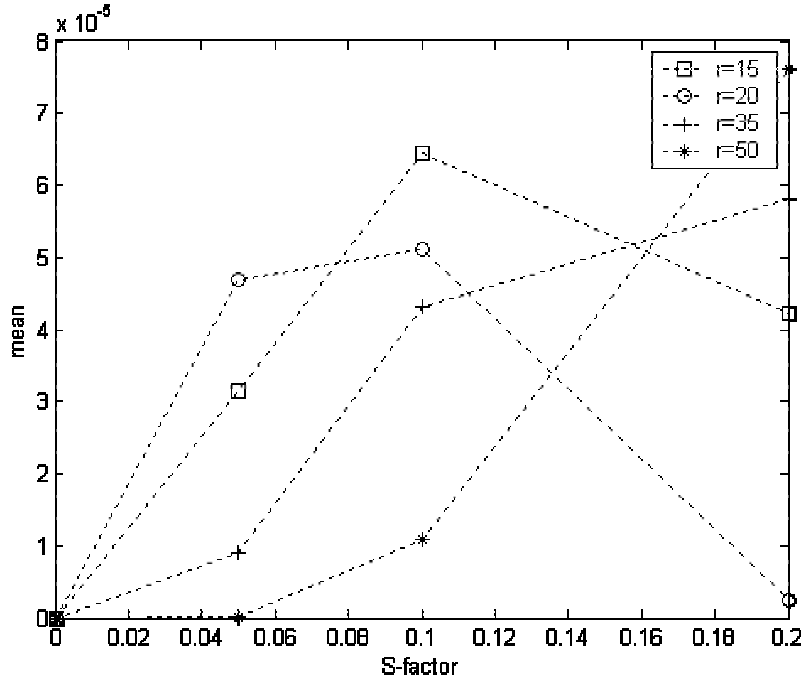

Figure 4.21: Effect of antenna mismatch on means for Ω_{Brel}, N=4

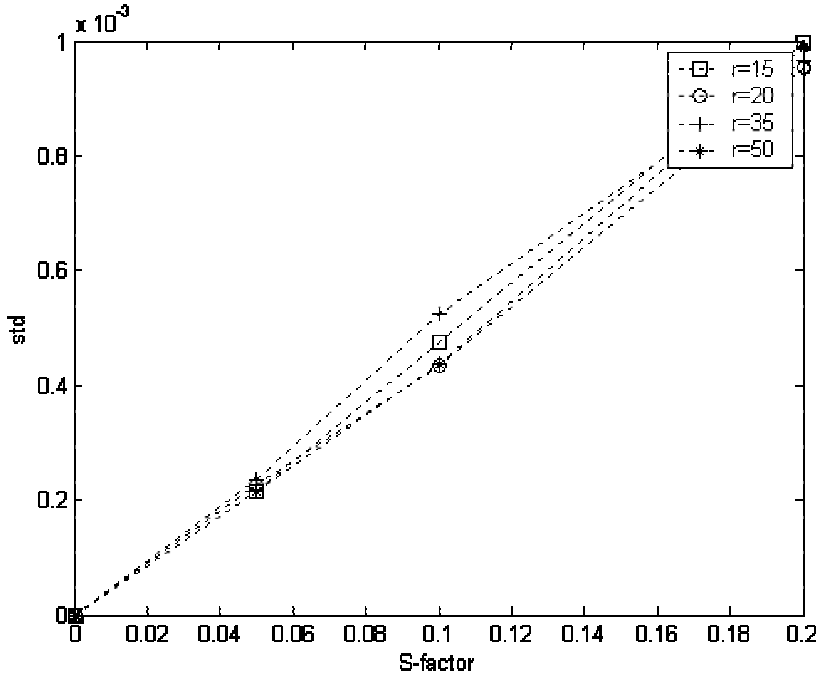

Figure 4.22: Effect of antenna mismatch on standard deviations for Ω_{Brel}, N=4

Although the figures reflecting the means for Ω_{Arel} and Ω_{Brel} do not show a trend with increasing S-factor, the standard deviations show a clear increase. This is attributed to the number of simulations run.

4.2.4 Errors due to gain factor

The following figures show the trends that Ω_{Arel}, Ω_{Brel}, and r_{rel} reflect when data for Table 4.5 is brought together:

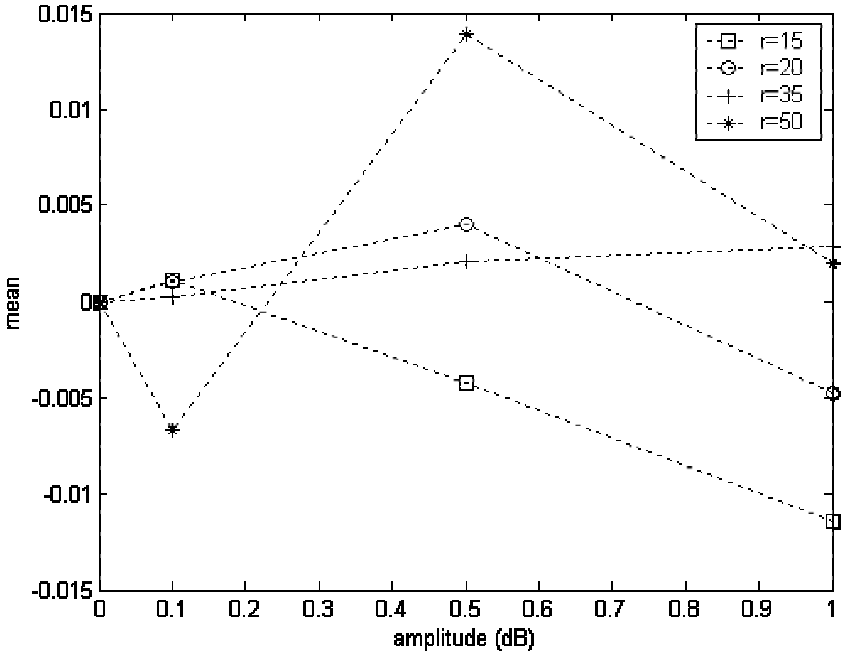

Figure 4.23: Effect of gain factor on means for r_{rel}, N=4

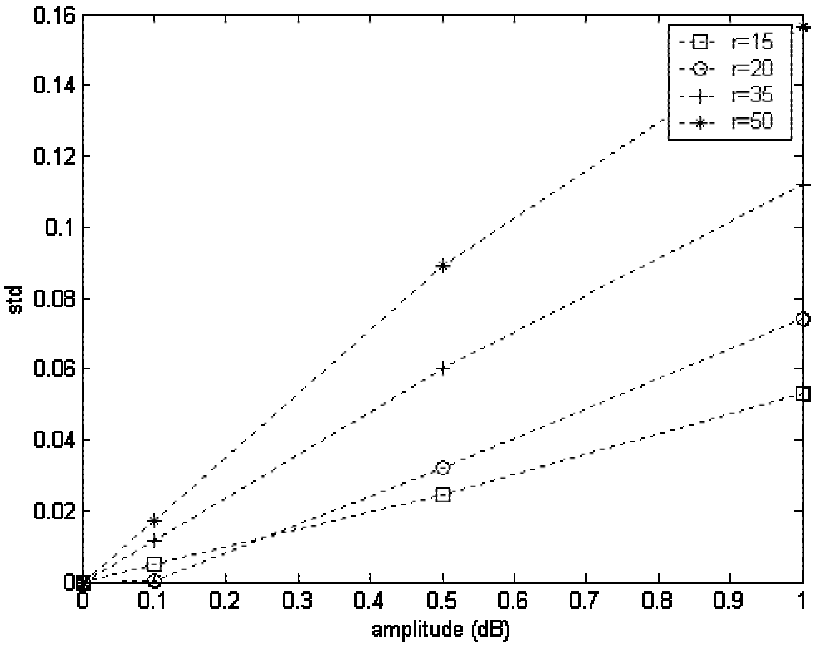

Figure 4.24: Effect of gain factor on standard deviations for r_{rel}, N=4

Figure 4.23 shows that the effect of gain factor on the overall range estimation accuracy is very small. With the standard deviation of the relative range estimation in Figure 4.24 varying not more than 0.15 for random gain factor variation with 1dB, the overall performance of the algorithm can be assumed to be pretty robust to this factor. Also, the trends in standard deviations show a clear increase in error with increasing amplitude change.

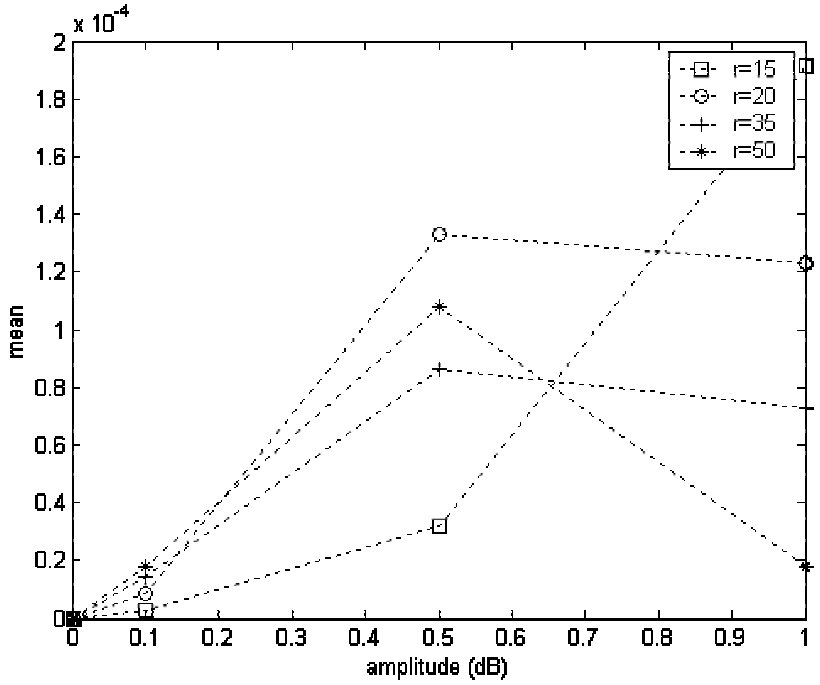

Figure 4.25: Effect of gain factor on means for Ω_{Arel}, N=4

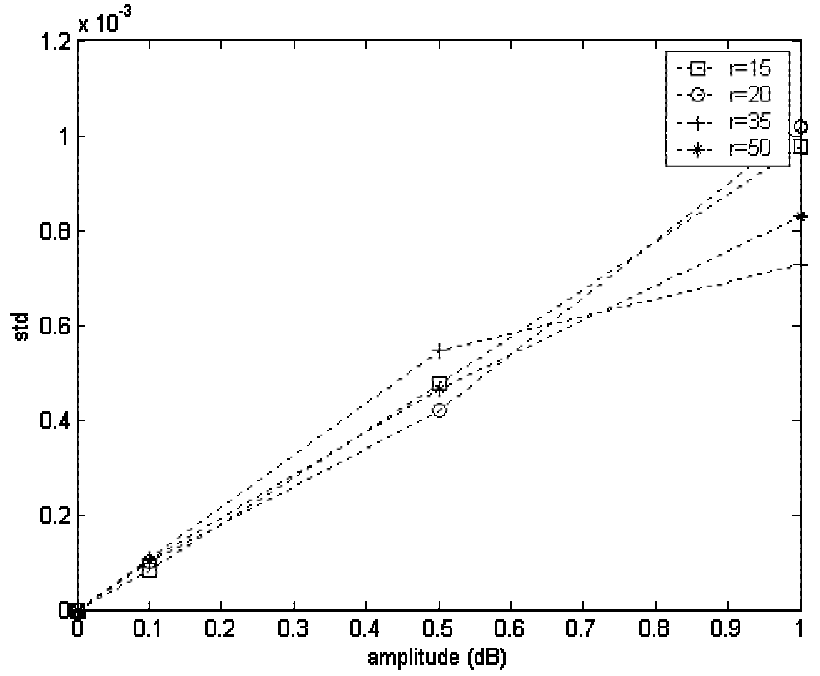

Figure 4.26: Effect of gain factor on standard deviations for Ω_{Arel}, N=4

Figures 4.25 and 4.26 above show the effect of the gain factor on Ω_{Arel}. The maximum change in mean is $2\text{x}10^{-4}$. The standard deviations show trends of increase towards the maximum value of $1.1\text{x}10^{-3}$.

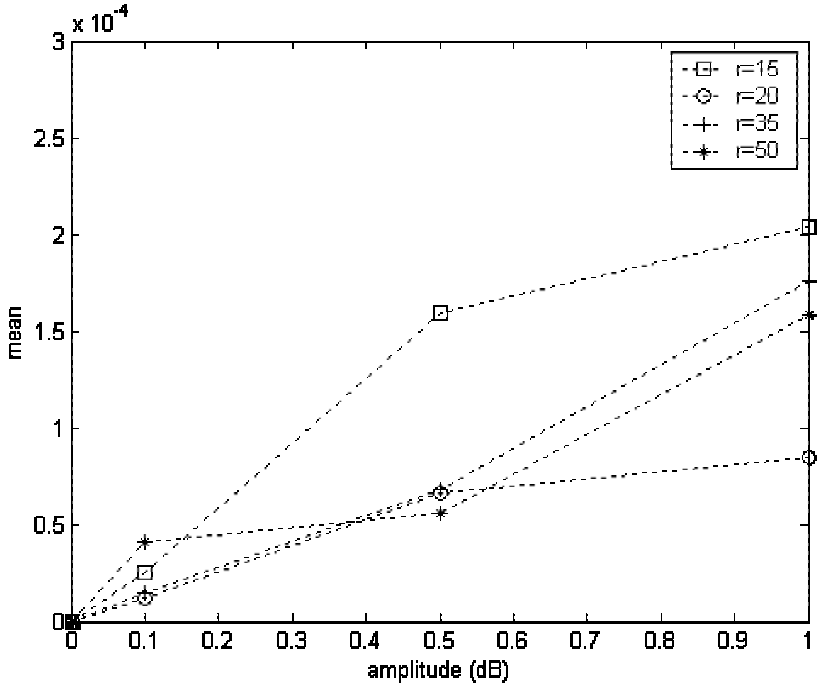

Figure 4.27: Effect of gain factor on means for Ω_{Brel}, N=4

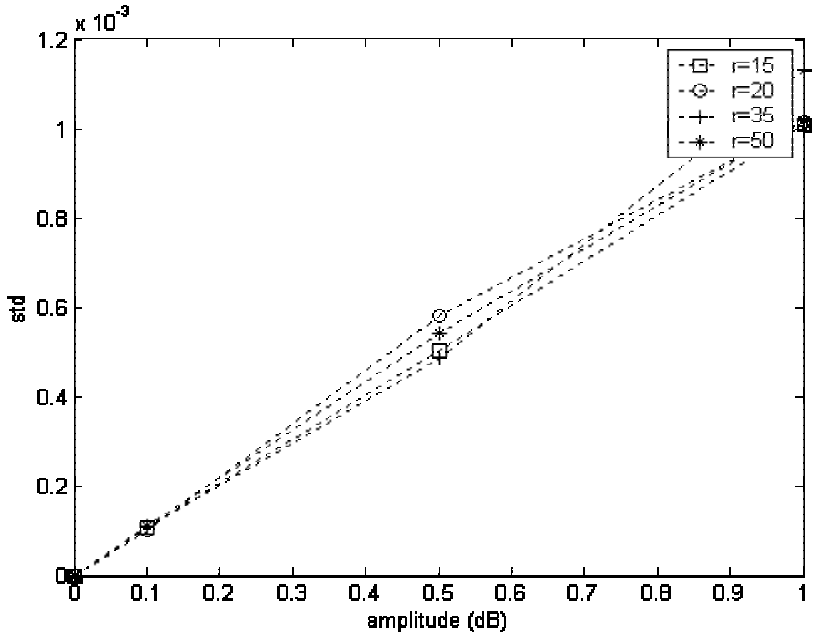

Figure 4.28: Effect of gain factor on standard deviations for Ω_{Brel}, N=4

Figures 4.27 and 4.28 above show the effect of the gain factor on Ω_{Brel}. The maximum change in mean is 2.1×10^{-4}. The standard deviations show trends of increase towards the maximum value of 1.1×10^{-3}. This is approximately the same as the figures representing Array A.

4.2.5 Errors due to phase shifter changes with N = 2

This section shows the effect of decreasing the number of antenna elements of each of the two arrays. The results can be compared to those presented earlier representing the N = 4 case for phase shifter errors.

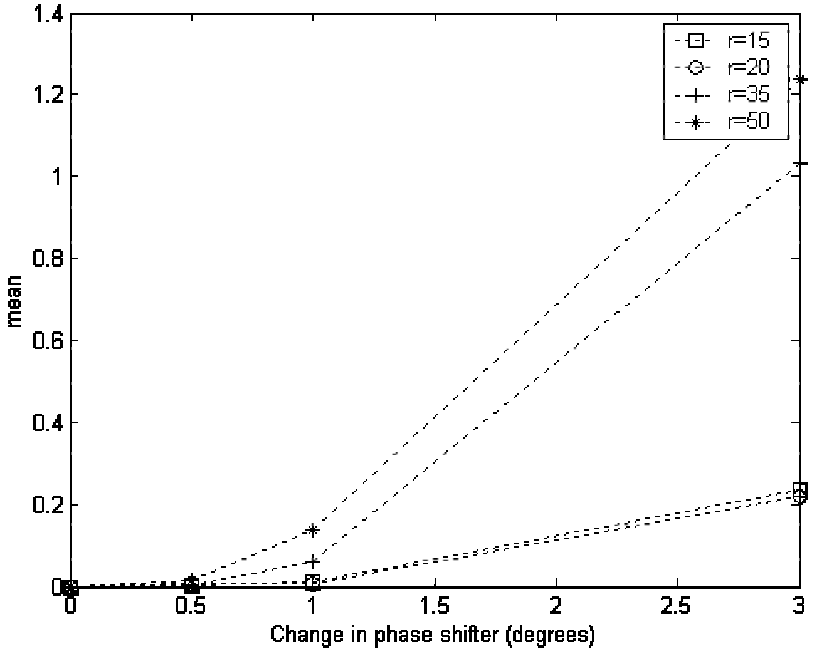

Figure 4.29: Effect of ΔP on means for r_{rel}, N=2

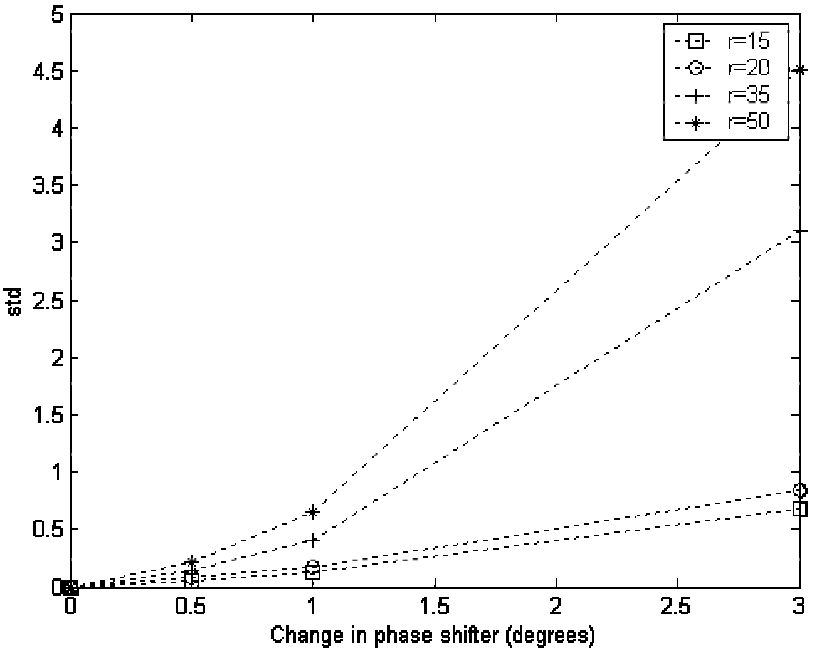

Figure 4.30: Effect of ΔP on standard deviations for r_{rel}, N=2

In comparison with Figures 4.11 and 4.12, we see that the maximums for the means and standard deviations using two elements on each array are much higher. Figure 4.11 representing means for N = 4 goes to a value of 0.55 whereas figure 4.29 goes to 1.3. Figure 4.12 showing standard deviations goes to a value of 1.6 whereas Figure 4.30 goes to a value of 4.6. Therefore, it is shown that increasing the number of elements makes the array response produce more accurate results in the presence of random phase variations.

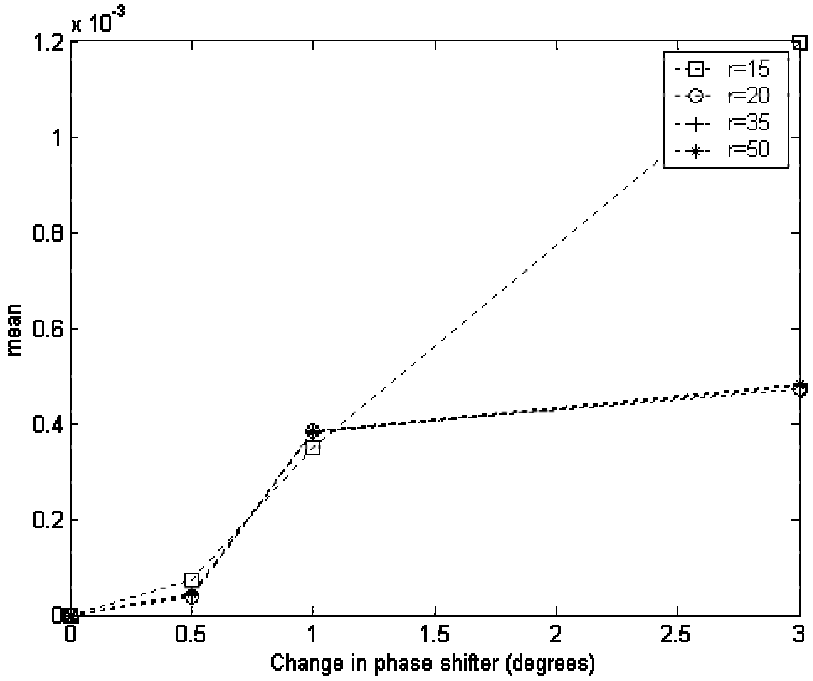

Figure 4.31: Effect of ΔP on means for Ω_{Arel}, N=2

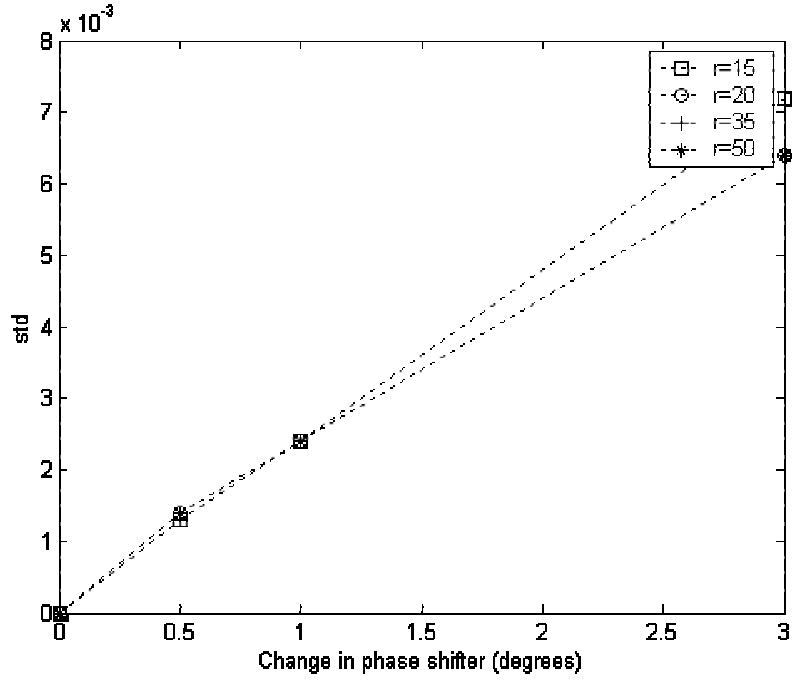

Figure 4.32: Effect of ΔP on standard deviations for Ω_{Arel}, N=2

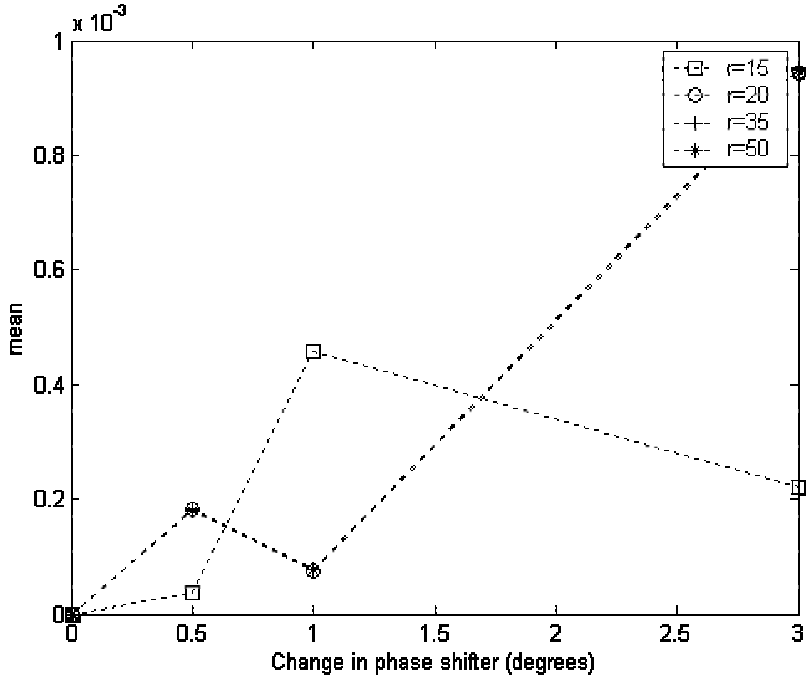

Figure 4.33: Effect of ΔP on means for Ω_{Brel}, N=2

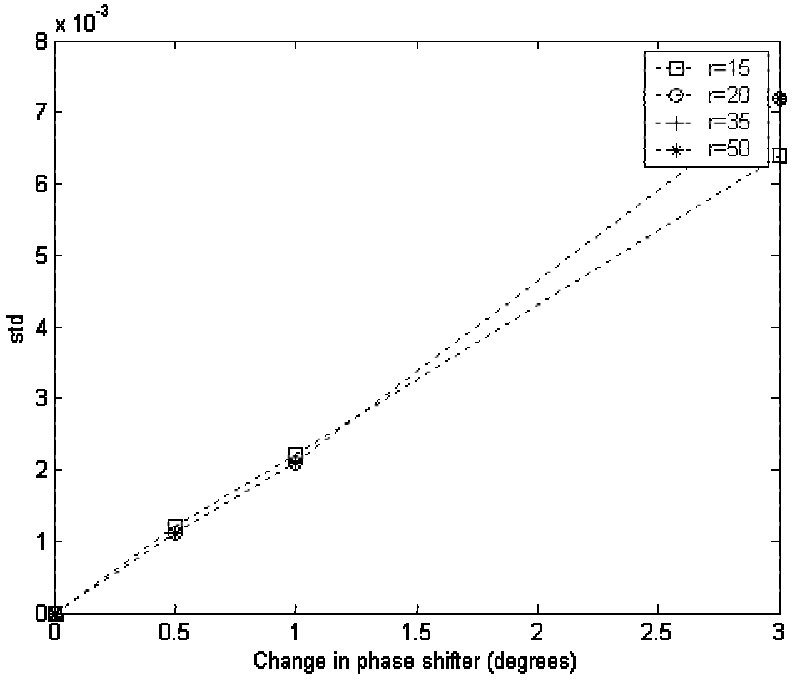

Figure 4.34: Effect of ΔP on standard deviations for Ω_{Brel}, N=2

In comparison with the figures for N=4, we have the same trend of increasing accuracy of the algorithm in estimating the angles of arrival for increasing number of antenna elements. Taking the case for Array A, we see that Figure 4.13 representing means for N = 4 goes to a value of 3×10^{-4} whereas Figure 4.31 goes to 1.2×10^{-3}. Figure 4.14 showing standard deviations has a maximum value of 2.5×10^{-3} whereas Figure 4.32 shows a maximum of 8×10^{-3}. Similar trends are seen for Array B.

4.2.6 Errors due to phase shifter changes with N = 8

This case has been run to further check the effect of increasing the number of elements in an antenna array. For a greater number of elements (N=8), the range estimation accuracy is greater when compared with N=2 or 4. The results shown below can be compared to the cases represented earlier.

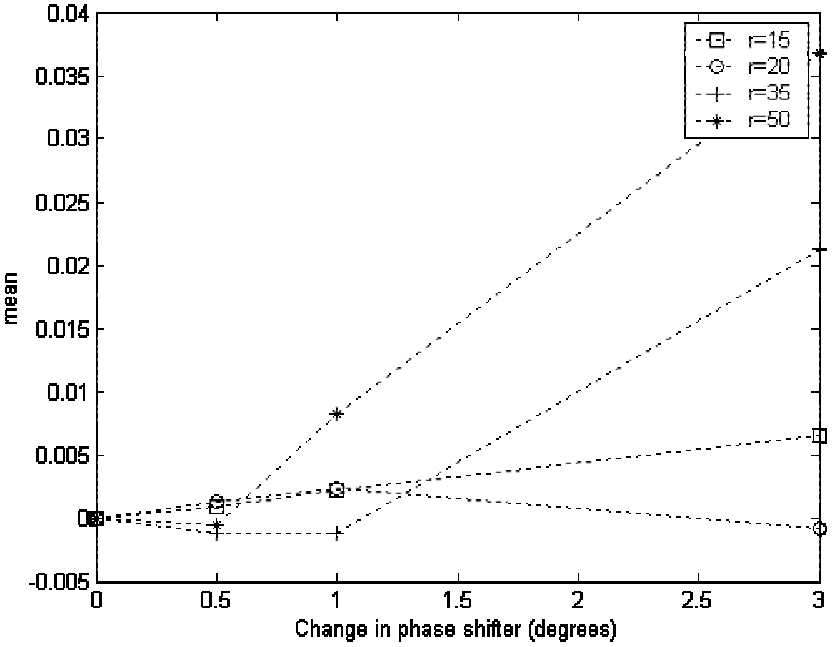

Figure 4.35: Effect of ΔP on means for r_{rel}, N=8

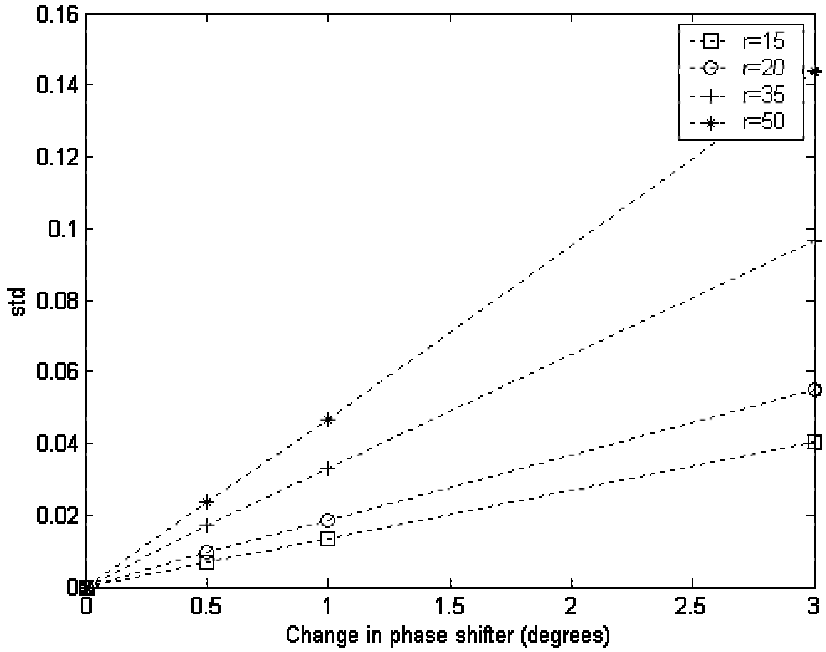

Figure 4.36: Effect of ΔP on standard deviations for r_{rel}, N=8

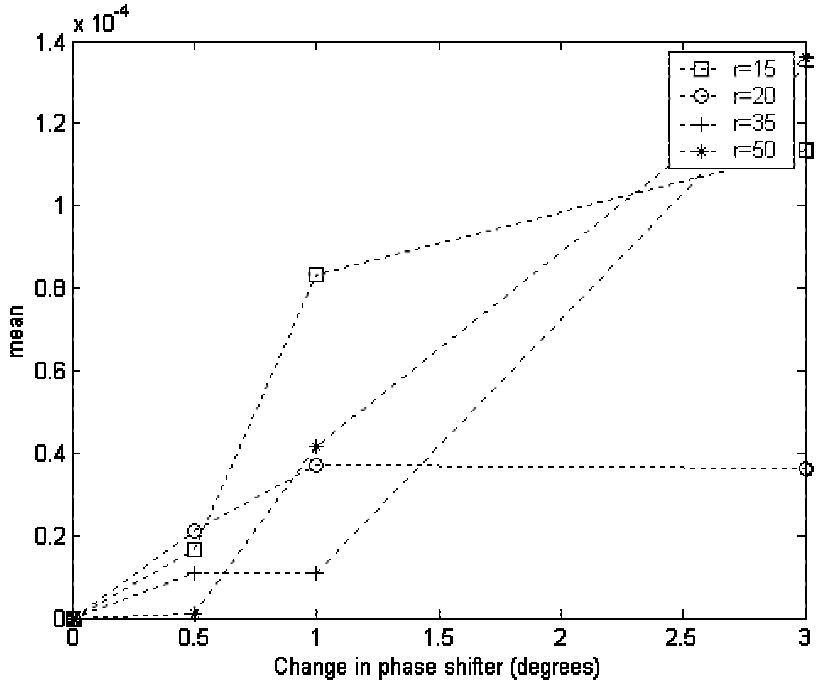

Figure 4.37: Effect of ΔP on means for Ω_{Arel}, N=8

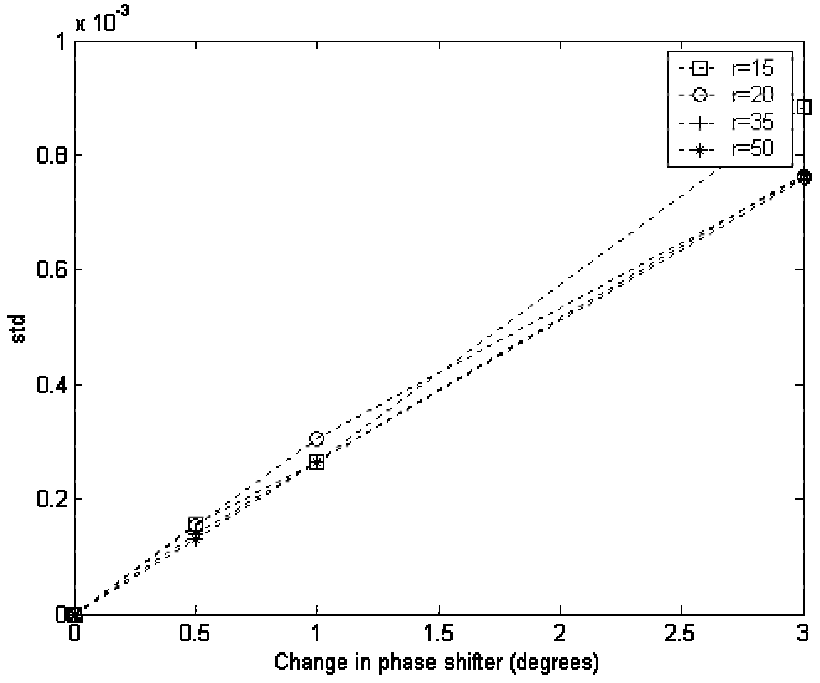

Figure 4.38: Effect of ΔP on standard deviations for Ω_{Arel}, N=8

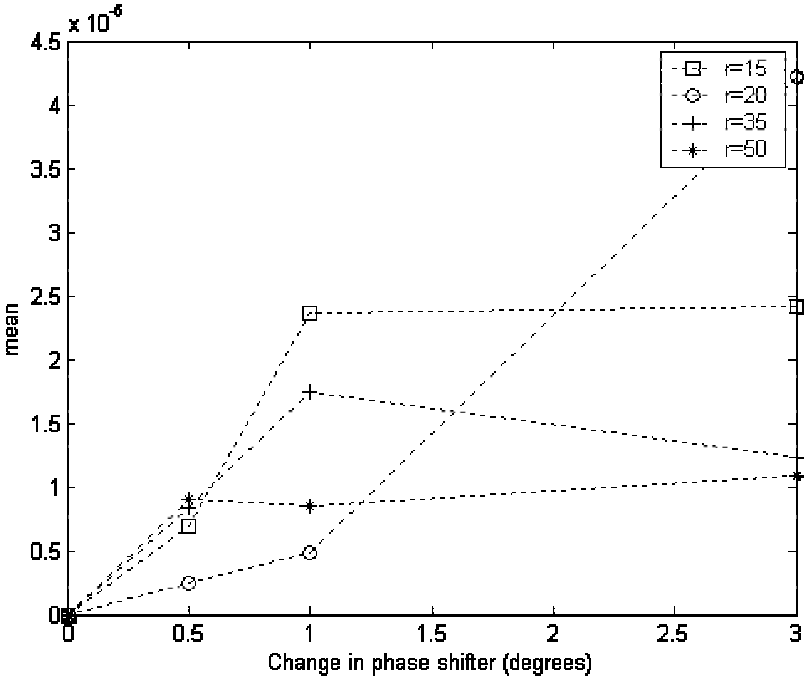

Figure 4.39: Effect of ΔP on means for Ω_{Brel}, N=8

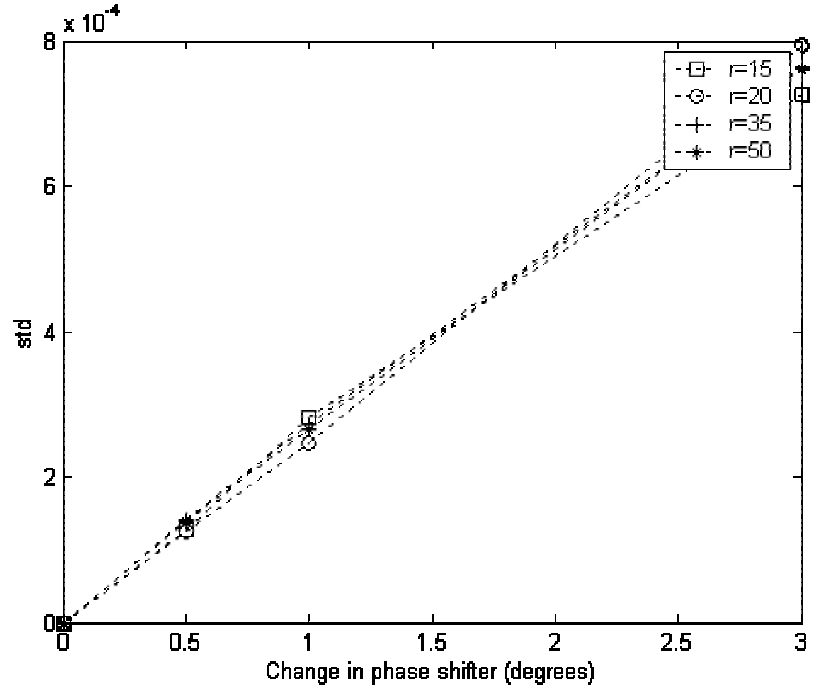

Figure 4.40: Effect of ΔP on standard deviations for Ω_{Brel}, N=8

4.2.7 Effect of azimuth

The following figures show the effect of changing the azimuth angle on the accuracy of the range estimation algorithm. The emitter was kept at a constant distance of 20m from the antenna array center. Furthermore, the simulations were run for the case where transmission line length differences are the source of random error.

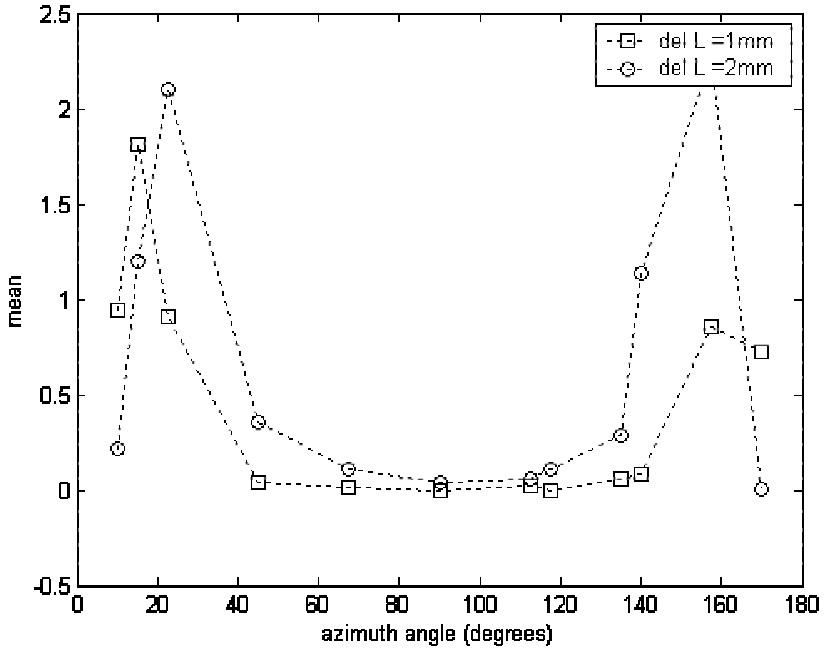

Figure 4.41: Effect of azimuth on means for N=4, r=20

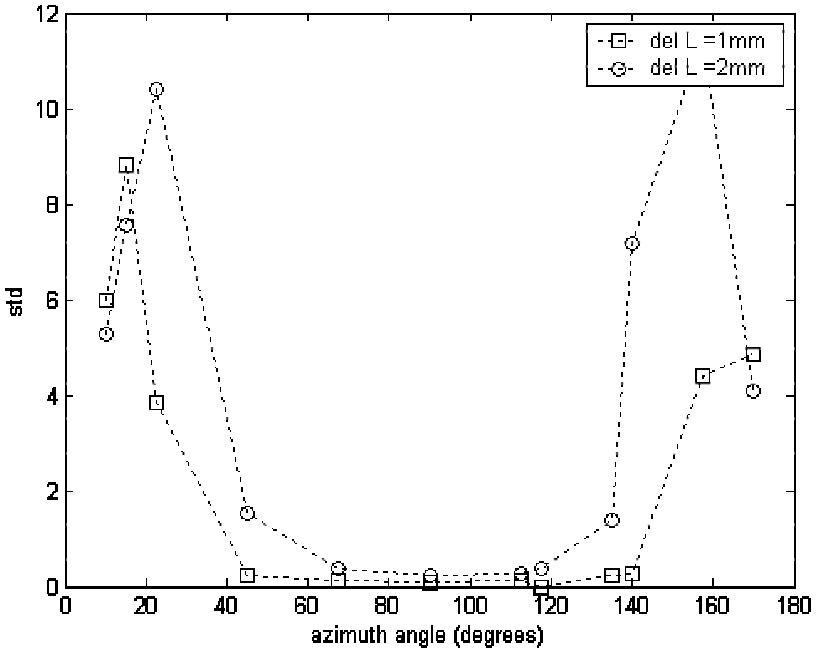

Figure 4.42: Effect of azimuth on standard deviations for N=4, r=20

As seen from Figures 4.41 and 4.42, the errors are low for the broadside angle which lies between 45^0 and 135^0. Furthermore, the lowest standard deviation for error is when the emitter and antenna array center are right in front of each other.

4.3 Tolerance levels for Range Estimation using MUSIC for N=4

The purpose of the earlier error analysis was to form a statistical analysis of the levels within which each error affects the over-all system errors represented in range and angles or arrival. Final assessment is given to that data in this section. For different tolerance levels, we have different estimated ranges. The tables below show the means and standard deviations of the relative error. Therefore, a 10% value represents an increase in the value of range by 10%, or an estimated range of 1.1 *r* where *r* is the actual range.

	r=15m		r=20m		r=35m		r=50m	
ΔL	Std	Mean	Std	Mean	Std	Mean	Std	Mean
1mm	10.27%	1.2%	9.67%	1.58%	28.4%	6.62%	9.87%	19.8%
2mm	22.92%	4.75%	23.18%	4.99%	471%	77.9%	984%	210%
3mm	53.6%	13%	42.8%	12.33%	951%	130%	1003%	278%

Table 4.7: Tolerances for different transmission line lengths

	r=15m		r=20m		r=35m		r=50m	
ΔP	Std	Mean	Std	Mean	Std	Mean	Std	Mean
0.5°	0.002%	0.01%	0.003%	0.004%	5.4%	0.2%	7.5%	0.27%
1°	4.4%	0%	5.96%	0.6%	15.32%	1%	14.1%	1.67%
3°	14.3%	1.65%	20.4%	4.3%	38.1%	8.9%	155%	45.37%

Table 4.8: Tolerances for different phase shifts

	r=15m		r=20m		r=35m		r=50m	
Γ	Std	Mean	Std	Mean	Std	Mean	Std	Mean
$0 \Leftrightarrow 0.05$	0.92%	0.08%	1.55%	0.35%	2.77%	0.27%	3.42%	0.51%
$0 \Leftrightarrow 0.1$	2.15%	0.31%	3.13%	0.26%	5.79%	0.34%	7.89%	0.37%
$0 \Leftrightarrow 0.2$	5.19%	0.56%	6.14%	0.48%	13.22%	1.69%	17.51%	3.99%

Table 4.9: Tolerances for different antenna mismatch factors

	r=15m		r=20m		r=35m		r=50m	
ΔA	Std	Mean	Std	Mean	Std	Mean	Std	Mean
$\pm 0.1dB$	0.49%	0.1%	0.01%	0.1%	1.15%	0.02%	1.69%	0%
$\pm 0.5dB$	2.44%	0%	3.2%	0.04%	6.03%	0.02%	8.9%	1.39%
$\pm 1dB$	5.3%	0%	7.4%	0%	11.2%	0.29%	15.63%	0.2%

Table 4.10: Tolerances for different gain factors

4.4 Tolerance levels for Range Estimation using MUSIC for N=2

This section gives the results with two elements on each array. As expected, the performance degrades when in comparison with Table 4.8. Table 4.11 shows the means and standard deviations of the relative error.

	r=15m		r=20m		r=35m		r=50m	
ΔP	Std	Mean	Std	Mean	Std	Mean	Std	Mean
0.5°	5.63%	0.08%	8.12%	0.42%	14.4%	0.12%	21.6%	1.47%
1°	12.42%	1.03%	17.36%	0.52%	39.57%	5.87%	65.06%	13.82%
3°	67.3%	23.6%	84%	22%	311%	103.5%	451%	124%

Table 4.11: Tolerances for different phase shifts

4.5 Tolerance levels for Range Estimation using MUSIC for N=8

This section gives the results when eight elements are used on each array. Table 4.12 shows a dramatic decrease in the means and standard deviations of the relative error when compared with Tables 4.8 and 4.11.

	r=15m		r=20m		r=35m		r=50m	
ΔP	Std	Mean	Std	Mean	Std	Mean	Std	Mean
0.5°	0.7%	0.083%	0.94%	0.12%	1.72%	0%	2.38%	0%
1°	1.33%	0.22%	1.85%	0.23%	3.28%	0%	4.66%	0.82%
3°	4.05%	0.65%	5.48%	0%	9.67%	2.13%	14.38%	3.68%

Table 4.12: Tolerances for different phase shifts

Chapter 5

Error Analysis Using Modified Root Pisarenko

This chapter covers the results for the error analysis using MRP as the Direction-finding Algorithm. The first section describes errors such as transmission line length differences, phase shifter changes, amplitude changes to the signal, and mismatches used to check the sensitivity of the range estimation algorithm. The second section gives plots representing Monte Carlo simulations run for relative errors in estimated ranges and angles of arrival. Also, the effect of increasing the number of passive elements on the range estimation is checked by using extended arrays of 10 elements each. The third section gives tolerance tables for the analysis involving MRP. The results given in this section can be used as a bound for certain conditions in which the antenna is to be used.

5.1 Description of Error Analysis

The error analysis of the MRP algorithm follows the same definitions as what was described in Section 4.1 for the MUSIC algorithm. However, some changes made to the introduced errors are given below.

5.1.1 Transmission line change

The introduced error has 4 ranges within which the uniformly distributed random errors lie:

1) $\pm 0.2mm$

2) $\pm 0.5mm$

3) $\pm 0.7mm$

4) $\pm 1mm$

Table 5.1 is a list of simulation cases that were run for changes in transmission line length changes for different ranges (r), azimuth angles (ϕ), elevation angles (θ), and cable length differences (ΔL).

r (m)	Azimuth (ϕ)	Elevation (θ)	ΔL
15	120	90	$\pm 0.2mm$
15	120	90	$\pm 0.5mm$
15	120	90	$\pm 0.7mm$
15	120	90	$\pm 1mm$
20	120	90	$\pm 0.2mm$
20	120	90	$\pm 0.5mm$
20	120	90	$\pm 0.7mm$
20	120	90	$\pm 1mm$
35	120	90	$\pm 0.2mm$
35	120	90	$\pm 0.5mm$
35	120	90	$\pm 0.7mm$
35	120	90	$\pm 1mm$
50	120	90	$\pm 0.2mm$
50	120	90	$\pm 0.5mm$
50	120	90	$\pm 0.7mm$
50	120	90	$\pm 1mm$

Table 5.1: Error analysis data points for ΔL

5.1.2 Phase shifter error

As mentioned in Chapter 4, phase shifters are used to tune in the received frequencies from the different antenna elements to one frequency. Taking practical limitations into account, errors are introduced within a certain tolerance as the phase shifter settings are dependent upon physical tuning using a knob. The introduced error has 3 random ranges within which it may vary:

1) $\pm 0.5^{\circ}$
2) $\pm 1^{\circ}$
3) $\pm 3^{\circ}$

The following simulations were run for changes in phase shifter errors:

r (m)	Azimuth (ϕ)	Elevation (θ)	ΔP
15	120	90	$\pm 0.5^{0}$
15	120	90	$\pm 1^{0}$
15	120	90	$\pm 3^{0}$
20	120	90	$\pm 0.5^{0}$
20	120	90	$\pm 1^{0}$
20	120	90	$\pm 3^{0}$
35	120	90	$\pm 0.5^{0}$
35	120	90	$\pm 1^{0}$
35	120	90	$\pm 3^{0}$
50	120	90	$\pm 0.5^{0}$
50	120	90	$\pm 1^{0}$
50	120	90	$\pm 3^{0}$

Table 5.2: Error analysis data points for ΔP

5.1.3 Antenna Mismatch

The reflection coefficients vary randomly within the following ranges:

1) $\Gamma = 0 \Leftrightarrow 0.05$
2) $\Gamma = 0 \Leftrightarrow 0.1$
3) $\Gamma = 0 \Leftrightarrow 0.2$

The following simulations were run to analyze the effect on the overall performance due to antenna mismatch:

r (m)	Azimuth (ϕ)	Elevation (θ)	Γ
15	120	90	$0 \Leftrightarrow 0.05$
15	120	90	$0 \Leftrightarrow 0.1$
15	120	90	$0 \Leftrightarrow 0.2$
20	120	90	$0 \Leftrightarrow 0.05$
20	120	90	$0 \Leftrightarrow 0.1$
20	120	90	$0 \Leftrightarrow 0.2$
35	120	90	$0 \Leftrightarrow 0.05$
35	120	90	$0 \Leftrightarrow 0.1$
35	120	90	$0 \Leftrightarrow 0.2$
50	120	90	$0 \Leftrightarrow 0.05$
50	120	90	$0 \Leftrightarrow 0.1$
50	120	90	$0 \Leftrightarrow 0.2$

Table 5.3: Error analysis data points for the antenna mismatch factor

5.1.4 Gain factor

The following simulations were run for the gain factor:

r (m)	Azimuth (ϕ)	Elevation (θ)	x
15	120	90	$\pm 0.1dB$
15	120	90	$\pm 0.5dB$
15	120	90	$\pm 1dB$
20	120	90	$\pm 0.1dB$
20	120	90	$\pm 0.5dB$
20	120	90	$\pm 1dB$
35	120	90	$\pm 0.1dB$
35	120	90	$\pm 0.5dB$
35	120	90	$\pm 1dB$
50	120	90	$\pm 0.1dB$
50	120	90	$\pm 0.5dB$
50	120	90	$\pm 1dB$

Table 5.4: Error analysis data points for the effect of amplitude

5.1.5 IF Mismatch

As described in Section 4.1.4, the reflection coefficients for the mixer mismatch are taken to vary randomly within the following ranges:

1) $0 \Leftrightarrow 0.05$
2) $0 \Leftrightarrow 0.1$
3) $0 \Leftrightarrow 0.1416$

The following simulations were run for the mixer mismatch with given values of Γ:

r (m)	Azimuth (ϕ)	Elevation (θ)	Γ
15	120	90	$0 \Leftrightarrow 0.05$
15	120	90	$0 \Leftrightarrow 0.1$
15	120	90	$0 \Leftrightarrow 0.1416$
20	120	90	$0 \Leftrightarrow 0.05$
20	120	90	$0 \Leftrightarrow 0.1$
20	120	90	$0 \Leftrightarrow 0.1416$
35	120	90	$0 \Leftrightarrow 0.05$
35	120	90	$0 \Leftrightarrow 0.1$
35	120	90	$0 \Leftrightarrow 0.1416$
50	120	90	$0 \Leftrightarrow 0.05$
50	120	90	$0 \Leftrightarrow 0.1$
50	120	90	$0 \Leftrightarrow 0.1416$

Table 5.5: Error analysis data points for the VSWR mismatch factor

5.2 Simulations for the Error Analysis Using MRP

The simulations shown in this section have been derived using Monte Carlo simulations. For each simulation, 100 runs were performed where the number was dependent on the time consumed. Furthermore, each simulation generated three different histograms that have already been described earlier in Section 4.2. The simulations run in this section were performed under coupled conditions. Also, no transformation for decoupling was introduced. This was done to see the effect of introducing extra antenna elements, as will be shown in Section 5.3.

5.2.1 Errors due to transmission line change

The following figures show the trends that Ω_{Arel}, Ω_{Brel}, and r_{rel} reflect when data for Table 5.1 is brought together.

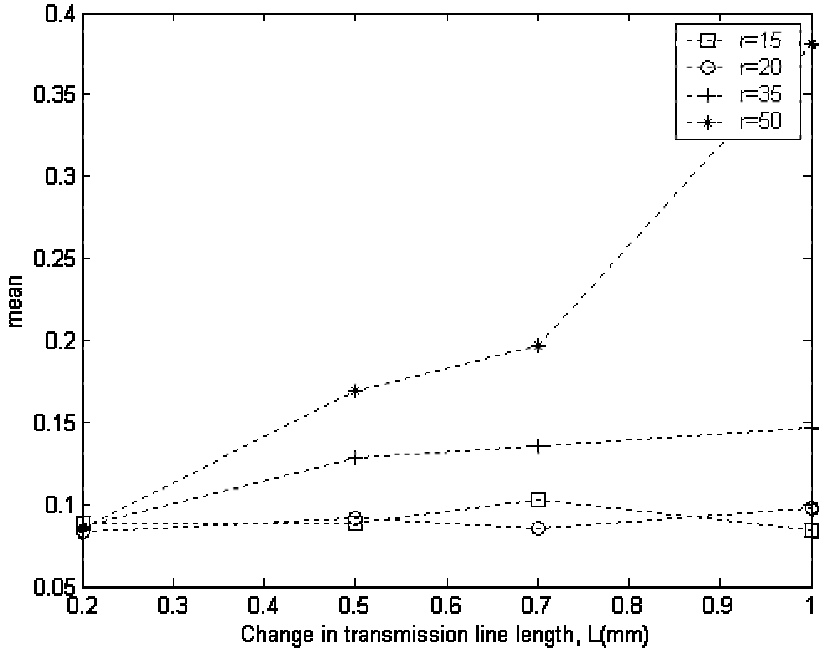

Figure 5.1: Effect of ΔL on means for r_{rel}, N=4

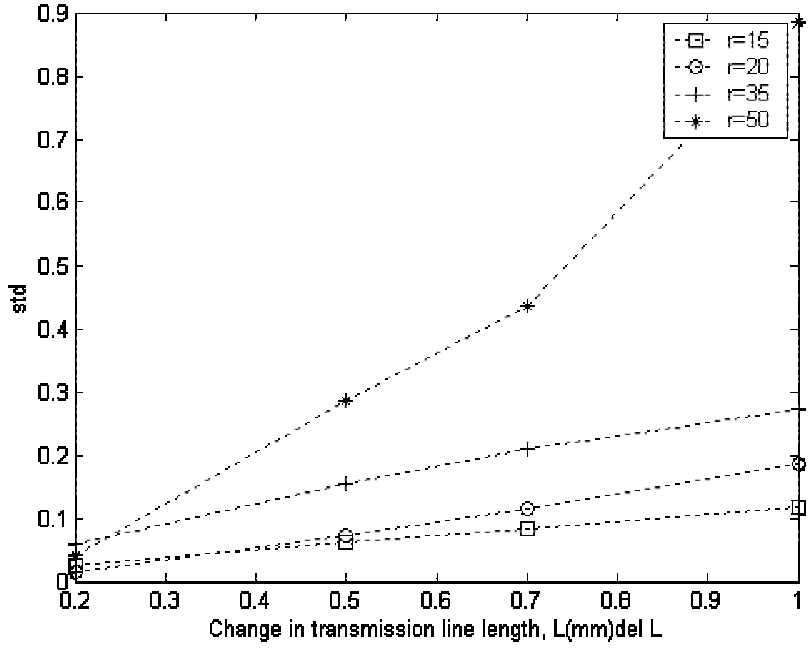

Figure 5.2: Effect of ΔL on standard deviations for r_{rel}, N=4

Figures 5.1 and 5.2 show an increasing mean and standard deviation for error in estimated range with increasing transmission line length errors. For errors distributed over more than $\pm 1mm$, the algorithm does not function properly as it gives an estimate that is almost twice the value of the original range. Also, standard deviations increase in accordance with increasing means.

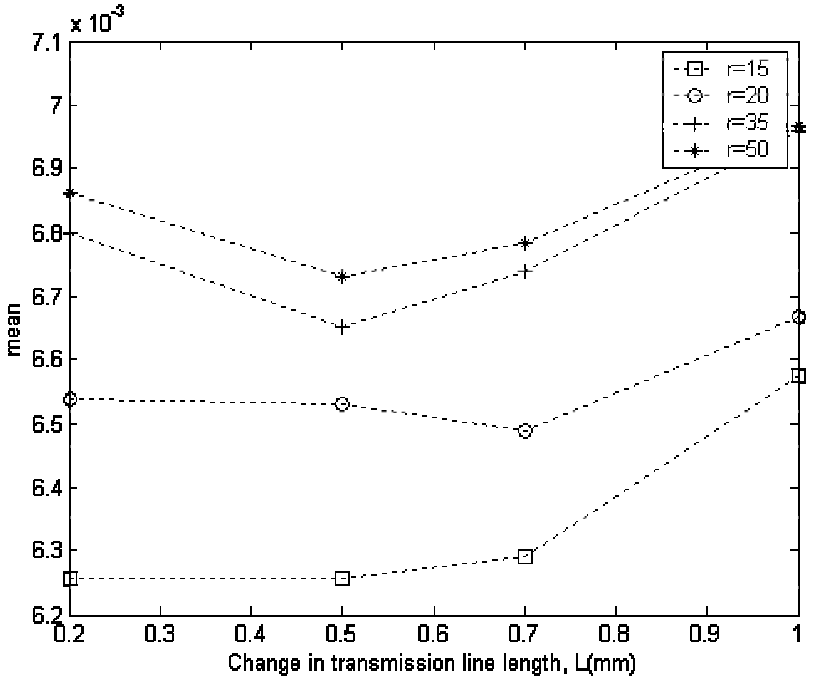

Figure 5.3: Effect of ΔL on means for Ω_{Arel}, N=4

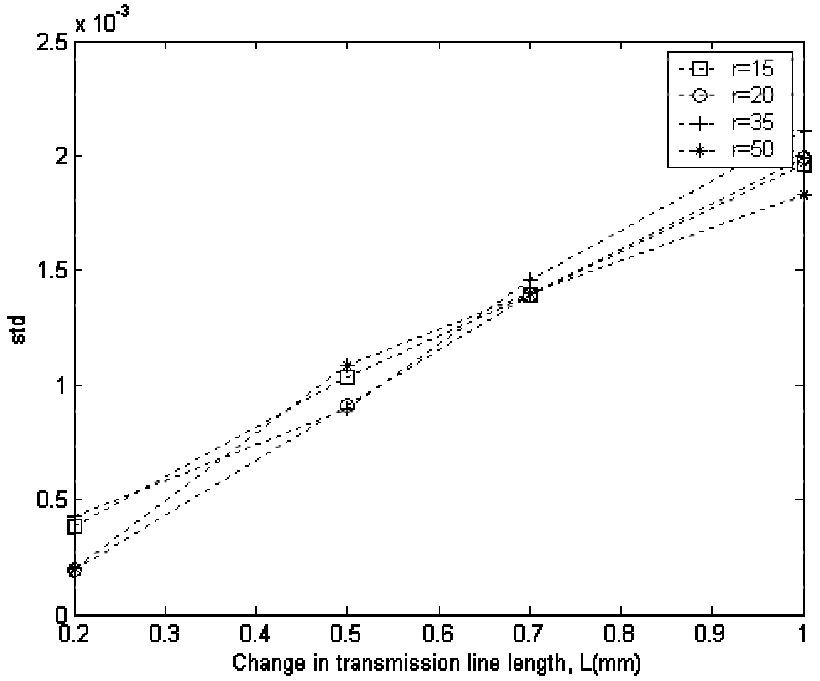

Figure 5.4: Effect of ΔL on standard deviations for Ω_{Arel}, N=4

Figure 5.3 shows an almost constant mean for the angle Ω_{Arel} with small changes brought due to the transmission line length errors. With increasing range, the error in the mean is greater. Figure 5.4 shows the increasing standard deviation with increasing error in transmission line lengths. Therefore, the results are consistent.

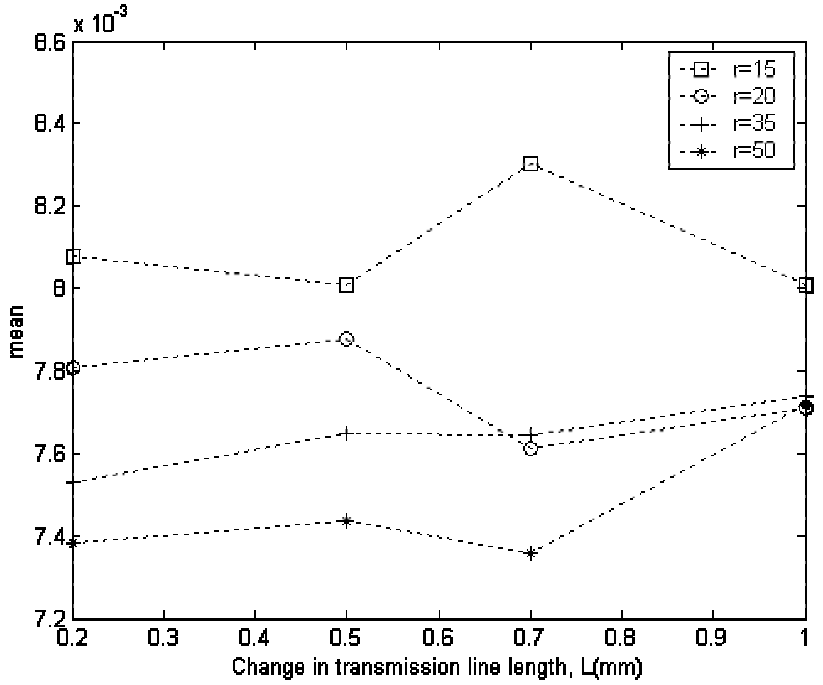

Figure 5.5: Effect of ΔL on means for Ω_{Brel}, N=4

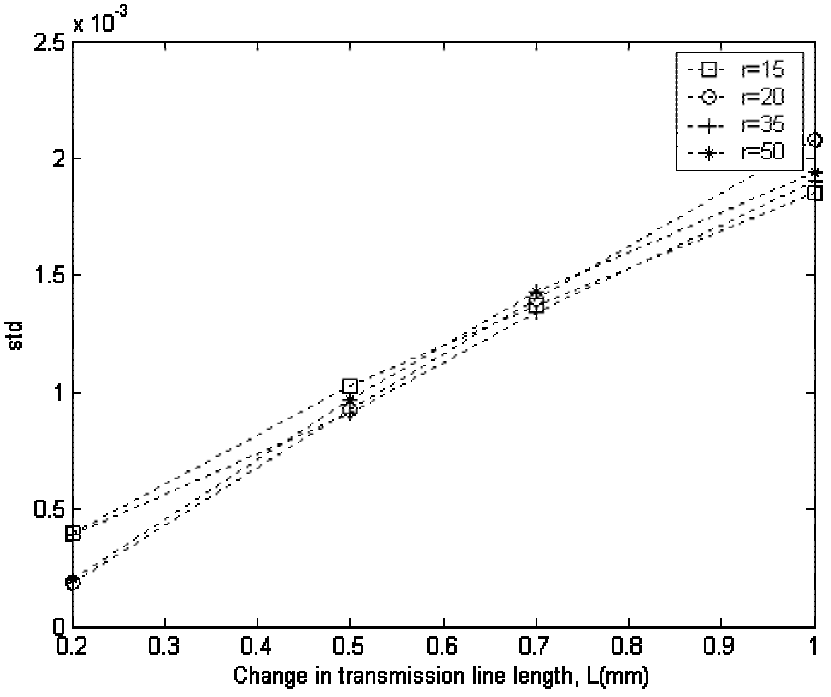

Figure 5.6: Effect of ΔL on standard deviations for Ω_{Brel}, N=4

Figure 5.5 shows the error parameter for Ω_{Brel} as was the case in Figure 5.3. However, it reflects the opposite trend with increasing range. This is the case because any

inconsistencies in the angles give greater error. The range estimation formula is dependent on the smallest of errors.

5.2.2 Errors using phase shifter changes

The following figures show the trends that Ω_{Arel}, Ω_{Brel}, and r_{rel} reflect when data for Table 5.2 is brought together.

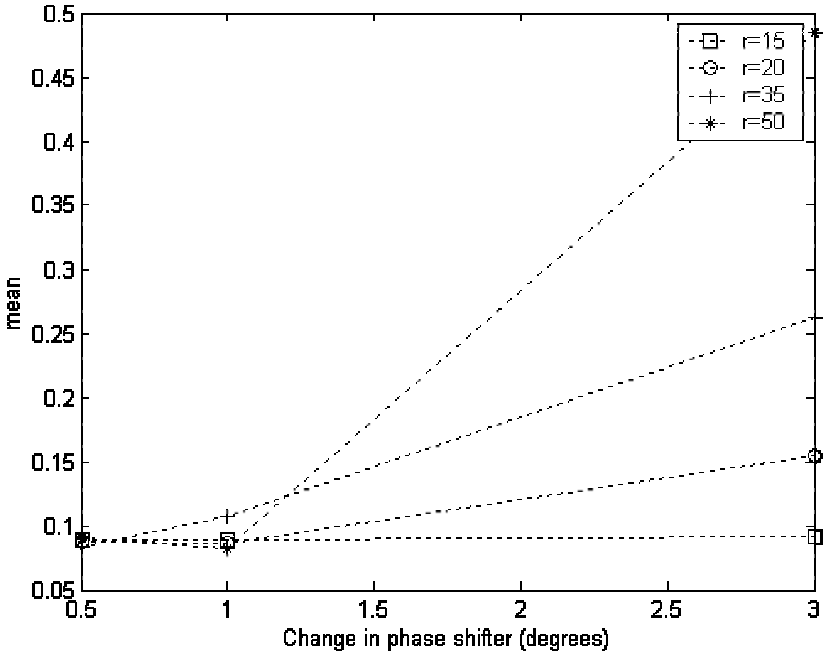

Figure 5.7: Effect of ΔP on means for r_{rel}, N=4

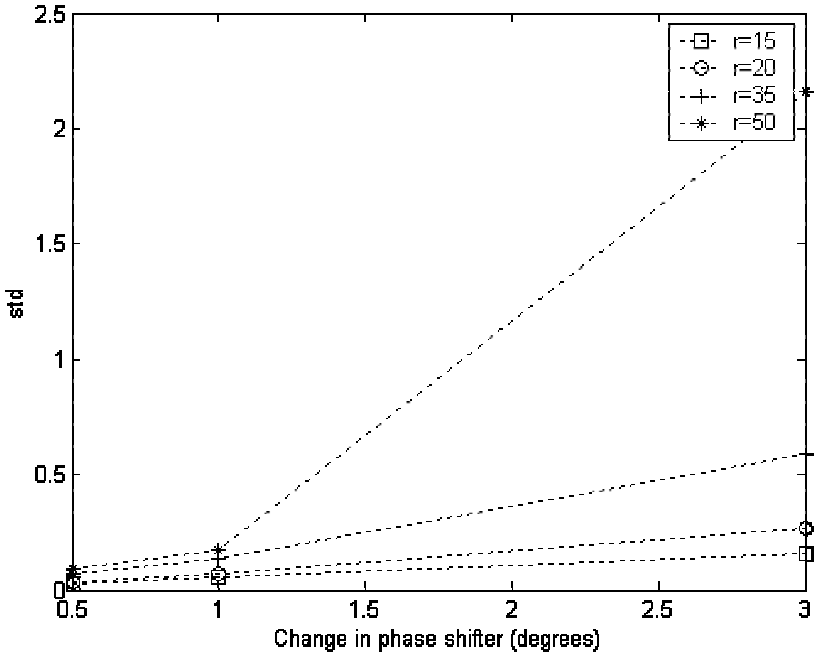

Figure 5.8: Effect of ΔP on standard deviations for r_{rel}, N=4

Figures 5.7 and 5.8 show that the range errors increase with increasing differences in the eight phase shifter angle errors. Standard deviations follow the trends for increasing means.

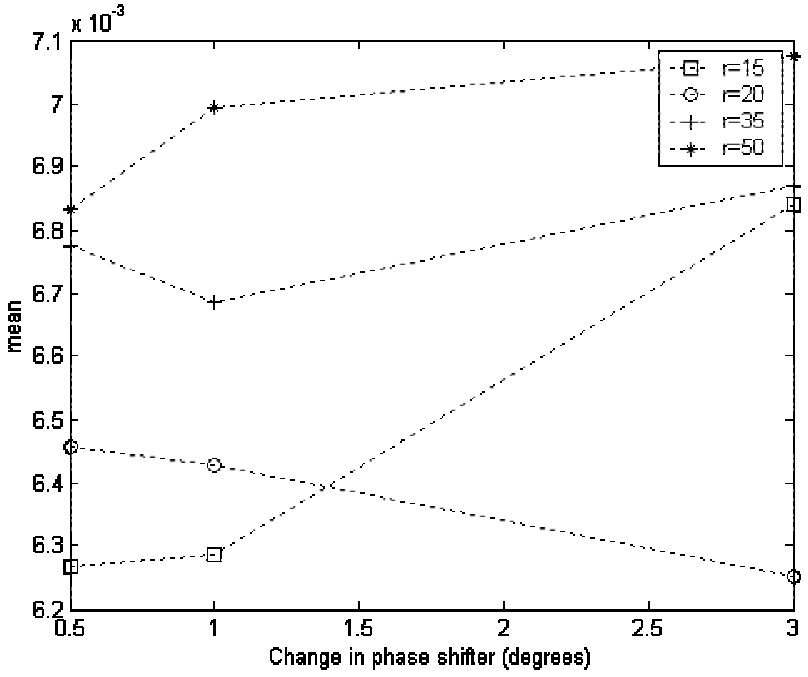

Figure 5.9: Effect of ΔP on means for Ω_{Arel}, N=4

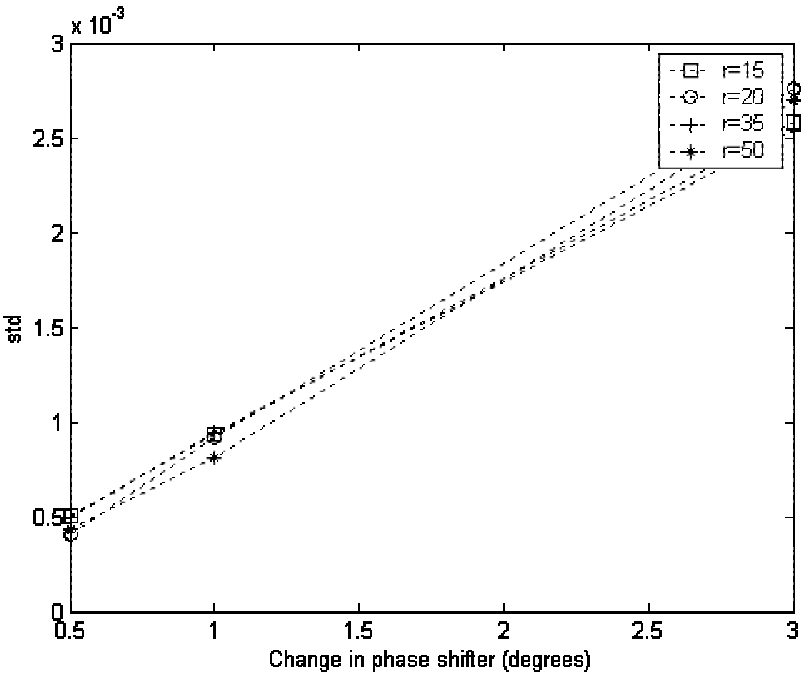

Figure 5.10: Effect of ΔP on standard deviations for Ω_{Arel}, N=4

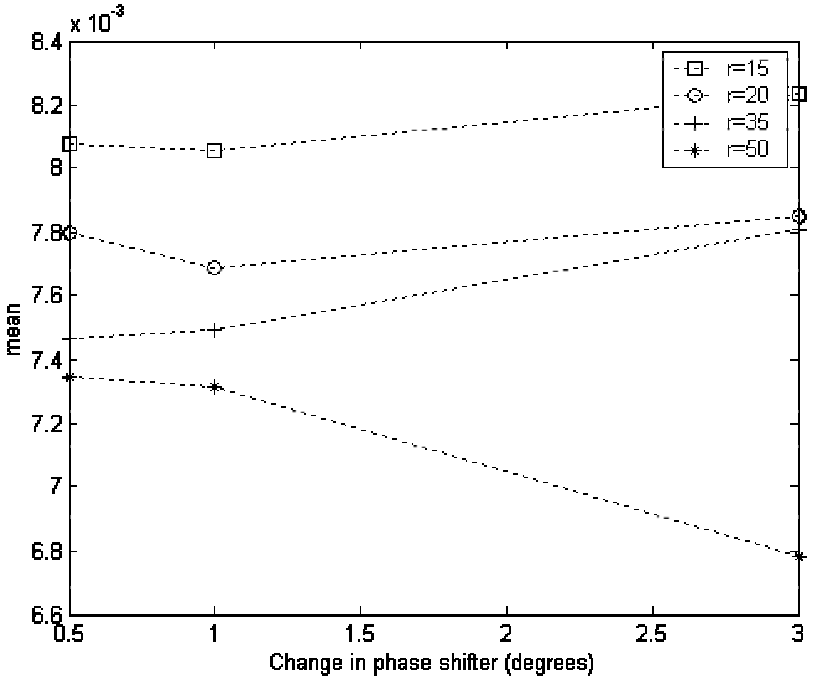

Figure 5.11: Effect of ΔP on means for Ω_{Brel}, N=4

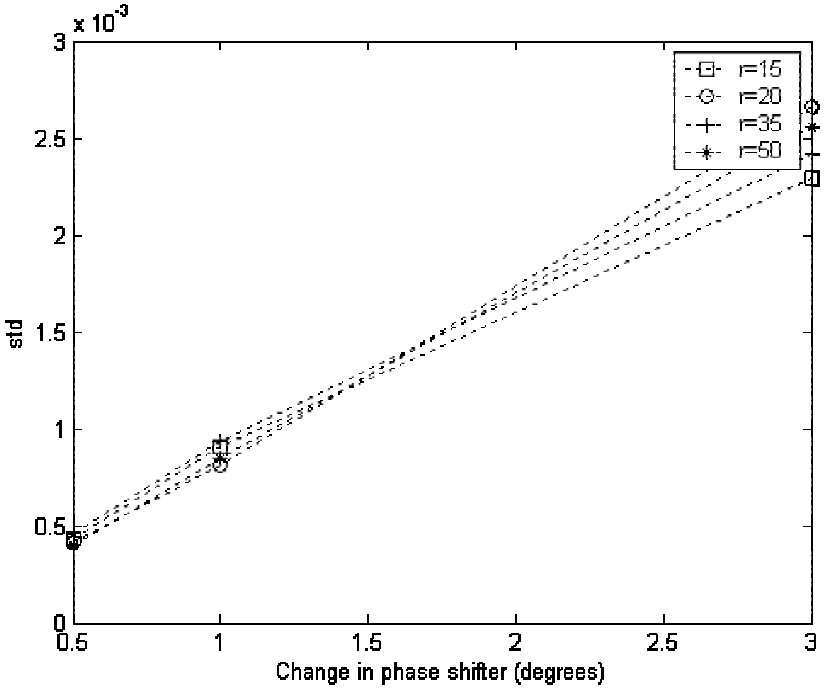

Figure 5.12: Effect of ΔP on standard deviations for Ω_{Brel}, N=4

The results for angle errors are consistent. Comparing Figure 5.9 to Figure 5.11, it can be seen that the former has increasing errors for relative means with increasing emitter ranges. However, the latter gives us the opposite trend. This can be attributed to the sensitivity of the range estimation algorithm to the errors in estimated angles for both the arrays. Standard deviations for Ω_{Arel} and Ω_{Brel} show the increasing trends which correspond to the increasing errors with range. This is similar to the case for transmission line lengths.

5.2.3 Errors due to antenna mismatch

The following figures show the trends that Ω_{Arel}, Ω_{Brel}, and r_{rel} reflect when data for Table 5.3 is brought together.

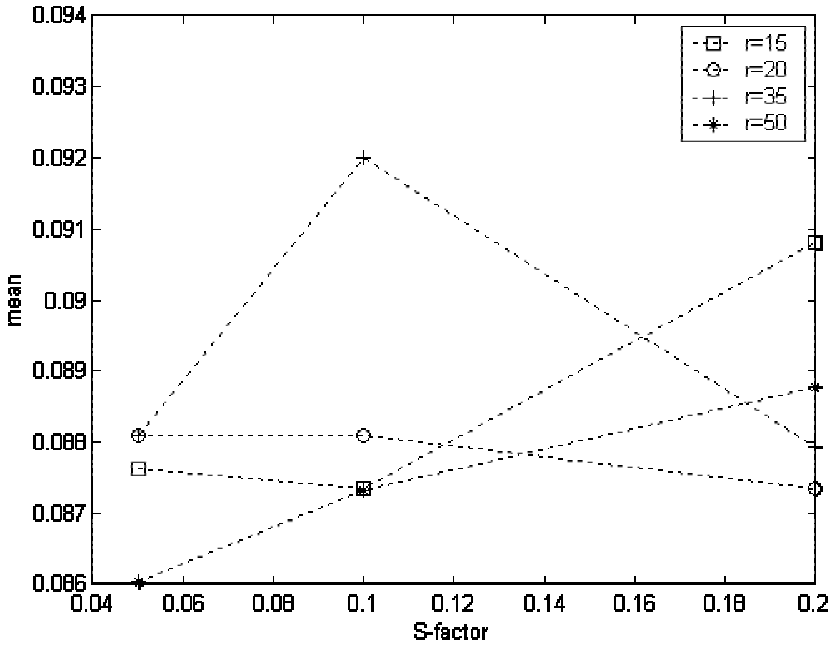

Figure 5.13: Effect of antenna mismatch on means for r_{rel}, N=4

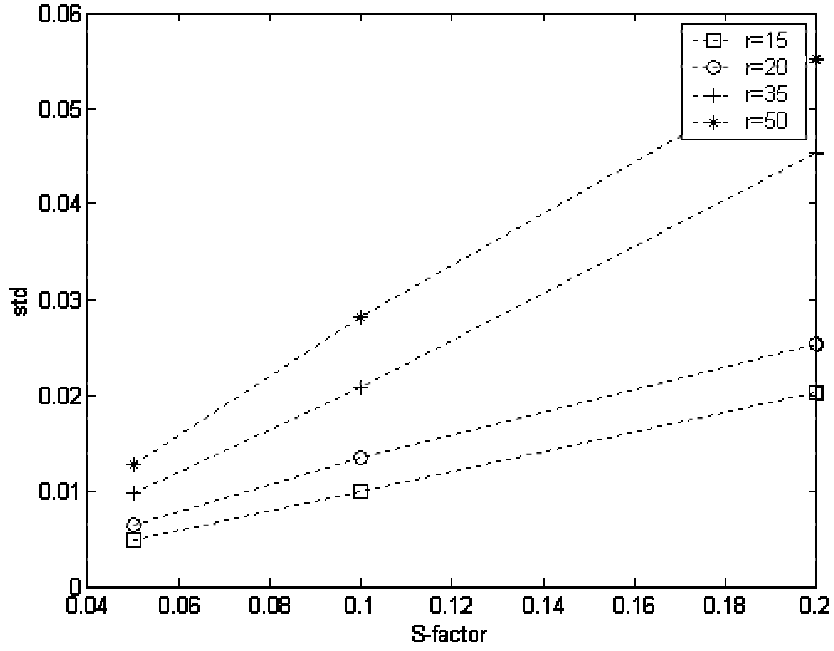

Figure 5.14: Effect of antenna mismatch on standard deviations for r_{rel}, N=4

Although Figure 5.13 does not show an increasing trend in error with increasing randomness of the S-factor, we can see this very clearly in Figure 5.14 showing the standard deviations for different ranges. Furthermore, it should be noted that the change in means for r_{rel} are small in comparison to the change for the phase shifter and transmission line length errors.

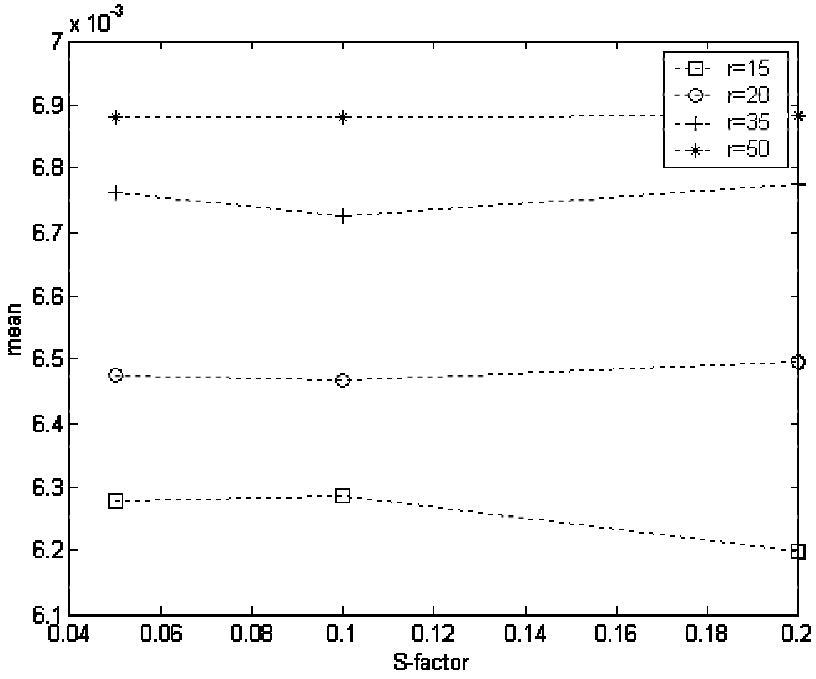

Figure 5.15: Effect of antenna mismatch on means for Ω_{Arel}, N=4

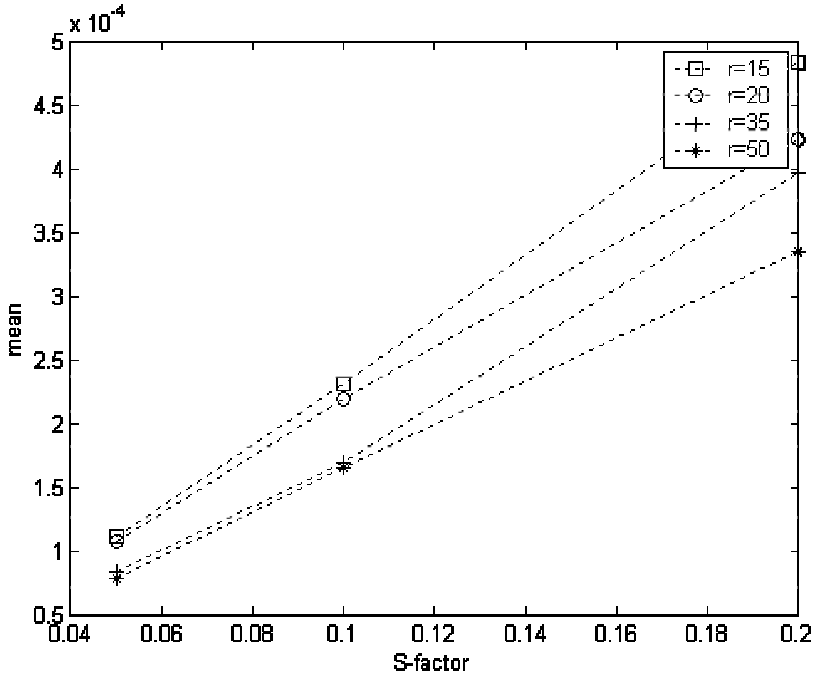

Figure 5.16: Effect of antenna mismatch on standard deviations for Ω_{Arel}, N=4

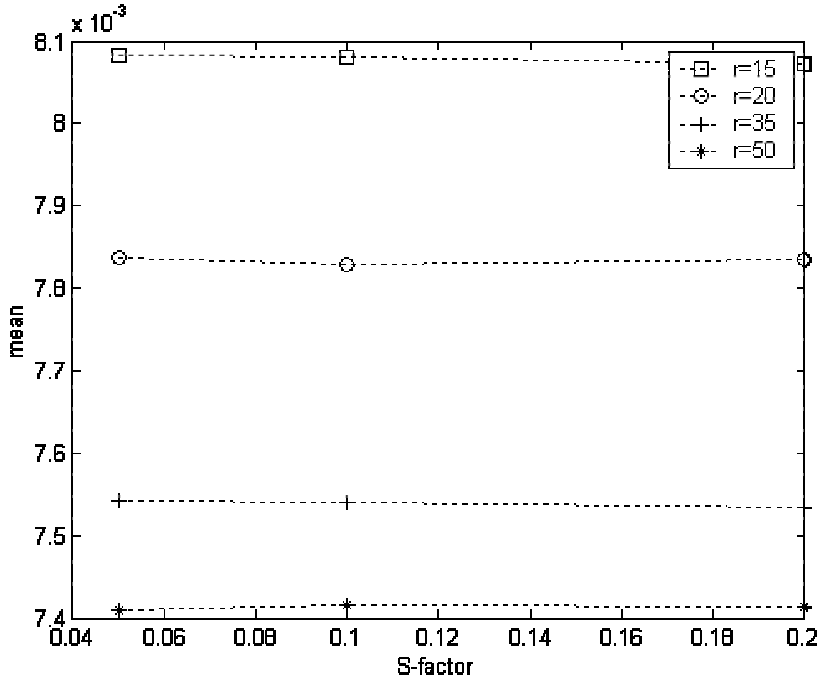

Figure 5.17: Effect of antenna mismatch on means for Ω_{Brel}, N=4

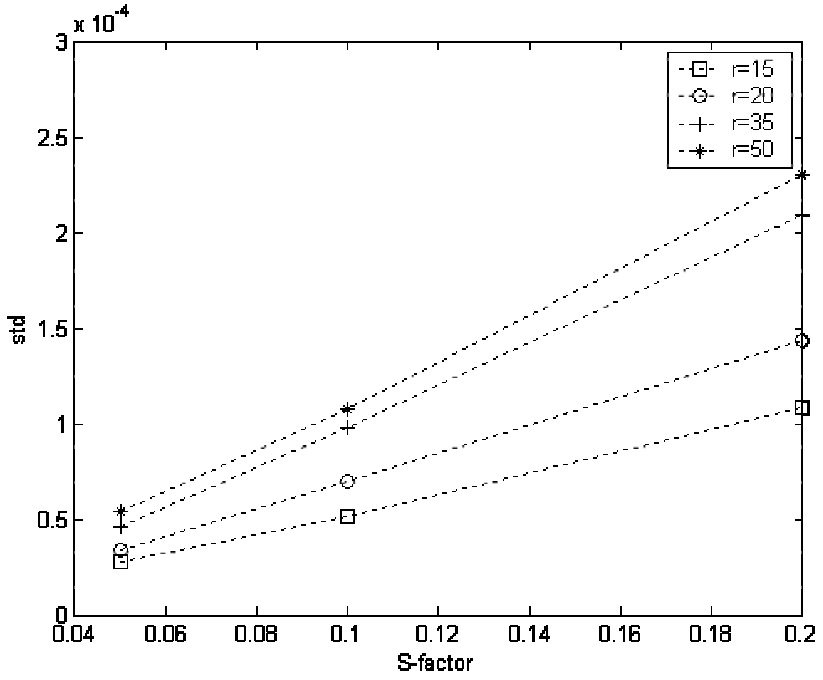

Figure 5.18: Effect of antenna mismatch on standard deviations for Ω_{Brel}, N=4

The results for angle errors are consistent. Comparing Figure 5.15 to Figure 5.17, it can be seen that the former has increasing errors for relative means with increasing emitter ranges. However, the latter gives us the opposite trend. Standard deviations show increasing trends.

5.2.4 Errors due to gain factor

The following figures show the trends that Ω_{Arel}, Ω_{Brel}, and r_{rel} reflect when data for Table 5.4 is brought together:

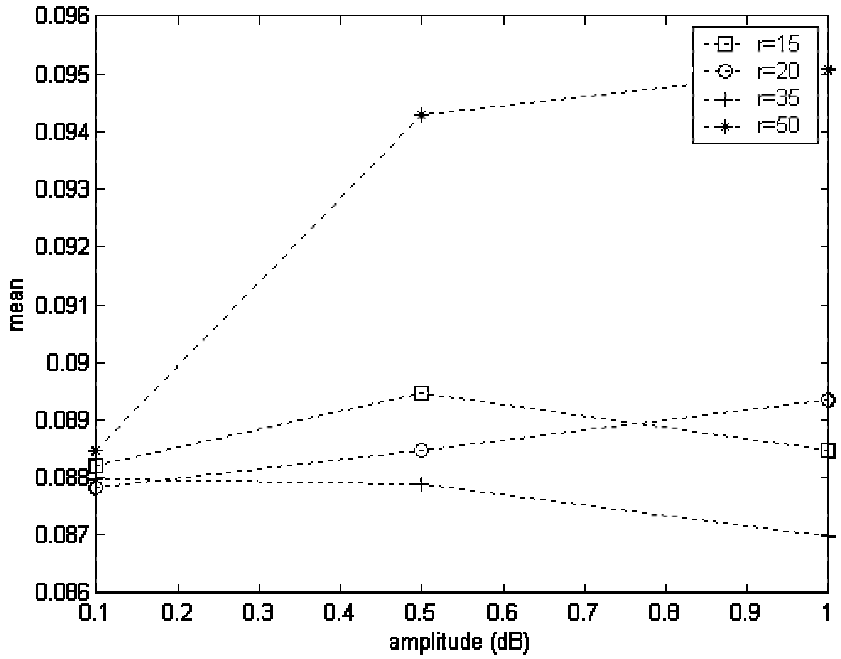

Figure 5.19: Effect of gain factor on means for r_{rel}, N=4

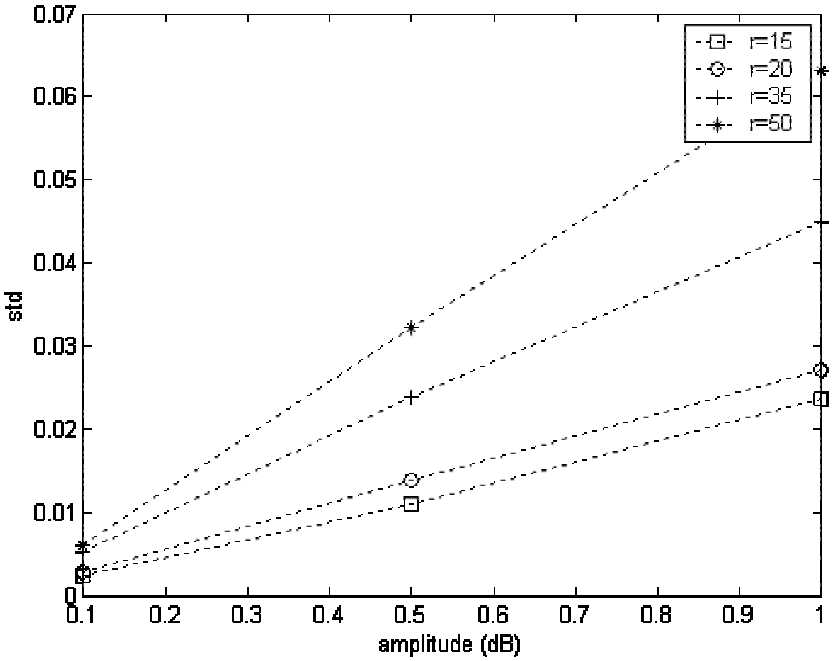

Figure 5.20: Effect of gain factor on standard deviations for r_{rel}, N=4

Although Figure 5.19 does not show a clear trend of increase with increasing amplitude changes, Figure 5.20 shows a very visible trend with range. Also, it should be noted that the effect of amplitude is small as standard deviations do not increase more than 0.07 for 1dB gains. The maximum change in means brought about by the amplitude is a factor of 0.1. This represents a 10% error in the estimated range.

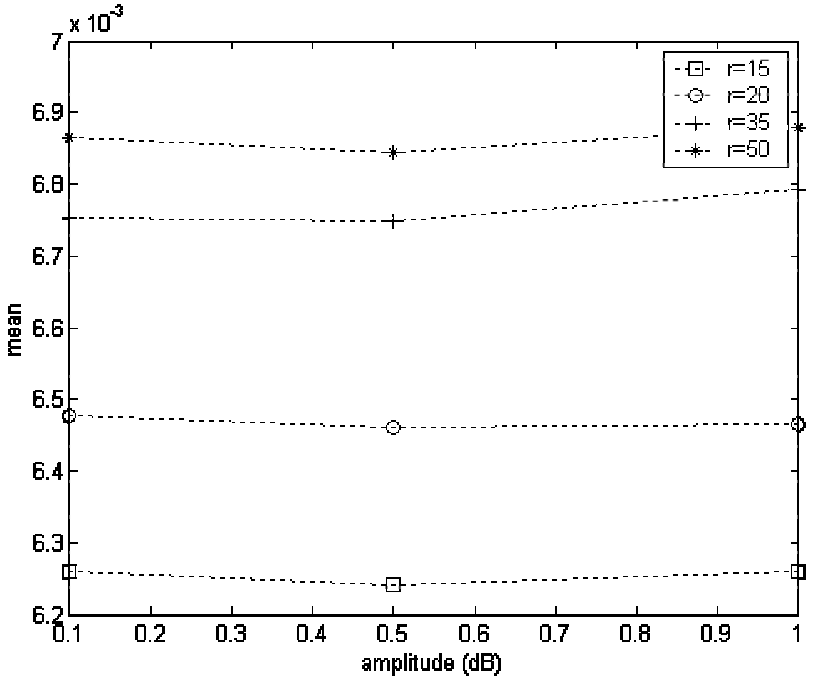

Figure 5.21: Effect of gain factor on means for Ω_{Arel}, N=4

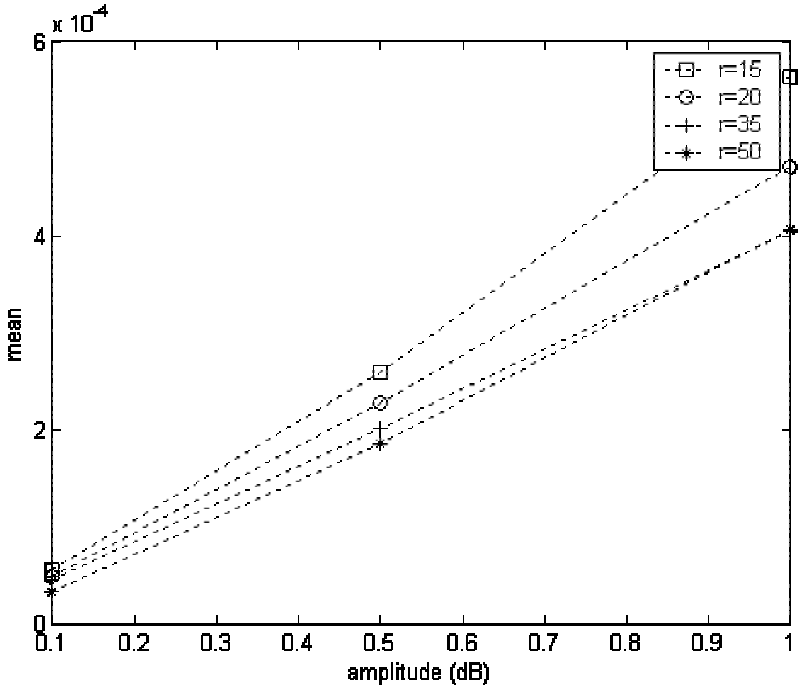

Figure 5.22: Effect of gain factor on standard deviations for Ω_{Arel}, N=4

Figures 5.21 and 5.22 show the effect of the gain factor on Ω_{Arel}. The maximum change in mean is approximately $6.9\text{x}10^{-3}$. The standard deviations show trends of increase towards the maximum value of $6\text{x}10^{-4}$.

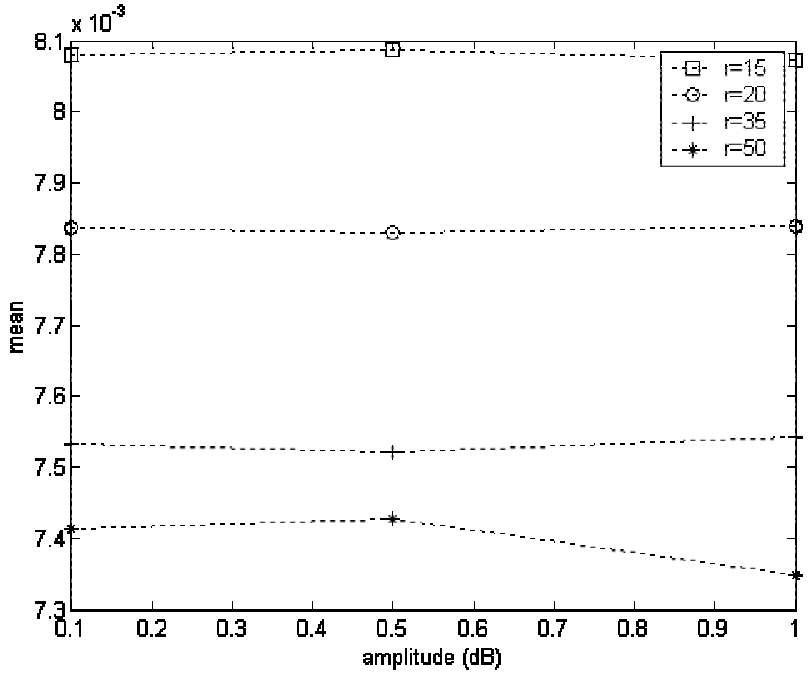

Figure 5.23: Effect of gain factor on means for Ω_{Brel}, N=4

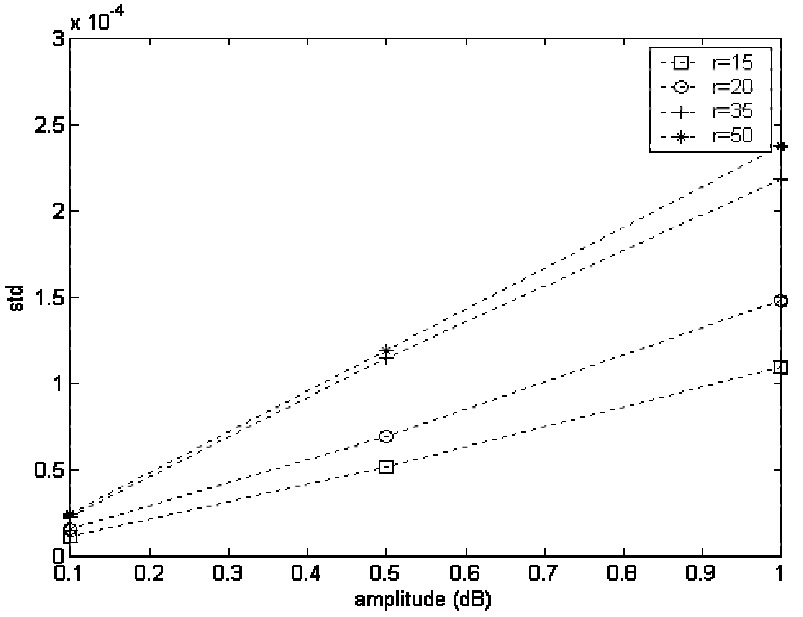

Figure 5.24: Effect of gain factor on standard deviations for Ω_{Brel}, N=4

Figures 5.23 and 5.24 show the effect of the gain factor on Ω_{Brel}. The maximum change in mean is approximately $8.1\text{x}10^{-3}$. The standard deviations show trends of increase towards the maximum value of $3\text{x}10^{-4}$. However, it should be noted that the trends oppose those presented in Figures 5.21 and 5.22.

5.2.5 Errors due to IF mismatch

The following figures show the trends that Ω_{Arel}, Ω_{Brel}, and r_{rel} reflect when data for Table 5.5 is brought together:

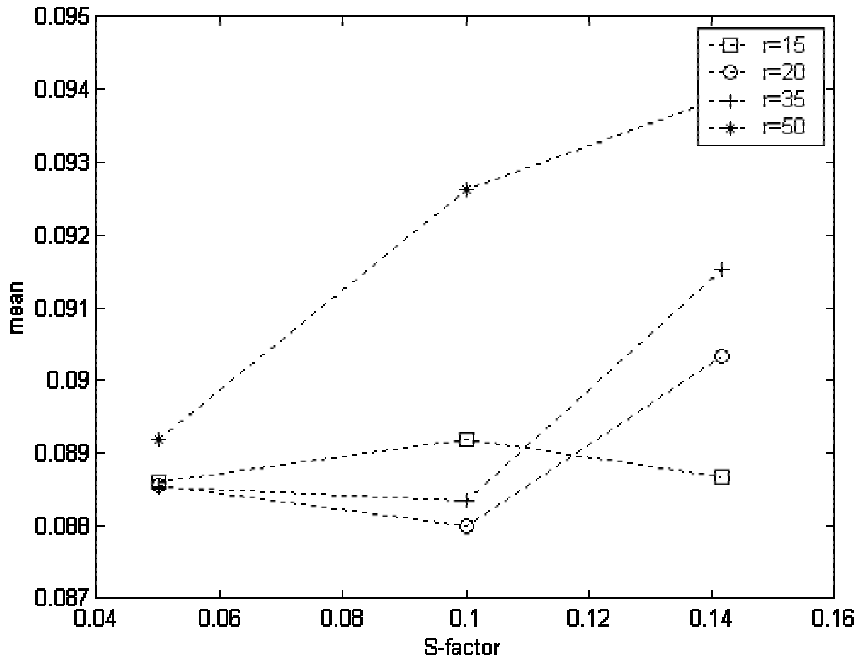

Figure 5.25: Effect of mixer mismatch on means for r_{rel}, N=4

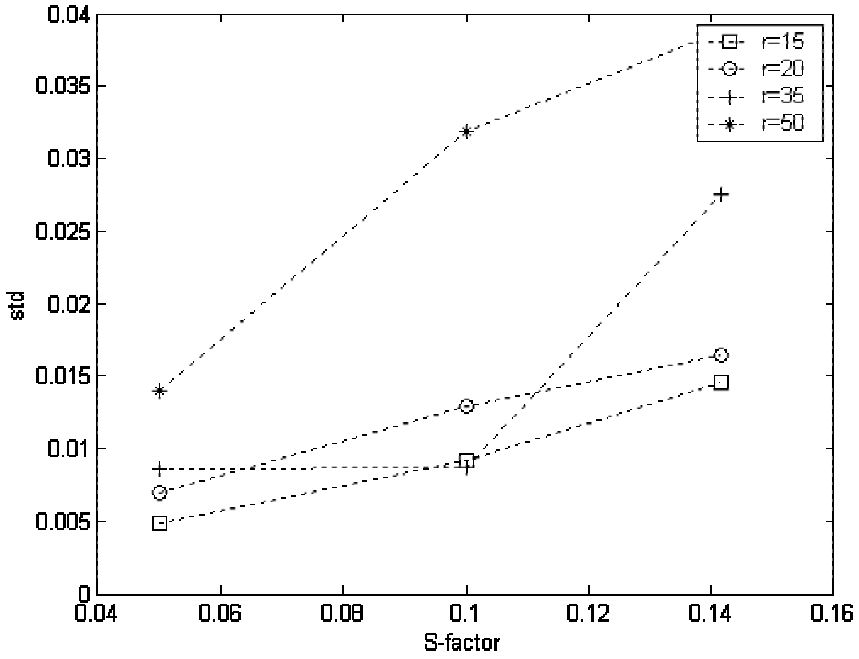

Figure 5.26: Effect of mixer mismatch on standard deviations for r_{rel}, N=4

Although Figure 5.25 does not show a trend, the standard deviations show clear increase with increasing S-factor randomness.

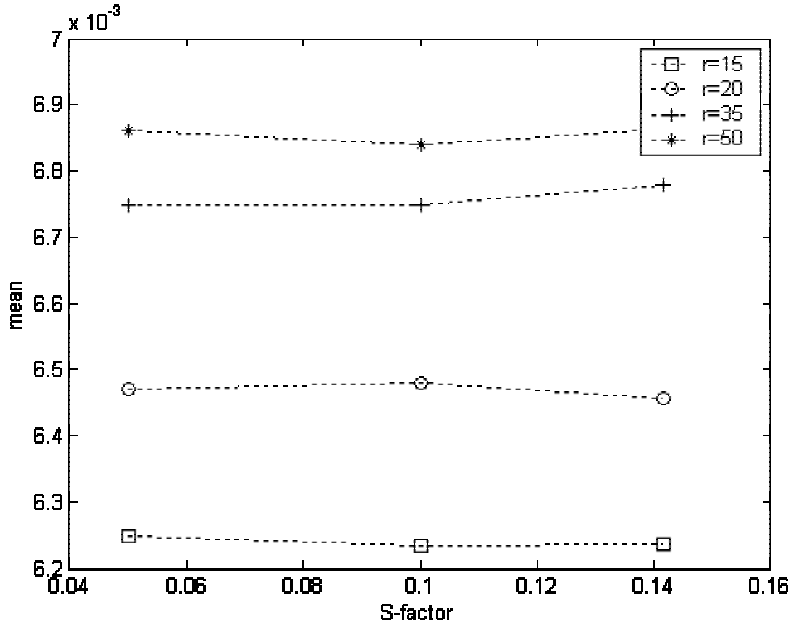

Figure 5.27: Effect of mixer mismatch on means for Ω_{Arel}, N=4

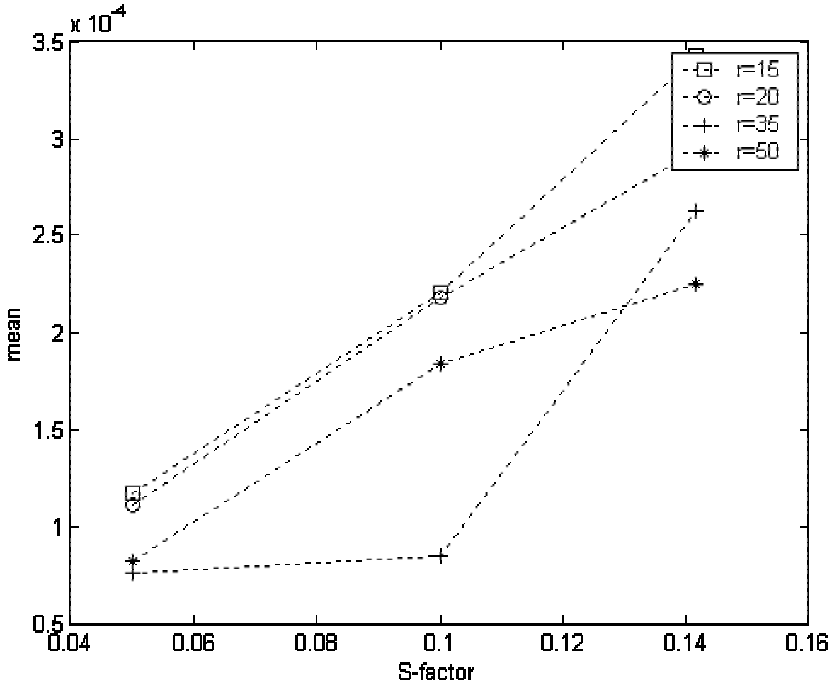

Figure 5.28: Effect of mixer mismatch on standard deviations for Ω_{Arel}, N=4

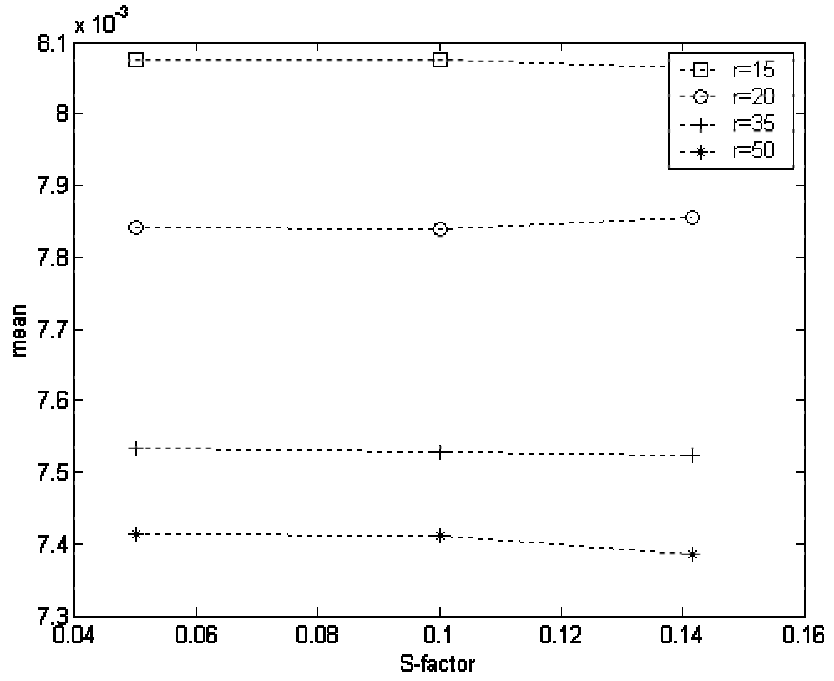

Figure 5.29: Effect of mixer mismatch on means for Ω_{Brel}, N=4

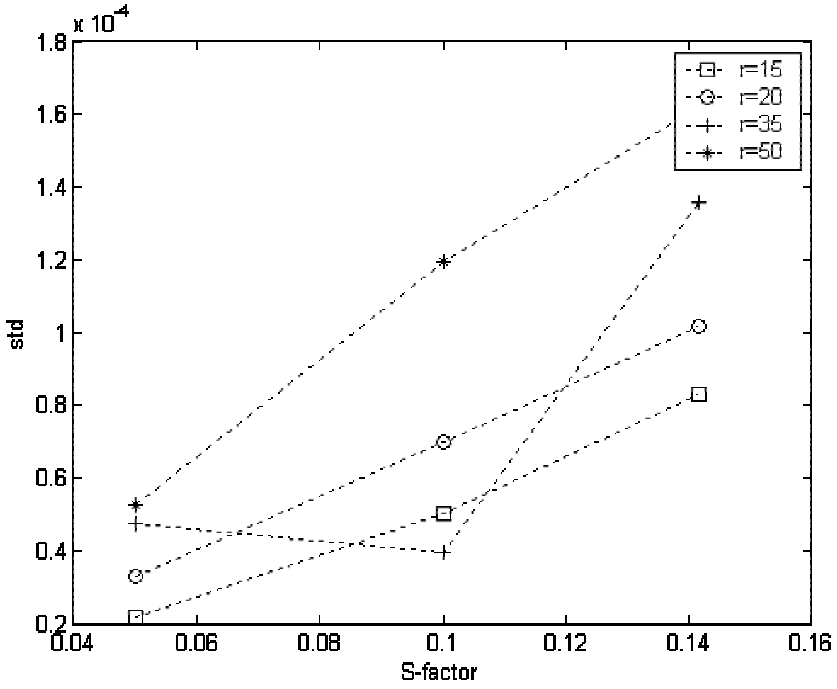

Figure 5.30: Effect of mixer mismatch on standard deviations for Ω_{Brel}, N=4

Figure 5.27 shows an almost constant mean for Ω_{Arel}. Also, as the range is increased, the mean errors increase. Figure 5.28 showing the standard deviations show an increasing trend. Also, it should be noted that 3.5×10^{-4} is the maximum change in standard deviations. Figure 5.29 shows an opposing trend when in comparison with Figure 5.27. However, it does show an increase in error with increasing randomness of the mismatch factor. From Figure 5.30, the maximum change in standard deviations for Ω_{Brel} can be taken as 1.8×10^{-4} for the 50m emitter range.

5.3 Simulations Using MRP with Extended 10 Element Arrays

The results for this section shall be compared with those presented in Section 5.2 so that the effects of coupling can be seen. Also, this shows the effectiveness of using the ten element array in comparison with the normal four element array without any

implementation of passive elements. The theoretical explanation for this has been presented earlier in Section 3.5.

5.3.1 Errors due to transmission line change

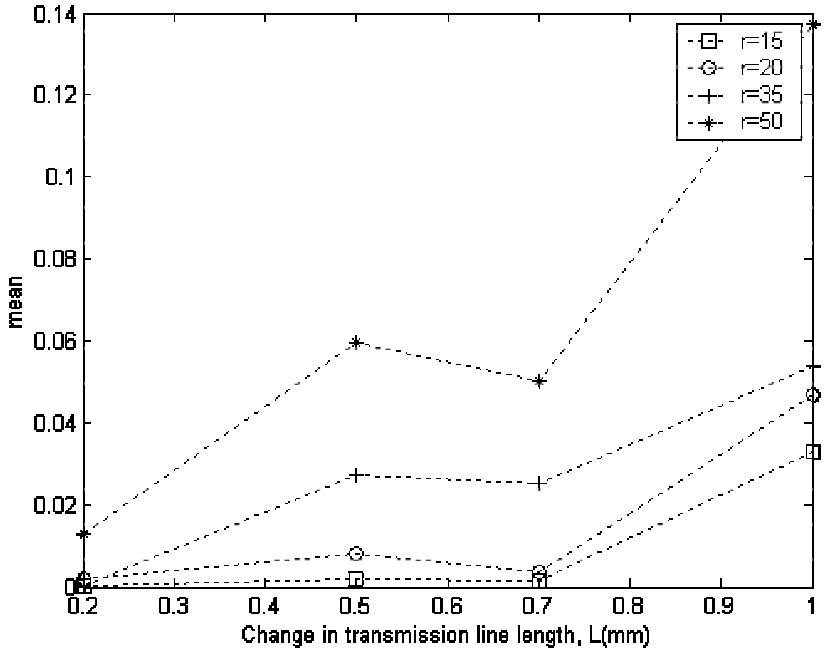

Figure 5.31: Effect of ΔL on means for r_{rel}, N=10

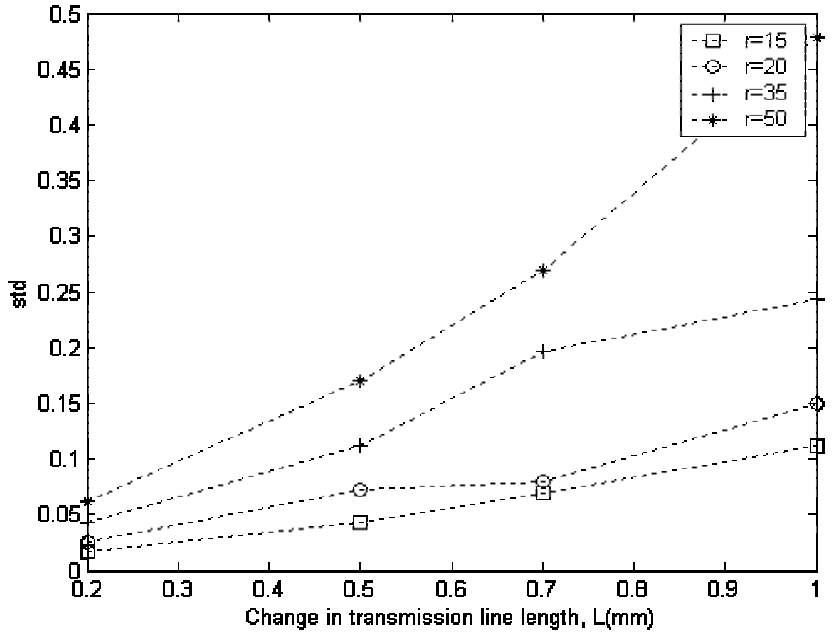

Figure 5.32: Effect of ΔL on standard deviations for r_{rel}, N=10

The effect of using an extended array is clearly visible when one compares Figures 5.31 and 5.32 with 5.1 and 5.2, respectively. Using 10 elements on each array gives us a maximum of 0.14 for mean of r_{rel}. With 4 elements, this factor was as high as 0.4. The standard deviations cross the 0.5 mark with 10 elements. For the 4 element case, the highest point is 0.9 as shown in Figure 5.2.

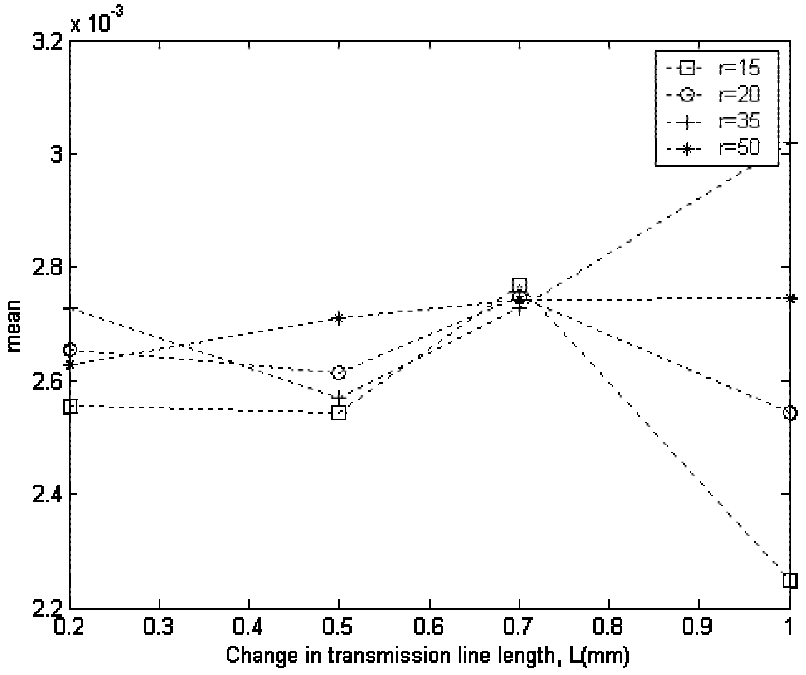

Figure 5.33: Effect of ΔL on means for Ω_{Arel}, N=10

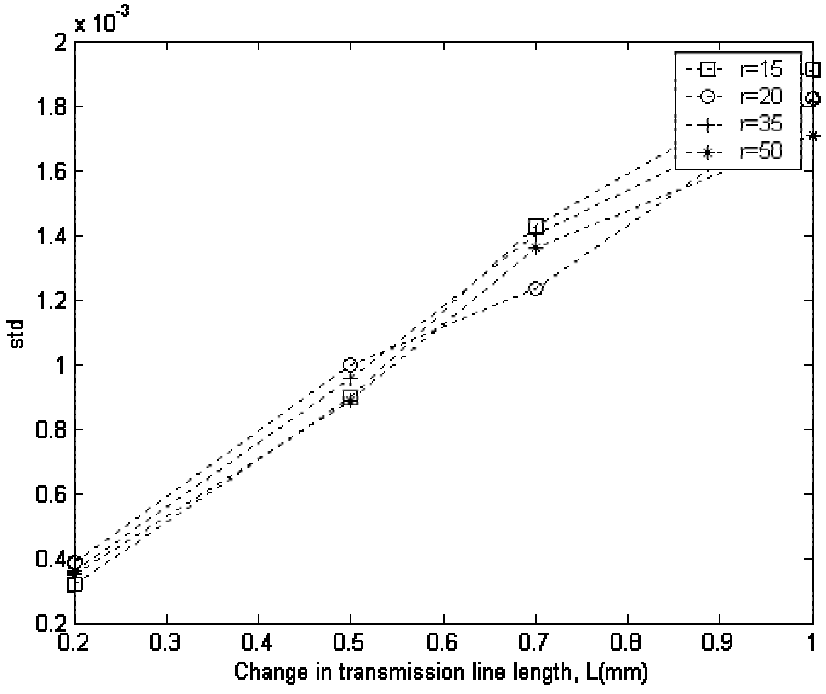

Figure 5.34: Effect of ΔL on standard deviations for Ω_{Arel}, N=10

Figure 5.33 does not show the mean trends very clearly. However, in comparison with Figure 5.3, we can see that the maximum point on the plot reduces from 7×10^{-3} to

3×10^{-3}. Also, the increasing trends can be seen from the standard deviations shown in Figure 5.34.

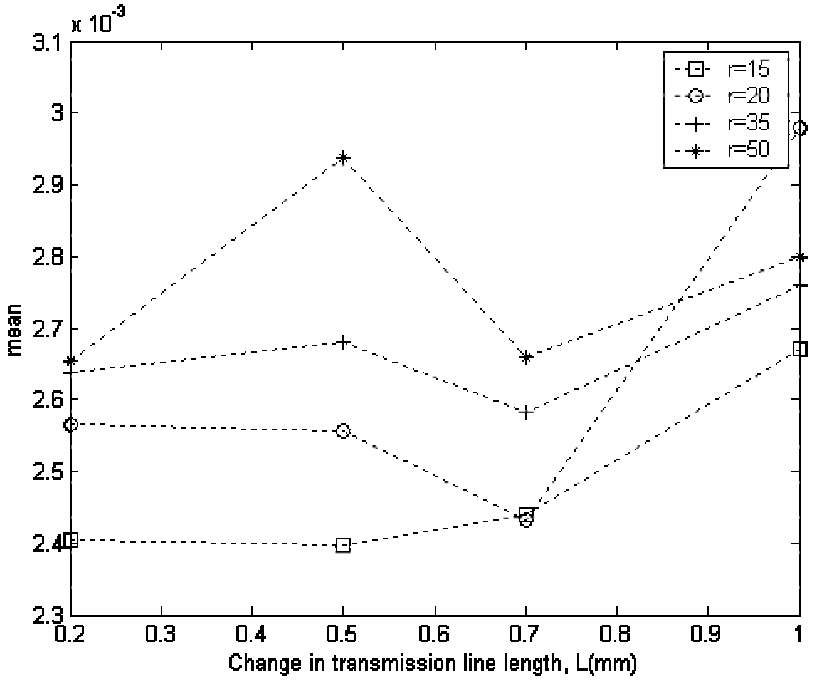

Figure 5.35: Effect of ΔL on means for Ω_{Brel}, N=10

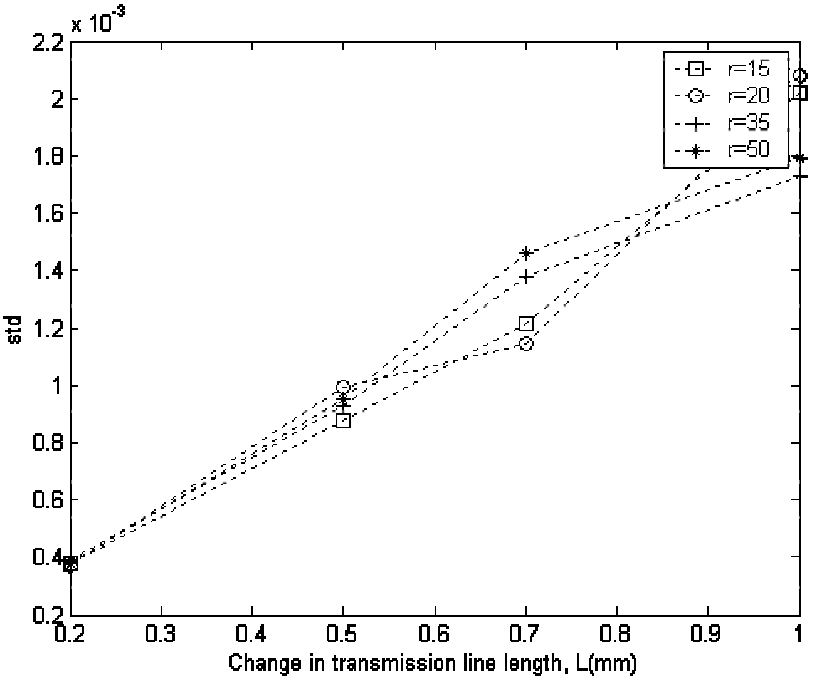

Figure 5.36: Effect of ΔL on standard deviations for Ω_{Brel}, N=10

Figure 5.35 can be compared with Figure 5.5 to see that the overall means drop for Ω_{Brel} when one uses the extended array. It is seen that the maximum point on the plot reduces from 8×10^{-3} to 3×10^{-3}.

5.3.2 Errors due to phase shifter changes

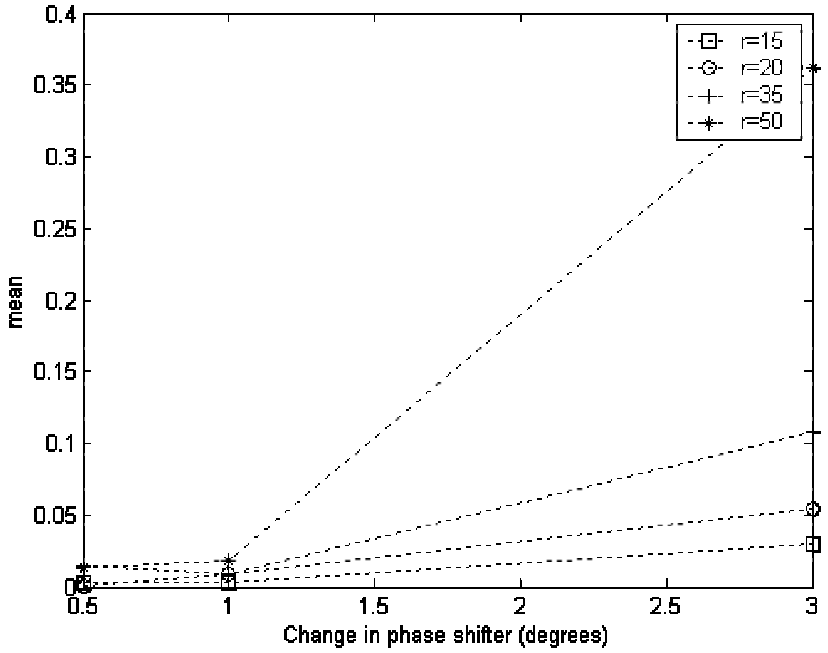

Figure 5.37: Effect of ΔP on means for r_{rel}, N=10

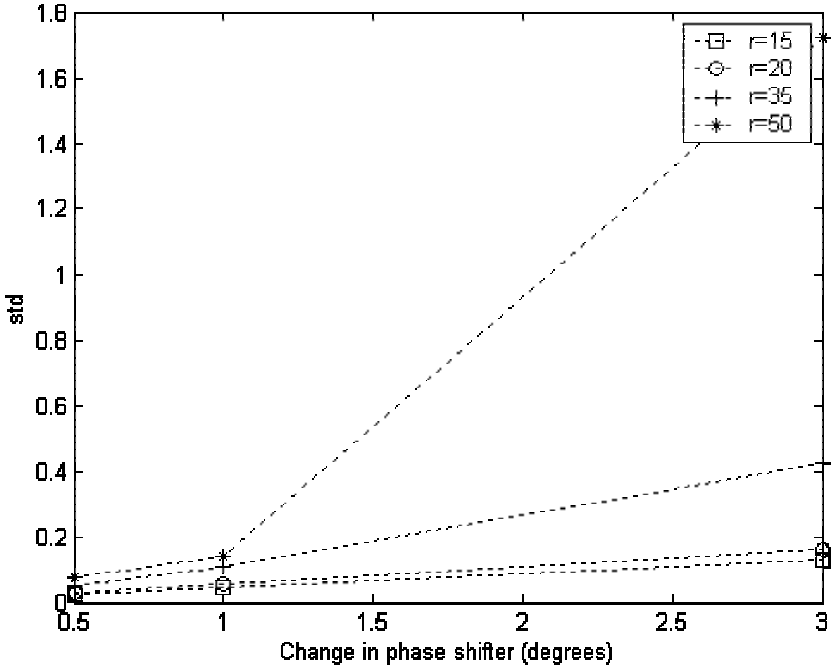

Figure 5.38: Effect of ΔP on standard deviations for r_{rel}, N=10

Figure 5.37 shows a maximum of 0.36 as the mean for r_{rel}. Using a four element array increases value to a 0.5. This represents a large increase in relative value. Also, it should be noted that these figures are magnifications of the figures representing transmission line length changes. Standard deviations follow the trends shown in the figure representing increase in relative means.

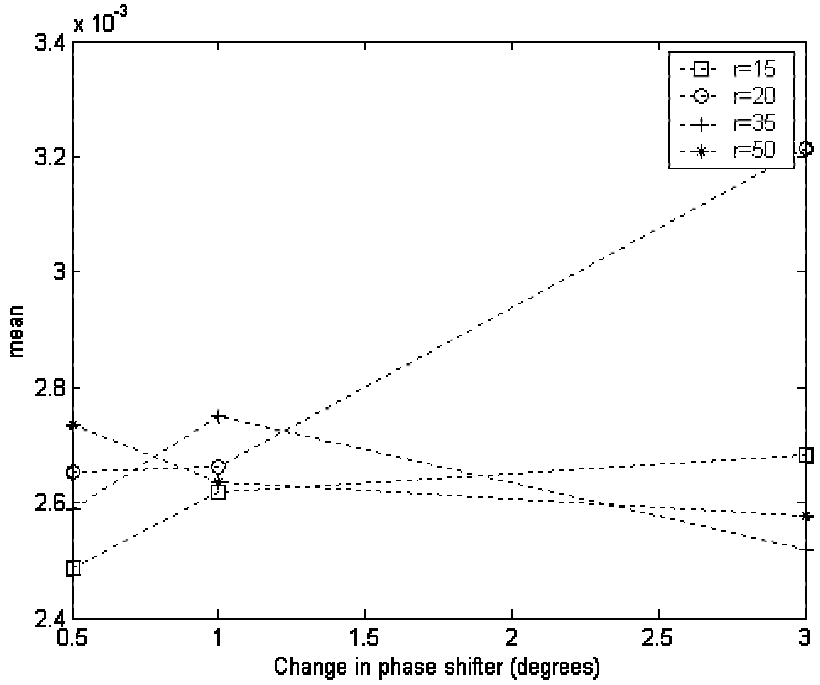

Figure 5.39: Effect of ΔP on means for Ω_{Arel}, N=10

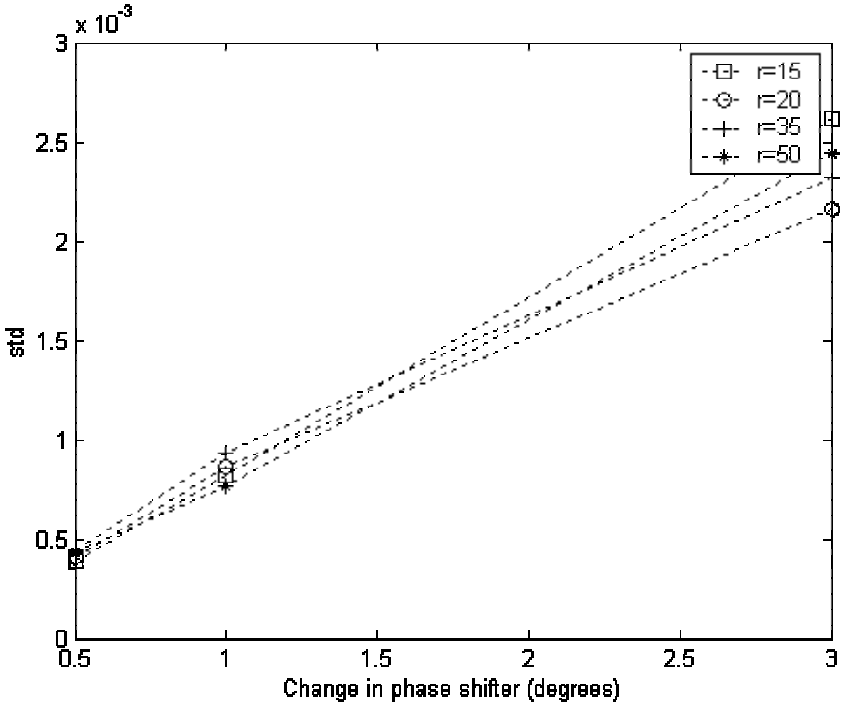

Figure 5.40: Effect of ΔP on standard deviations for Ω_{Arel}, N=10

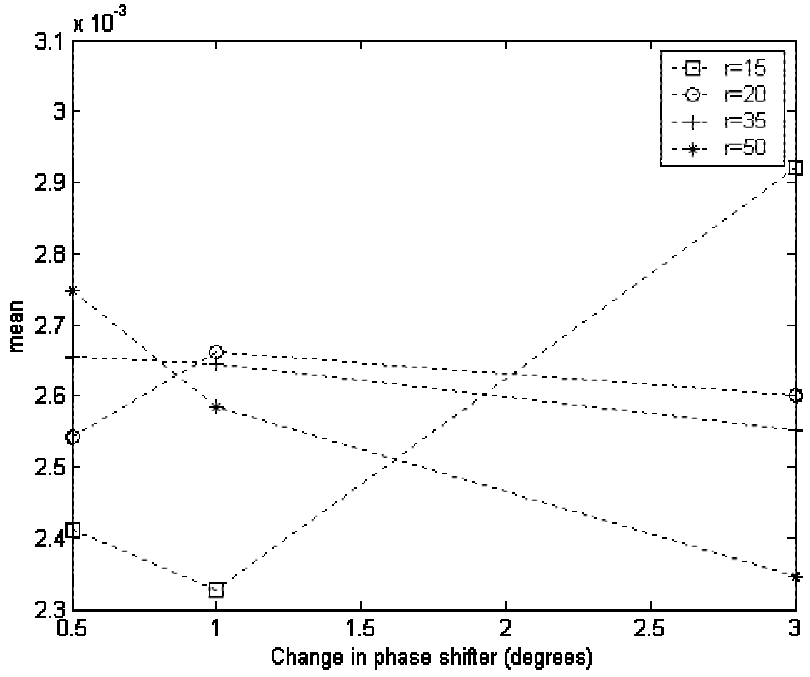

Figure 5.41: Effect of ΔP on means for Ω_{Brel}, N=10

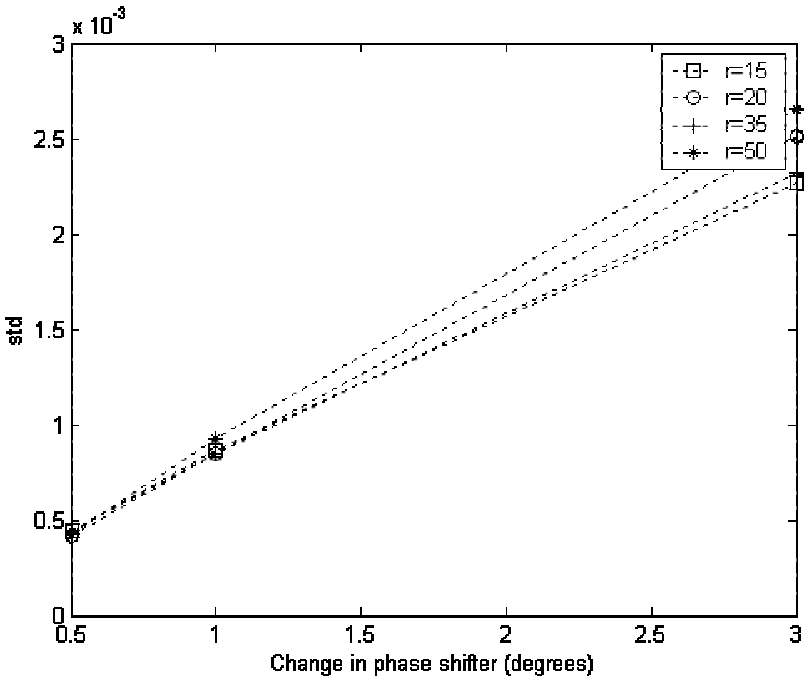

Figure 5.42: Effect of ΔP on standard deviations for Ω_{Brel}, N=10

Figure 5.39 shows a maximum value of 3×10^{-3} for the estimation of relative error in angle Ω_{Arel}. This is compared to the figure representing four elements with a maximum of 7×10^{-3}. The standard deviations show the same trends as before representing an increase in variation for the means. Furthermore, Figure 5.41 shows a maximum value of 2.9×10^{-3}. This is compared to Figure 5.11 representing four elements with a maximum of 8.2×10^{-3}. The standard deviations show a regular increase.

5.3.3 Errors due to antenna mismatch

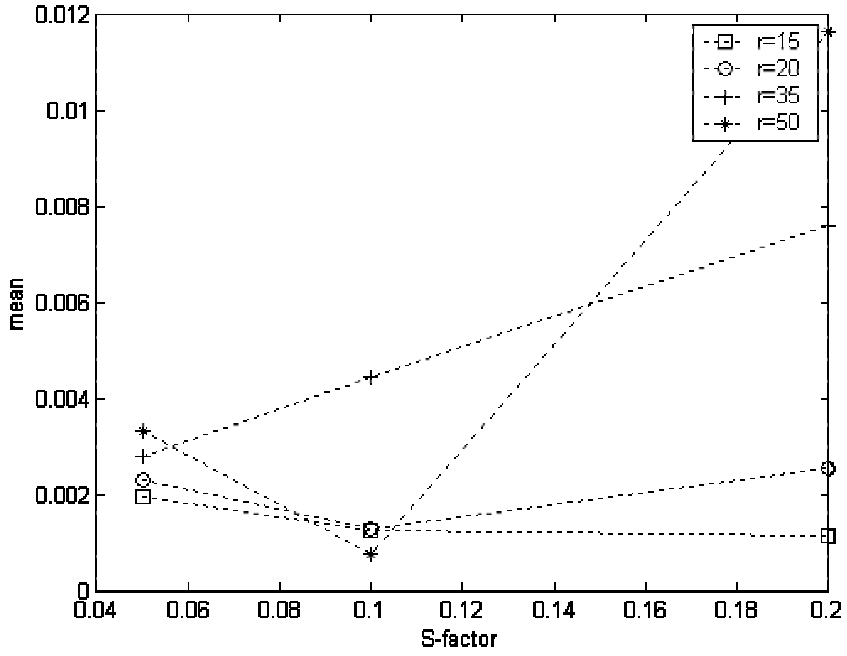

Figure 5.43: Effect of antenna mismatch on means for r_{rel}, N=10

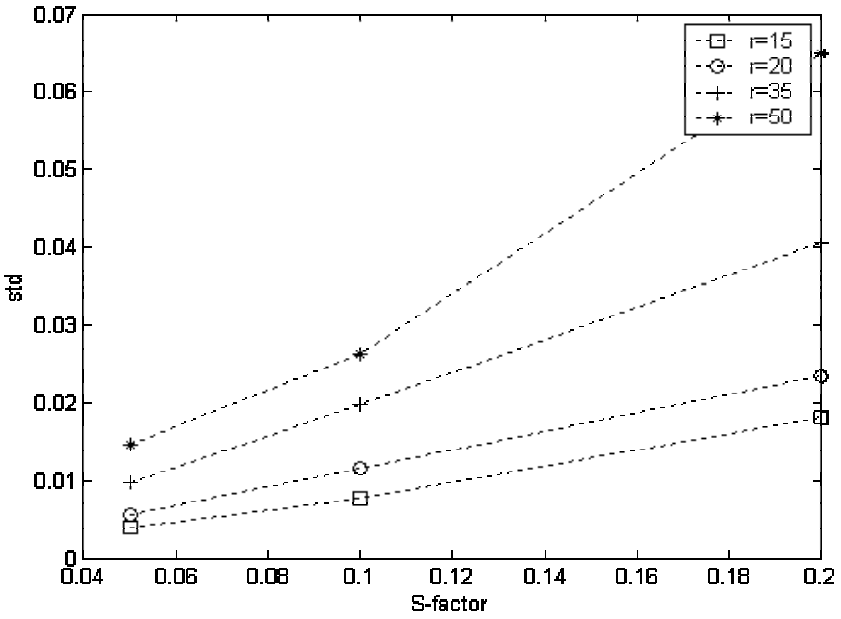

Figure 5.44: Effect of antenna mismatch on standard deviations for r_{rel}, N=10

With four elements the maximum mean for r_{rel} is 0.092. However, with the extended array, the maximum mean drops dramatically to 0.012. Figure 5.44 representing standard deviations show a constant increase.

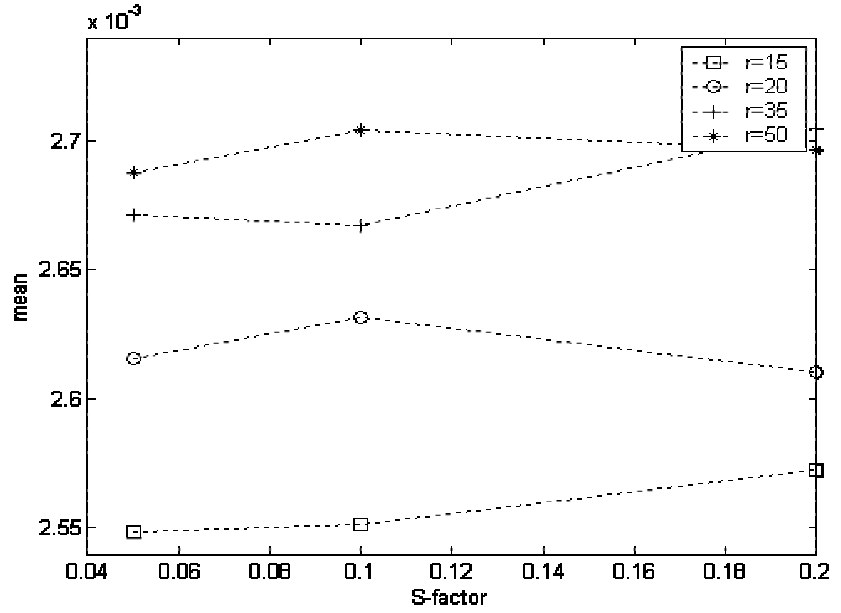

Figure 5.45: Effect of antenna mismatch on means for Ω_{Arel}, N=10

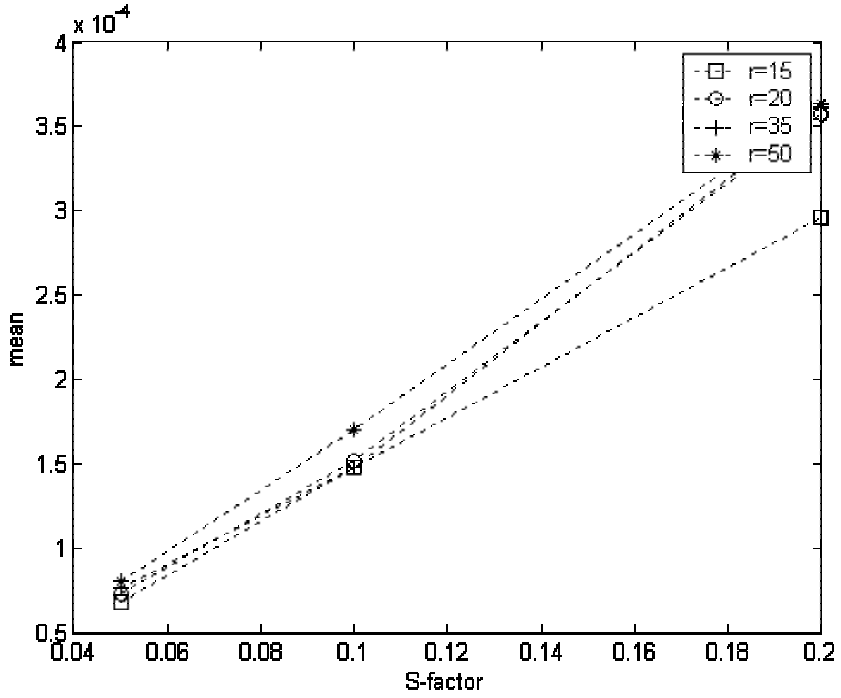

Figure 5.46: Effect of antenna mismatch on standard deviations for Ω_{Arel}, N=10

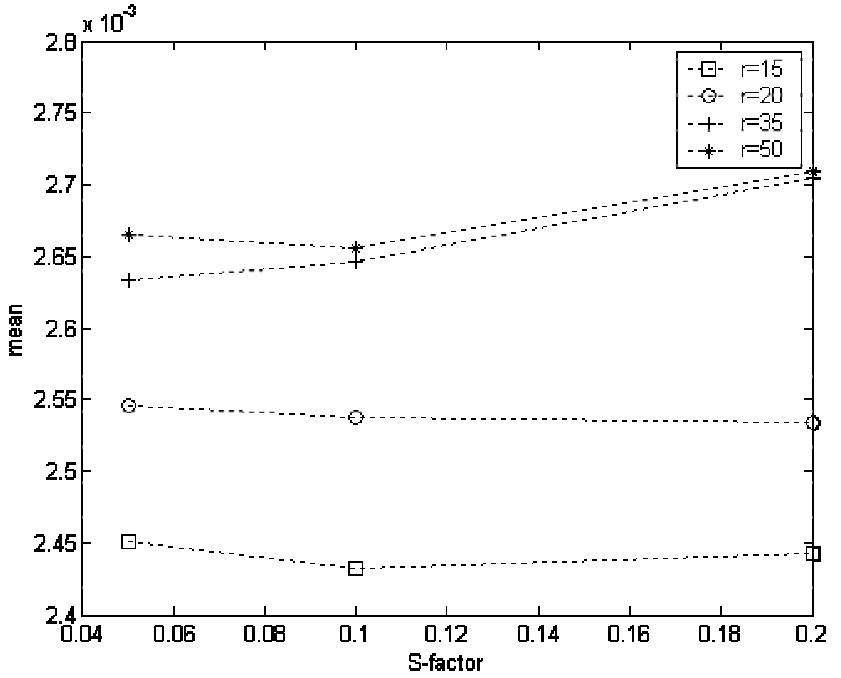

Figure 5.47: Effect of antenna mismatch on means for Ω_{Brel}, N=10

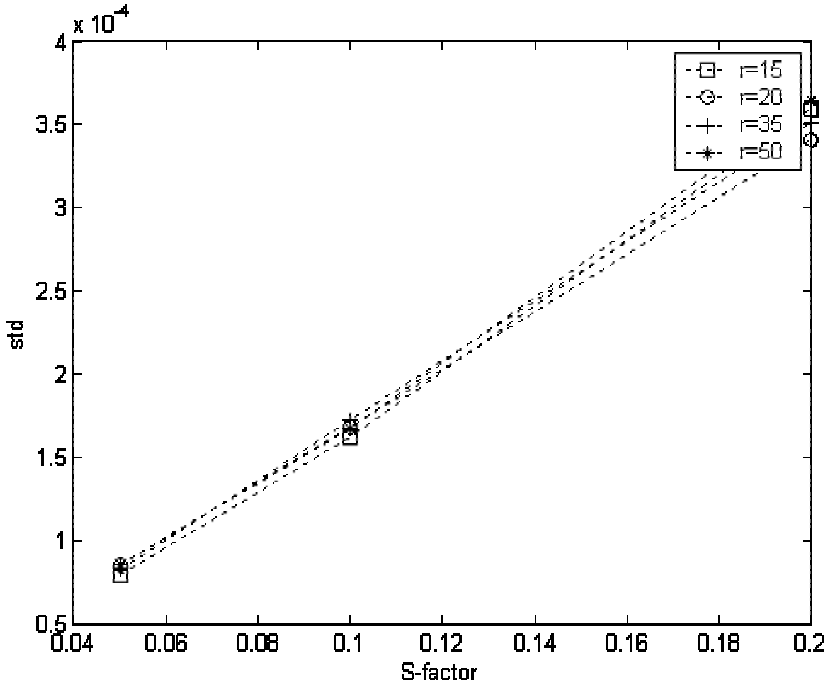

Figure 5.48: Effect of antenna mismatch on standard deviations for Ω_{Brel}, N=10

Figure 5.45 shows a maximum value of 2.5×10^{-3}. This is compared to the Figure 5.15 representing four elements with a maximum of 7×10^{-3}. Figure 5.47 shows a maximum value of 2.75×10^{-3}. This is compared to Figure 5.17 representing four elements with a maximum of 8.1×10^{-3}. The standard deviations show a regular increase.

5.3.4 Errors due to gain factor

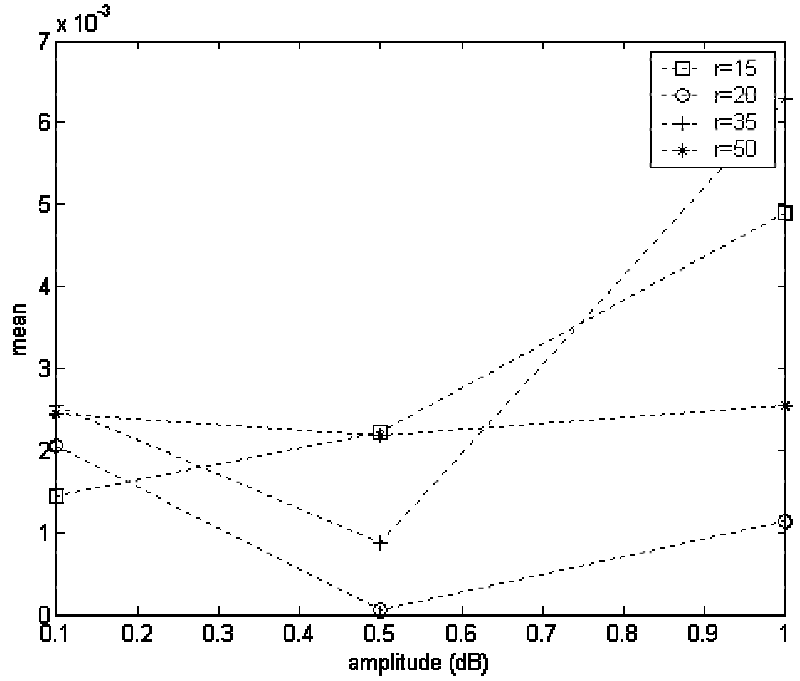

Figure 5.49: Effect of gain factor on means for r_{rel}, N=10

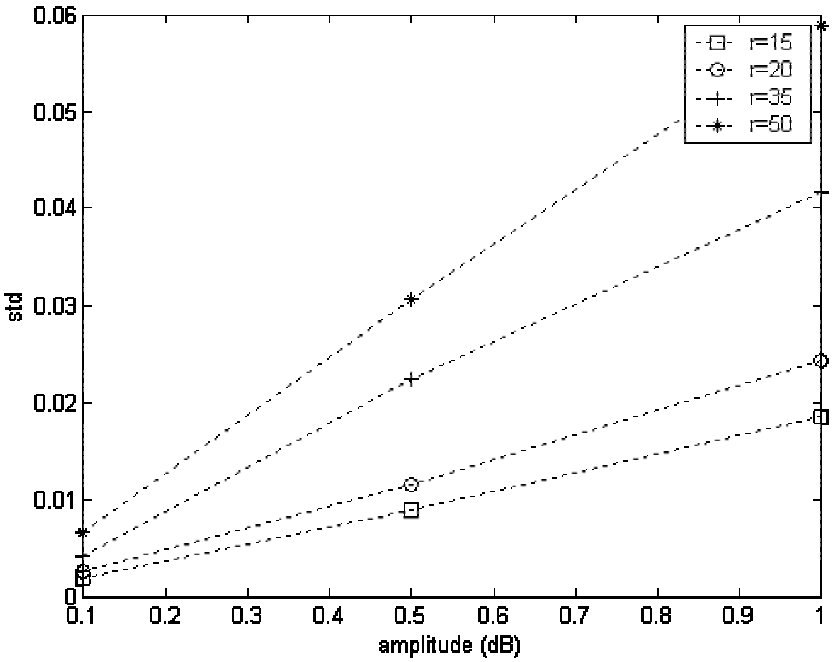

Figure 5.50: Effect of gain factor on standard deviations for r_{rel}, N=10

As shown by Figure 5.49, the effect of increasing the amplitude factor on the overall range estimation accuracy can be almost negligible. However, this is not the case with Figure 5.19 that represents the case for 4 elements with a maximum of 0.096. Standard deviations show a constant increase.

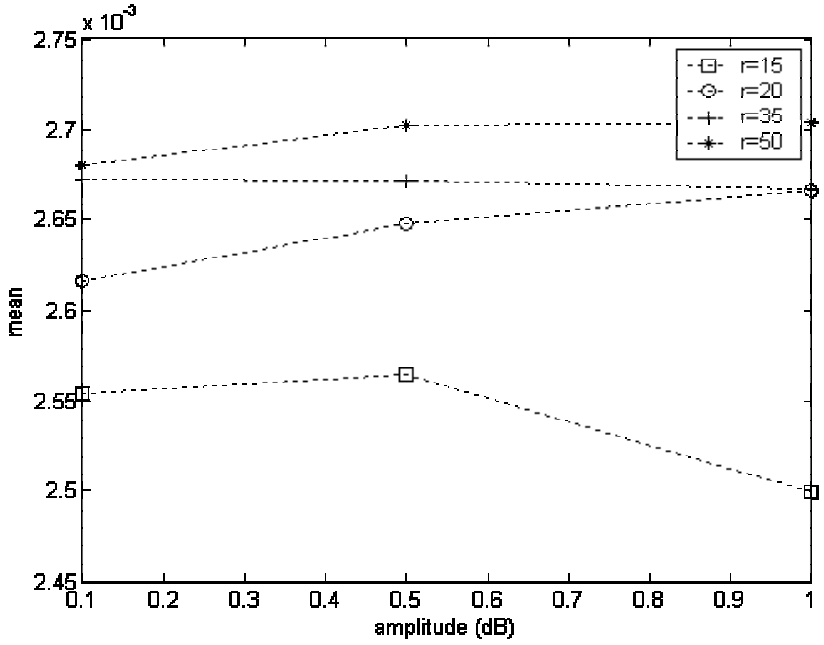

Figure 5.51: Effect of gain factor on means for Ω_{Arel}, N=10

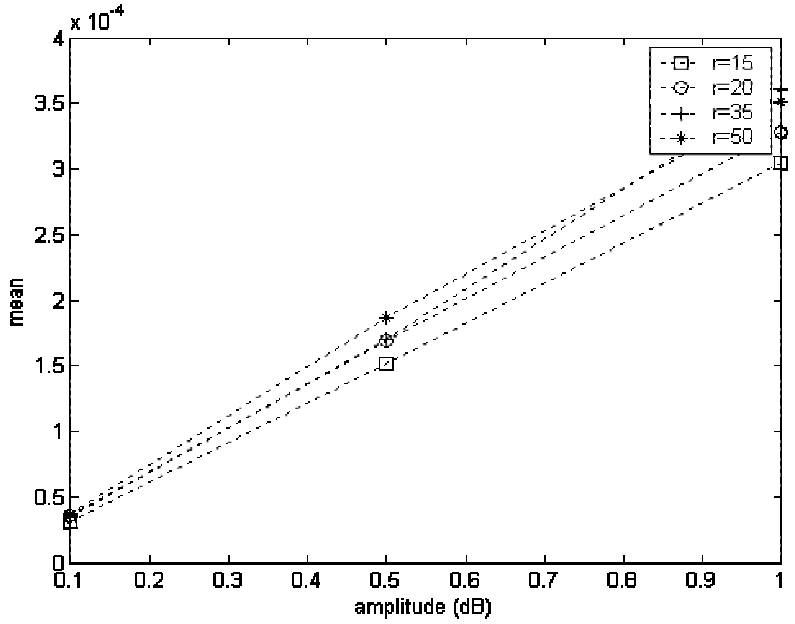

Figure 5.52: Effect of gain factor on standard deviations for Ω_{Arel}, N=10

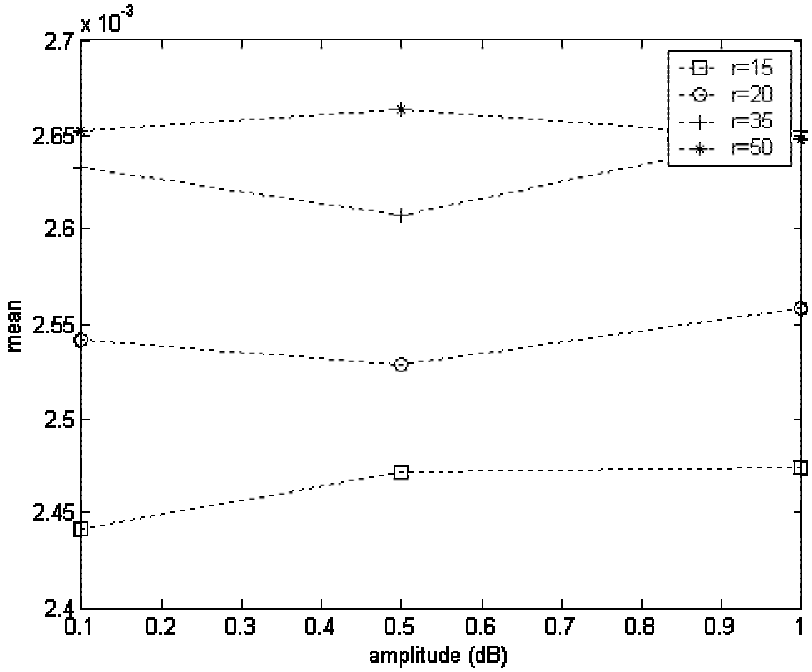

Figure 5.53: Effect of gain factor on means for Ω_{Brel} , N=10

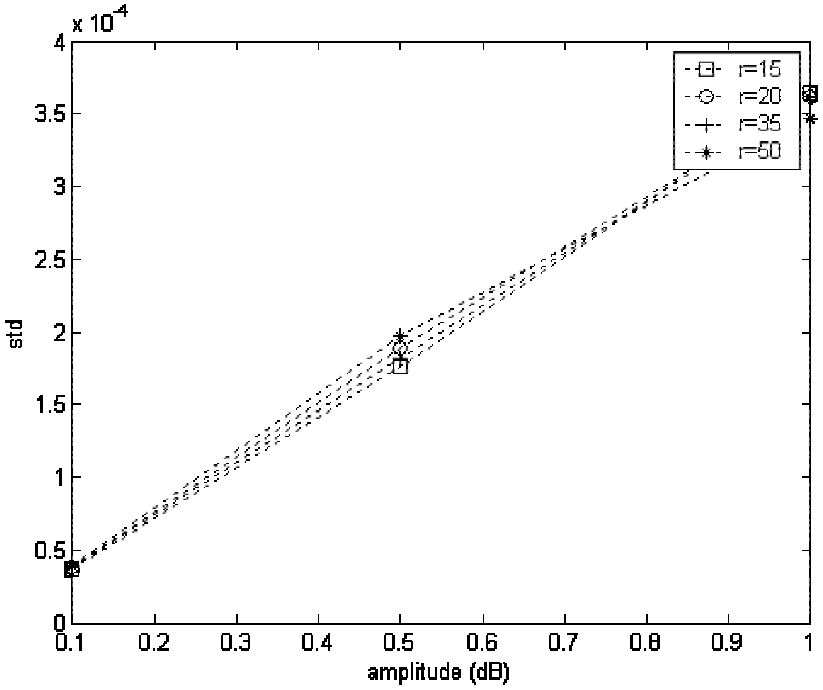

Figure 5.54: Effect of gain factor on standard deviations for Ω_{Brel} , N=10

Figure 5.51 shows a maximum value of 2.7×10^{-3}. This is compared to Figure 5.21 representing four elements with a maximum of 6.85×10^{-3}. Figure 5.53 shows a maximum value of 2.65×10^{-3}. This is compared to Figure 5.23 representing four elements with a maximum of 8×10^{-3}. The standard deviations show a regular increase.

5.3.5 Errors due to IF mismatch

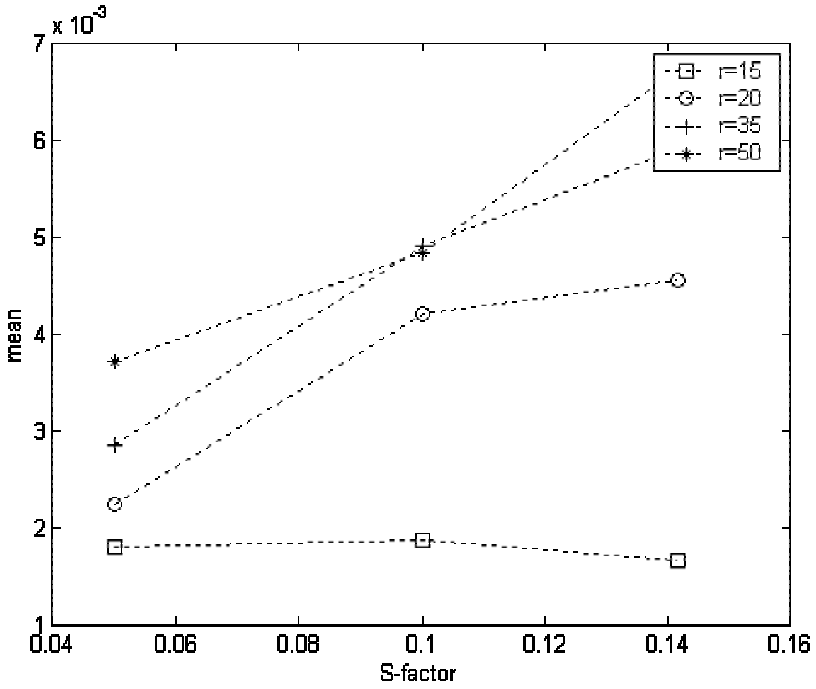

Figure 5.55: Effect of mixer mismatch on means for r_{rel}, N=10

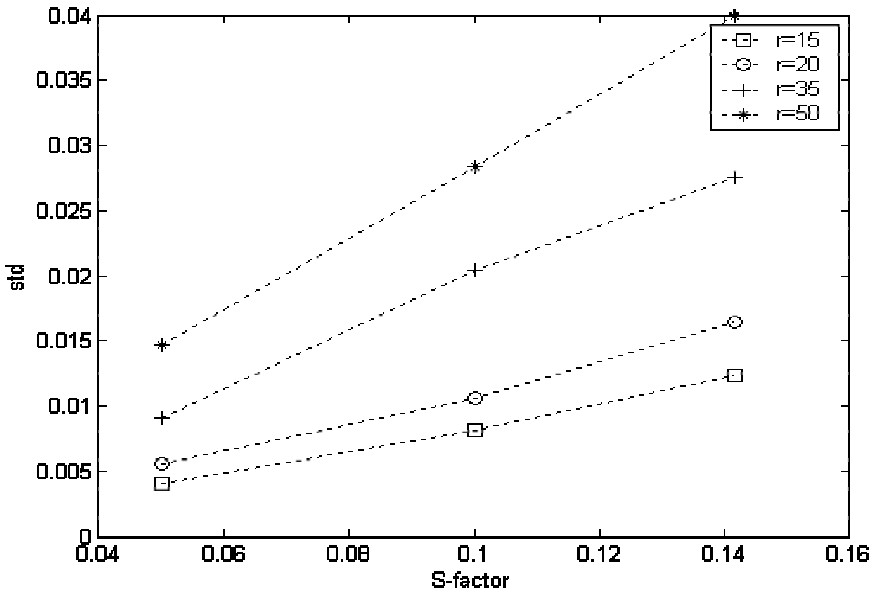

Figure 5.56: Effect of mixer mismatch on standard deviations for r_{rel}, N=10

As shown by Figure 5.55, the effect of increasing the randomness of the mixer mismatch on the overall range estimation accuracy can be almost negligible. However, this is not the case with Figure 5.25 that represents the case for 4 elements with a maximum of 0.094. Standard deviations show a constant increase.

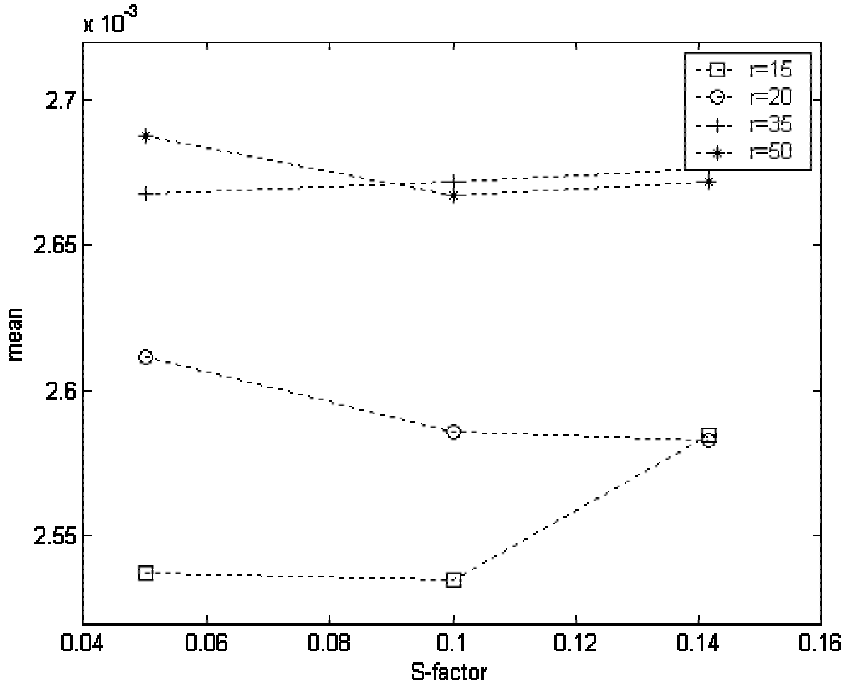

Figure 5.57: Effect of mixer mismatch on means for Ω_{Arel}, N=10

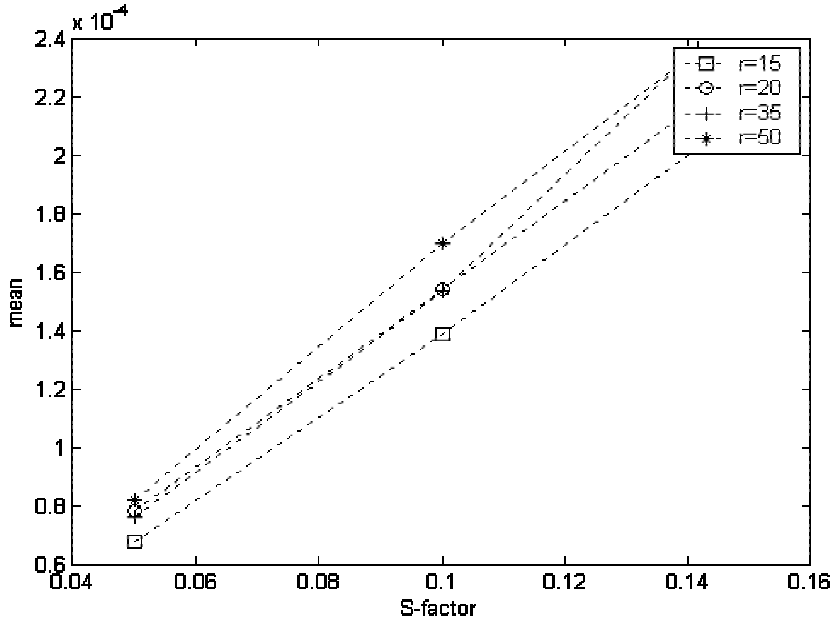

Figure 5.58: Effect of mixer mismatch on standard deviations for Ω_{Arel}, N=10

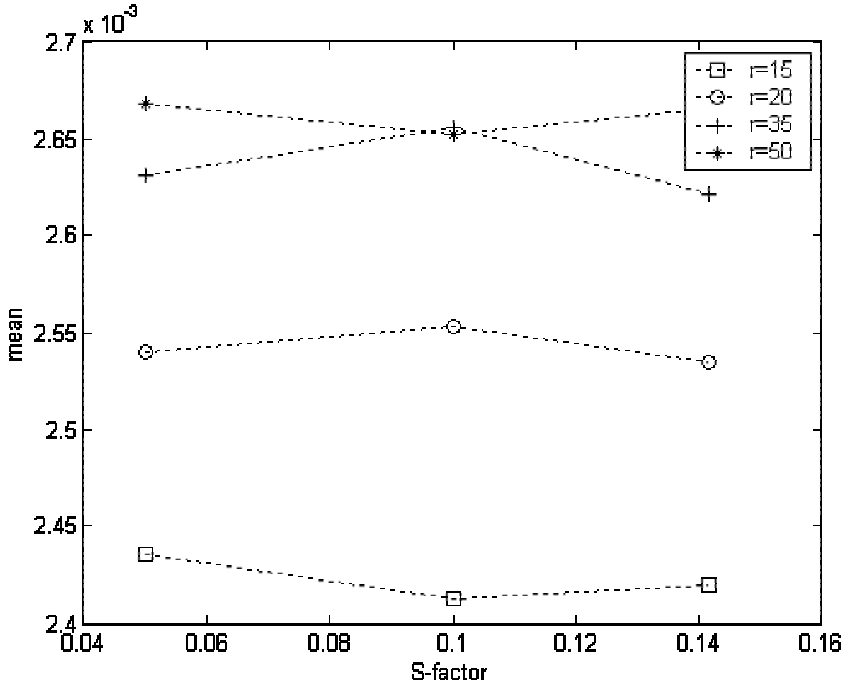

Figure 5.59: Effect of mixer mismatch on means for Ω_{Brel}, N=10

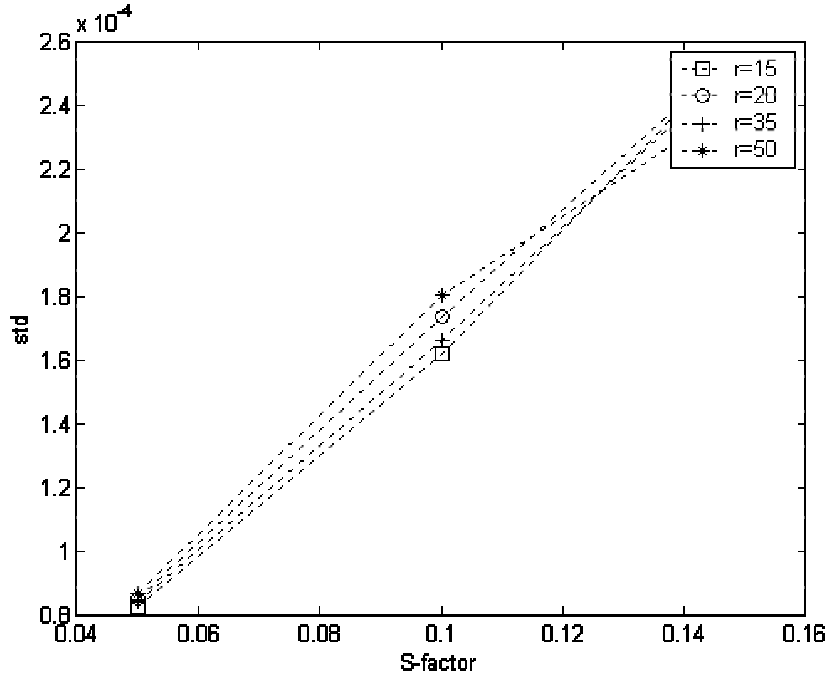

Figure 5.60: Effect of mixer mismatch on standard deviations for Ω_{Brel}, N=10

Figure 5.57 shows a maximum value of 2×10^{-3}. This is compared to Figure 5.27 representing four elements with a maximum of 6.85×10^{-3}. Figure 5.59 shows a

maximum value of 2.68×10^{-3}. This is compared to Figure 5.29 representing four elements with a maximum of 8×10^{-3}. The standard deviations show a regular increase.

5.4 Tolerance levels for Range Estimation using MRP for N=4

The purpose of the earlier error analysis was to form a statistical analysis of the levels within which each error affects the over-all system errors represented in range and angles or arrival. Final assessment is given to that data in this section. For different tolerance levels, we have different estimated ranges. The tables below show the means and standard deviations of the relative error. Therefore, a 10% value represents an increase in the value of range by 10%, or an estimated range of 1.1 *r* where *r* is the actual range.

	r=15m		*r*=20m		*r*=35m		*r*=50m	
ΔL	Std	Mean	Std	Mean	Std	Mean	Std	Mean
0.2mm	2.5%	8.9%	1.5%	8.3%	6%	8.7%	4%	8.5%
0.5mm	6%	9%	7.5%	9.3%	15.5%	12.9%	28.5%	16.9%
0.7mm	7.5%	10.5%	11.5%	9%	21%	22%	44%	19%
1mm	10.5%	8.5%	18.5%	9.75%	27%	14.7%	89%	38.2%

Table 5.6: Tolerances for different transmission line lengths

	r=15m		*r*=20m		*r*=35m		*r*=50m	
ΔP	Std	Mean	Std	Mean	Std	Mean	Std	Mean
0.5°	2.8%	8.8%	3.4%	8.7%	6.6%	8.3%	8.8%	9%
1°	5.5%	8.9%	7%	8.7%	13.7%	10.7%	17.4%	8.2%
3°	16%	9.2%	26.7%	15.5%	58.7%	26.2%	216%	48.5%

Table 5.7: Tolerances for different phase shifts

	r=15m		r=20m		r=35m		r=50m	
Γ	Std	Mean	Std	Mean	Std	Mean	Std	Mean
$0 \Leftrightarrow 0.05$	0.48%	8.8%	0.64%	8.81%	0.98%	8.81%	1.3%	8.6%
$0 \Leftrightarrow 0.1$	0.99%	8.7%	1.33%	8.81%	2.1%	9.2%	2.8%	8.73%
$0 \Leftrightarrow 0.2$	2.02%	9.08%	2.54%	8.73%	4.53%	8.79%	5.52%	8.88%

Table 5.8: Tolerances for different antenna mismatch factors

	r=15m		r=20m		r=35m		r=50m	
Γ	Std	Mean	Std	Mean	Std	Mean	Std	Mean
$0 \Leftrightarrow 0.05$	0.49%	8.86%	0.7%	8.86%	0.86%	8.85%	1.4%	8.92%
$0 \Leftrightarrow 0.1$	0.93%	8.92%	1.3%	8.8%	0.88%	8.83%	3.2%	9.26%
$0 \Leftrightarrow 0.2$	1.46%	8.87%	1.65%	9.03%	2.75%	9.15%	3.9%	9.39%

Table 5.9: Tolerances for different IF mismatch factors

	r=15m		r=20m		r=35m		r=50m	
ΔA	Std	Mean	Std	Mean	Std	Mean	Std	Mean
$\pm 0.1dB$	0.25%	8.82%	0.27%	8.9%	0.52%	8.8%	0.61%	8.85%
$\pm 0.5dB$	1%	8.95%	1.37%	8.85%	2.38%	8.79%	3.22%	9.43%
$\pm 1dB$	2.37%	8.85%	2.72%	8.94%	4.49%	8.7%	6.31%	9.51%

Table 5.10: Tolerances for different gain factors

5.5 Tolerance levels for Range Estimation using MRP for extended 10 element arrays

This section summarizes the results with the extended 10 element arrays which are better than those presented in Section 5.4. The tables below show the means and standard deviations of the relative error.

	r=15m		r=20m		r=35m		r=50m	
ΔL	Std	Mean	Std	Mean	Std	Mean	Std	Mean
0.2mm	1.7%	0.025%	2.58%	0.2%	4.3%	0.01%	6.27%	0.13%
0.5mm	4.24%	0.2%	7.21%	0.8%	11.12%	2.72%	17.02%	5.94%
0.7mm	6.87%	0.16%	8.01%	0.34%	19.6%	2.8%	26.98%	5.1%
1mm	11.16%	3.28%	14.96%	4.7%	24.3%	5.4%	47.9%	13.72%

Table 5.11: Tolerances for different transmission line lengths

	r=15m		r=20m		r=35m		r=50m	
ΔP	Std	Mean	Std	Mean	Std	Mean	Std	Mean
0.5°	2.13%	0.31%	2.8%	0.11%	5.25%	1.41%	7.52%	1.29%
1°	4.26%	0.33%	5.55%	0.88%	10.74%	0.84%	14.02%	1.81%
3°	12.82%	3.04%	15.96%	5.43%	42.17%	10.81%	172.2%	36.22%

Table 5.12: Tolerances for different phase shifts

	r=15m		r=20m		r=35m		r=50m	
Γ	Std	Mean	Std	Mean	Std	Mean	Std	Mean
$0 \Leftrightarrow 0.05$	0.4%	0.2%	0.56%	0.23%	0.97%	0.28%	1.46%	0.33%
$0 \Leftrightarrow 0.1$	0.77%	1.2%	1.17%	1.26%	1.97%	0.44%	2.63%	0.08%
$0 \Leftrightarrow 0.2$	1.81%	0.11%	2.34%	0.25%	4.06%	0.76%	6.49%	1.16%

Table 5.13: Tolerances for different antenna mismatch factors

	r=15m		r=20m		r=35m		r=50m	
Γ	Std	Mean	Std	Mean	Std	Mean	Std	Mean
$0 \Leftrightarrow 0.05$	0.4%	0.18%	0.55%	0.22%	0.91%	0.28%	1.47%	0.37%
$0 \Leftrightarrow 0.1$	0.81%	0.19%	1.05%	0.42%	2.04%	0.5%	2.84%	0.48%
$0 \Leftrightarrow 0.2$	1.23%	0.17%	1.64%	0.46%	2.76%	0.59%	4%	0.67%

Table 5.14: Tolerances for different IF mismatch factors

	r=15m		r=20m		r=35m		r=50m	
ΔA	Std	Mean	Std	Mean	Std	Mean	Std	Mean
$\pm 0.1dB$	0.18%	0.14%	0.25%	0.21%	0.41%	0.24%	0.66%	0.25%
$\pm 0.5dB$	0.88%	0.22%	1.14%	0.04%	2.24%	0.09%	3.06%	0.22%
$\pm 1dB$	1.85%	0.49%	2.42%	0.11%	4.16%	0.63%	5.9%	0.25%

Table 5.15: Tolerances for different gain factors

Chapter 6
Conclusions and Future Work

This thesis covered the error analysis for estimating the range of emitters using a Range Limited Antenna and using different direction-finding algorithms. MUSIC and Modified Root Pisarenko were applied to different conditions of error so that the final impact on estimating the range of the emitter could be realized. Several Monte Carlo simulations were performed to form a statistical analysis that could be used in reference with the antenna. Upon simulating physical errors in the antenna set-up, it was realized that the range estimation algorithm is sensitive to the slightest of phase shifts, cable gains, mixer mismatches, and antenna mismatches. Furthermore, the effects of mutual coupling have also been analyzed. An important part of the analysis is the use of an extended antenna array using elements that shows how effective it is in terms of equalizing the radiation patterns. This was necessary for the performance of MRP.

The final sections of Chapters 4 and 5 assess the overall analysis so that tolerance levels for the range estimation could be formed. Section 4.3 shows that by using MUSIC with two 4-element arrays for emitters lying within 50m, tolerance levels below 10% can be achieved by keeping transmission line length differences within 1mm, phase shifter differences within 1°, Γ (reflection coefficient) within 0.2 and ΔA (gain factor) within $\pm 1dB$. Section 4.4 analyzes the effect of decreasing the number of antenna elements on each array by taking the case representing phase shifter differences. As expected, the performance degrades. Section 4.5 analyzes the improvement in performance by increasing the number of antenna elements to 8 on each array. Tolerance levels within 10% for N=8 can be achieved by having phase shifter differences within 3°.

Section 5.4 shows that by using Modified Root Pisarenko with two 4-element arrays for emitters lying within 50m, tolerance levels below 10% can be achieved by keeping transmission line length differences within 0.5mm, phase shifter differences within 1°,

Γ (reflection coefficient) within 0.2 and ΔA (gain factor) within $\pm 1dB$. Section 5.5 analyzes an extended 10-element array. The performance improves as tolerance levels below 10% can be achieved by keeping transmission line length differences within 1mm, phase shifter differences within 3°, Γ (reflection coefficient) within 0.2 and ΔA (gain factor) within $\pm 1dB$. For all cases, the range estimation is very sensitive to estimated angles of arrival. Furthermore, taking practical conditions into account, it may become difficult, although not impossible, to have useful range results unless component tolerances are kept within tight bounds.

A continuation of this work could be the application of different direction-finding algorithms such as Root MUSIC, Prony, and Modified Pisarenko and comparing their performance with MUSIC and MRP. Also, the effects of multipath could be taken into account. Another development could be the analysis when more than one emitter is used. Furthermore, several input parameters could be varied to see their effect on the overall performance. Of these, emitter power, bit duration, filtered signal SNR, emitter gain, etc. could give interesting results. 3D figures could be generated by developing algorithms that would cover all elevation and azimuth angles for a specific input emitter range.

Appendix A

Derivation of Estimated Range using Angles of Arrival

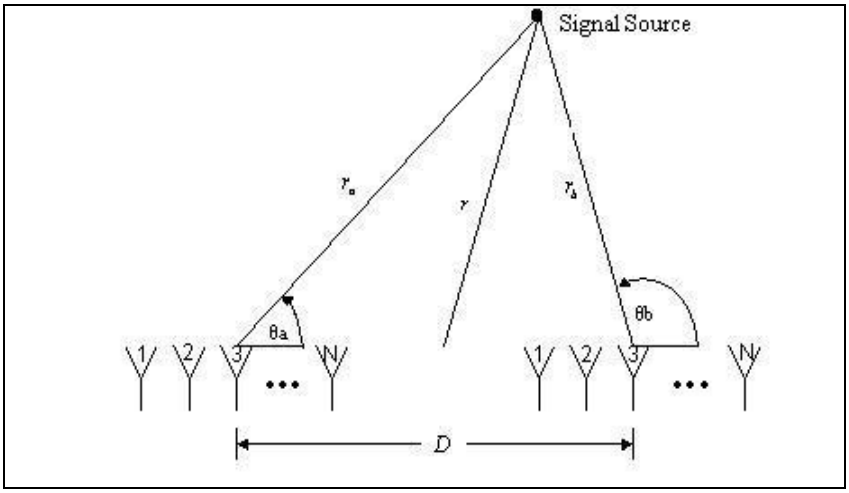

The above figure shows *r* to be the accurate distance of the emitter from the center of the antenna array. An estimated distance is denoted by *R*. Applying sine theorem on the above figure, it can be seen that:

$$\frac{\sin(\pi-\theta_b)}{r_a}=\frac{\sin(\theta_a)}{r_b}=\frac{\sin(\theta_b-\theta_a)}{D} \tag{A-1}$$

Further expansion gives:

$$\frac{\sin(\theta_b)}{r_a}=\frac{\sin(\theta_a)}{r_b}=\frac{\sin(\theta_b)\cos(\theta_a)-\sin(\theta_a)\cos(\theta_b)}{D} \tag{A-2}$$

Applying the cosine theorem on the above figure, we have:

$$R^2=D^2\left\{\frac{1}{4}+\frac{{r_a}^2}{D^2}-\frac{r_a}{D}\cos\theta_a\right\} \tag{A-3}$$

Substituting from (A-1), the following equations are formed:

$$R^2 = D^2\left\{\frac{1}{4} + \frac{\sin^2\theta_b}{\sin^2(\theta_a - \theta_b)} - \frac{\sin\theta_b}{\sin(\theta_b - \theta_a)}\cos\theta_a\right\} \tag{A-4}$$

$$R^2 = D^2\left\{\frac{1}{4} + \frac{\sin^2\theta_b - \sin\theta_b\cos\theta_a\sin(\theta_b - \theta_a)}{\sin^2(\theta_a - \theta_b)}\right\} \tag{A-5}$$

$$R^2 = D^2\left\{\frac{1}{4} + \frac{\sin^2\theta_b - \sin\theta_b\cos\theta_a[\sin\theta_b\cos\theta_a - \sin\theta_a\cos\theta_b]}{\sin^2(\theta_a - \theta_b)}\right\} \tag{A-6}$$

$$R^2 = D^2\left\{\frac{1}{4} + \frac{\sin^2\theta_b - \sin^2\theta_b\cos^2\theta_a + [\sin\theta_a\sin\theta_b\cos\theta_a\cos\theta_b]}{\sin^2(\theta_a - \theta_b)}\right\} \tag{A-7}$$

$$R^2 = D^2\left\{\frac{1}{4} + \frac{\sin^2\theta_b\sin^2\theta_a + \sin\theta_a\sin\theta_b\cos\theta_a\cos\theta_b}{\sin^2(\theta_a - \theta_b)}\right\} \tag{A-8}$$

$$R^2 = D^2\left\{\frac{1}{4} + \frac{\sin\theta_a\sin\theta_b[\sin\theta_b\sin\theta_a + \cos\theta_a\cos\theta_b]}{\sin^2(\theta_a - \theta_b)}\right\} \tag{A-9}$$

$$R^2 = D^2\left\{\frac{1}{4} + \frac{\sin\theta_a\sin\theta_b\cos(\theta_a - \theta_b)}{\sin^2(\theta_a - \theta_b)}\right\} \tag{A-10}$$

$$R = D\sqrt{\left\{\frac{1}{4} + \frac{\sin\theta_a\sin\theta_b\cos(\theta_a - \theta_b)}{\sin^2(\theta_a - \theta_b)}\right\}} \tag{A-11}$$

References

[Bahl1] *Bahl, I.; Bhartia, P.,* "Microstrip Antennas," Artech House, Massachusetts, 1980

[Ban1] *Balanis, C.A.,* "Antenna Theory: Analysis and Design," pp. 724-725, John Wiley & Sons, 1997

[Ban2] *Balanis, C.A.,* "Antenna Theory: Analysis and Design," 1st Edition, Publisher John Wiley & Sons, pp. 207, 1982

[Ban3] *Balanis, C.A.,* "*Antenna* Theory: Analysis and Design," pp. 412 - 434, 2nd Edition, John Wiley & Sons, Inc., 1997

[Camp1] *Campbell, D.,* "Adaptive Beamforming using a Microphone Array for Hands-free Telephony," Masters of Science Thesis, Virginia Tech, February, 1999

[Frid1] *Friedlander, B.,* "A Sensitivity Analysis of the Music Algorithm," IEEE Transactions on Acoustics, Speech, and Signal Processing, Vol 38, No. 10, 1990

[Garg1] *Garg, R.; Bhartia, P.; Bahl, I.; Ittipiboon, A.,* "Microstrip Antenna Design Handbook," pp. 2-3

[Garg2] *Garg, R.; Bhartia, P.; Bahl, I.; Ittipiboon, A.,* "Microstrip Antenna Design Handbook," pp. 759-766

[Kop1] *Kopriva, I.; Wasylkiwskyj, W.,* "Application of Direction-finding Algorithms to Antenna Arrays with Mutual Coupling,", private communication, pp. 2; Appendix 3, GWU, 2003

[Kop2] *Kopriva, I.,* "RLA Signal Processing Issues," private communication, GWU, 2003

[Kop3] *Kopriva, I.; Wasylkiwskyj, W.,* "Root Algorithms Based Direction of Arrival Estimation in the Presence of Mutual Coupling,", private communication, GWU, 2003

[Kop4] *Kopriva, I.; Wasylkiwskyj, W.,* "Root Algorithms Based Direction of Arrival Estimation in the Presence of Mutual Coupling,", private communication, Eq. 3, 6, 7, 9, 10; GWU, 2003

[Kop5] *Kopriva, I.; Wasylkiwskyj, W.,* "Application of Direction-finding Algorithms to Antenna Arrays with Mutual Coupling,", private communication, Eq. 1, 2, 3, 4, 5, 6, 7, 12, 13, 14, 20, 34, 35, 36, 37, 38; pp. 3-7; Appendix 3, GWU, 2003

[Lib1] *Liberti, J. C.; Rappaport, T. S.,* "Smart Antennas for Wireless Communications: IS-95 and Third Generation CDMA Applications," Eq. 3.3, 3.4, 3.5; pp. 60-65

[Lib2] *Liberti, J. C.; Rappaport, T. S.,* "Smart Antennas for Wireless Communications: IS-95 & 3rd Generation CDMA Applications," pp. 258-260, Prentice Hall PTR, 1st edition (April 1999)

[Lib3] *Liberti, J. C.; Rappaport, T. S.,* "Smart Antennas for Wireless Communications: IS-95 & 3rd Generation CDMA Applications," Eq. 9.8, 9.10, 9.11; pp. 258

[Sch1] *R. O. Schmidt*, "A Signal Subspace Approach to Multiple Emitter Location and Spectral Estimation," PhD Thesis, Stanford University, Stanford, CA, November 1981

[Spd1] *Spielman, D.; Paulraj, A.; Kaliath, T., "*Performance Analysis of the Music Algorithm Information Systems Laboratory," Stanford University

[Swi1] *Swindlehurst, A.; Kailath, T.,* "A Performance Analysis of Subspace Based Methods in the Presence of Model Errors – Part 1: The Music Algorithm," pp. 3

[Was1] *Wasylkiwskyj, W.; Eom, K.,* "RLA Design Employing DF Techniques,", private communication, GWU, 2003

[Was2] *Wasylkiwskyj, W.,* "Array Super-resolution Taking Account of Bandwidth and Mutual Coupling,", private communication (Rev7), pp. 21-24, August 26th, 2002
[Was3] *Wasylkiwskyj, W., "*Array Super-resolution Taking Account of Bandwidth and Mutual Coupling,", private communication, Eq. A-6, A-42, A-44; pp. 21-31; August 26th, GWU, 2002
[Was4] *Wasylkiwskyj, W.; Eom, K.,* "RLA Design Employing DF Techniques,", private communication, GWU, 2003

Vita

Zarak A. Khan was born in London, UK on 5th March, 1978. He received his Bachelor of Electronic Engineering from Ghulam Ishaq Khan Institute of Engineering Sciences and Technology, Pakistan in May 2001. He was enrolled as an M.S. Student at Virginia Polytechnic Institute and State University in Fall 2001. His work interests include RF propagation, network planning and optimization techniques.